AN ABSTRACT OF THE THESIS OF

Harry R. Anderson for the degree of Master of Science in Electrical & Computer Engineering presented on October 16, 1984.

Title: Theoretical and Experimental Investigations of FSK Data Transmission in the Noise and Interference Environment of Broadband Two-Way Cable Television Systems

Redacted for privacy

Abstract approved: _____
Rudolf S. Engelbrecht

Two-way transmission of data on broadband community cable television systems is considered in this thesis. A discussion of the data transmission environment is presented which attempts to characterize the channel noise and interference which degrades data transmission performance. The analysis considers channel degradation resulting from additive gaussian noise and various amplitudes and frequencies of sinewave interference which simulate the noise and interference environment likely to be found on cable systems. To assess the impact of the channel noise and interference, noncoherent binary frequency shift keying (FSK) using frequency discriminator detection was chosen as the basis for a theoretical and experimental investigation. To simplify the analysis, a linear model of frequency discriminator detection is presented which provides useful results in situations where the signal-to-noise ratio is high. The model was tested against laboratory experiments using an idealized FSK data transmission channel with controlled amounts of noise and interference. A comparison of theoretical and experimental results show reasonably good agreement, thus

validating the model for certain noise and interference circumstances which are applicable to data transmission on two-way cable television systems. The results show that with an FSK carrier-to-sinewave interference ratio of 6 dB, an increase in carrier-to-noise ratio of approximately 5 dB is required to achieve the same 1×10^{-9} error rate. The usefulness of the study results for predicting FSK data transmission performance can be improved by incorporating empirical statistical data on interference ingress in the return path of the cable system.

Theoretical and Experimental Investigations of FSK Data Transmission in the Noise and Interference Environment of Broadband Two-Way Cable Television Systems

by

Harry R. Anderson

A THESIS

submitted to

Oregon State University

in partial fullfillment of
the requirements for the
degree of

Master of Science

Completed October 16, 1984

Commencement June 1985

APPROVED:

Redacted for privacy

Rudolf S. Engelbrecht, Associate Professor of Electrical & Computer Engineering in charge of major

Redacted for privacy

S. J. T. Owen, Head of the Department of Electrical & Computer Engineering

Redacted for privacy

Dean of the Graduate School

Date thesis is presented: October 16, 1984

TABLE OF CONTENTS

LIST OF FIGURES

Figure	Page

LIST OF TABLES

THEORETICAL AND EXPERIMENTAL INVESTIGATIONS OF FSK DATA TRANSMISSION IN THE NOISE AND INTERFERENCE ENVIRONMENT OF BROADBAND TWO-WAY CABLE TELEVISION SYSTEMS

INTRODUCTION

The growing requirement for data communications by businesses, institutions, and households has directed attention to community-wide broadband cable systems as a possible carrier mechanism for these new services. Such systems are primarily designed to distribute television and music programming to homes. Because these systems are intended for one-way transmission of analog information from a central location to thousands of receiving points, their use for two-way data communications is not optimum. Consequently, a number of noise and interference problems are encountered which affect the data signals in ways which cannot be predicted by simple extrapolation from the performance of the one-way analog signals.

The theoretical and experimental analysis described in this thesis addresses some of these problems and develops a model which attempts to provide a conservative estimate of data communication performance. Although many data modulation-demodulation schemes are available to the communication system designer, this research deals specifically with non-coherent frequency shift keying (NCFSK or simply FSK in this document) when demodulated using frequency discriminator detection. It is not suggested that this modulation-demodulation method is optimum, but because of its simplicity it is widely used in currently available data communications equipment designed for use on

cable systems at moderate data signalling rates (up to 56 kbits per second).

A frequency discriminator detector responds to the instantaneous frequency of the input signal (derivative of the instantaneous phase), resulting in a nonlinear transfer of the input signal. The nonlinear effect means that superposition of the effects of various noise and interference inputs is not a strictly valid way to predict the output signal. The nonlinear effect on an input FSK signal corrupted by gaussian noise has been previously analyzed in the literature. However, FSK data performance with both noise and interference has not, to the author's knowledge, been dealt with in the literature. This research proposes a simplified linear model which is intended to be useable in situations with high signal-to-noise ratios and interference of varying amplitudes and frequencies.

Section 1 of this thesis is background information which describes the signal environment on current day cable systems. Very little actual measurement data on return path interference amplitudes is available, so assumptions about worst case conditions were used. The assumption that the signalling environment will be most often characterized by high signal-to-noise ratios and relatively low signal-to-interference ratios is explained in this section.

Section 2 is a theoretical analysis of FSK demodulation with frequency discrimination detection which first deals with noise and interference effects independently, and subsequently proposes a model in which it is assumed that low level noise is linearly transferred to the output baseband spectrum while the nonlinear effect of the interference is treated in a comprehensive fashion such that the "no-noise"

sample values of the demodulated data signal are shifted according to the amplitude and frequency of the interference. The data pulse sample error at the output of the model is thus a linear combination of the sample error due to the non-linear effect of the input interference and a gausssian-distributed sample error due to the input gaussian noise.

Section 3 describes the laboratory set up and associated measurements which were used to investigate actual FSK performance in the noise and interference environment analysized in Section 2. The intention of this work was to confirm, within reasonable experimental error, the applicability of the model proposed in Section 2. The laboratory results are idealized in that transmitter-receiver timing and synchronization problems are not present. The measured results therefore show performance which is worse than theoretical predictions but better than that obtained in practice.

Section 4 compares the theoretical and experimental results of Section 2 and Section 3, respectively, and draws conclusions on the viability of the model for predicting real data communication performance on community-wide broadband cable systems.

In keeping with standards established in electrical engineering literature, all footnotes, references, and bibliographic citations are indicated by sequential numbers enclosed in brackets (such as [1]), and listed at the end of the text as references.

SECTION 1 - BACKGROUND INFORMATION ON BROADBAND CABLE SYSTEMS

Development of Broadband Cable Systems

The demand for increasing numbers of communication services for both business and home uses over the last thirty years has driven the growth of wide area coaxial cable distribution networks. Such systems began as a means of distributing television programming in remote areas where the performance obtained with off-air reception using commonly available home receiving antennas was unacceptable. Early systems of this type typically had bandwidths of about 175 MHz (50 to 225 MHz), sufficient to carry 12 standard VHF television channels. These community cable systems were structured with a single central distribution point (headend) and networks of coaxial cable designed to provide signals to randomly distributed points which were passed by the distribution system, similar to electrical power distribution. In this respect these systems could be distinguished from point-to-point coaxial cable systems in use over short distances by telephone companies and others. Because of the cable attenuation at the higher frequencies, and the noise figure and output level limitations of intermediate repeater amplifiers, the extent of signal distribution for such early systems was limited to about five miles from the headend.

The improved television signal quality possible with the cable system as compared to off-air broadcasting, and the desire for more channels than could be made available via the spectrum allocated to television broadcasting, motivated improvements in amplifiers,

cable hardware, and signal processing equipment. The improved equipment allowed extending the distribution system to serve large portions of metropolitan areas.

A broadband cable into most homes in a city has additional potential beyond the one-way distribution of television programming from a central location. By frequency sharing techniques (frequency division multiplexing or FDM), signals can be also be originated in the home for transmission back up the cable to the headend or other intermediate distribution point. Such two-way (forward - return) technology has been an integral part of modern cable system design for the past fifteen years, especially in large cities where planners, viewing the cable system as a natural monopoly, have instituted franchise ordinances that cable systems be two-way capable. The envisioned uses of such two-way systems include pay-per-view billing for premium TV programs, interactive services such as shopping, banking, and voting from home, home security, and remote utility meter reading and load control. All of these services involve digital rather than analog data communications.

Although systems have been designed for two-way communications for some years, the capability has largely gone unutilized for two main reasons: 1) several technical problems involved with transmitting two-way data are yet to be resolved, and 2) the demand for such services has not been adequate to justify the cost of developing home interactive data terminals and solving the technical and operational problems associated with a high-reliability data service such as would be required for financial and billing transactions. Some specific aspects

of the technical problems involved with such two-way data transmission are the subject of this thesis.

Before discussing the architecture of modern cable systems in more detail, it should be noted that a parallel development of cable systems for purely business uses has occurred. These systems are referred to as local area networks (LAN's). They are usually confined to a single office building where they are used as a data bus to connect computer terminals with a central computer and other peripheral devices, such as printers and plotters, which may be located thoughout the building. LAN's are also used to connect machines and robots with central control computers along extensive assembly lines. LAN's differ from city cable systems in four major ways:

1. They are specifically designed for two-way data communication rather than one-way television with data as an add-on.
2. They are not exclusively frequency-division-multiplexed systems. Some of the most widely used employ baseband data transmission using time-division-multiplexing (TDM) and high average data rates (10 Mbits/second).
3. They use cable, repeater amplifiers and distribution hardware designed for limited area use (from terminal to terminal within a given building or complex of buildings).
4. They are used in a limited environment entirely on private property where sources of electromagnetic interference can be controlled.

Because of these differences, LAN's represent different, and generally less severe, data communication engineering problems from those posed by cable systems which pass all the homes in a city. The research

described in this thesis deals with community-wide cable systems connecting homes; henceforth "cable system" in this document will refer only to such systems.

Architecture of Community-Wide Cable Television Systems

Figure 1 shows a block diagram of a modern cable system. Signals originate at one or more headends from satellite downlinks, microwave, off-air broadcast, dedicated point-to-point cable, videotape, or video studio programming sources. From the headend the signals are distributed to hubs via "supertrunk" links which are typically multichannel microwave hops, large diameter coaxial cable, or multiple analog optical fiber. The hubs distribute signals to multiple trunks, each of which is connected to several feeder cables. Each feeder distributes programming to several homes via drop cables connected to a signal splitter on the feeder cable.

The forward path employs amplifiers spaced such that overall system gain to the farthest point in the system is unity (that is, the amplifiers provide frequency-equalized gain to just overcome the cable loss incurred since the preceeding amplifier). For return communication, a cascade of reverse amplifiers is used with crossover filters on the cable which essentially segment the available spectrum into forward (to the home) and return (from the home) bands. Although system specifications and hardware vary throughout the industry, and the amplifier technology is constantly improving, at this point in time the forward band is typically 50 to 400 or 450 MHz, while the return

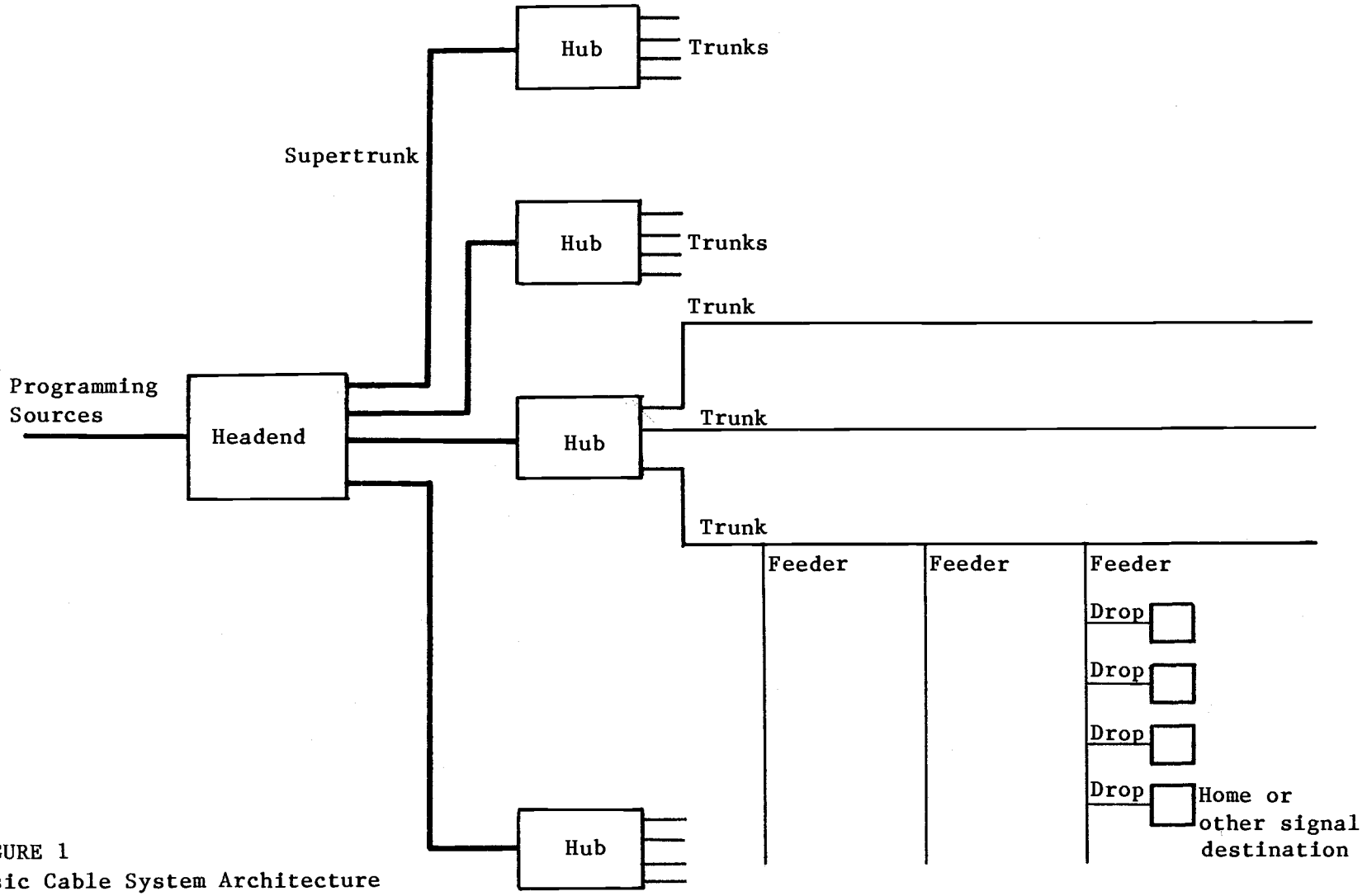

FIGURE 1
Basic Cable System Architecture

band is typically 5 to 30 MHz. The 30 to 50 MHz range is a guard band where the filter responses cross over.

The number of forward amplifiers in cascade on a trunk system can range up to about 30, limited by the noise and intermodulation distortion which builds up as the cascade length increases. The number of forward amplifiers in cascade on the feeders is typically not greater than three. Since the frequency band assigned to return transmission is much lower than the forward band, cable attenuation is lower and consequently return amplifiers can be more widely spaced on both the feeders and trunks.

The hub represents a distribution point where signals are usually demodulated from the supertrunk and remodulated on new frequencies for insertion on the distribution system. Two-way data regeneration can also take place at the hub and data from multiple trunks multiplexed after regeneration. Because regeneration is possible at the hubs, the data signal degradation of concern here occurs along the distribution leg consisting of a single trunk and its connected feeders and drop cables to homes. Figure 2 shows this distribution arm in more detail, along with the amplifiers and crossover filters.

As stated, the feeders are connected to drop cables which enter the homes for subsequent distribution to multiple TV receivers or other signal destination points. The connection from the feeder to the drop cable is made via directional couplers which provide a degree of isolation between homes connected to the same feeder between amplifiers.

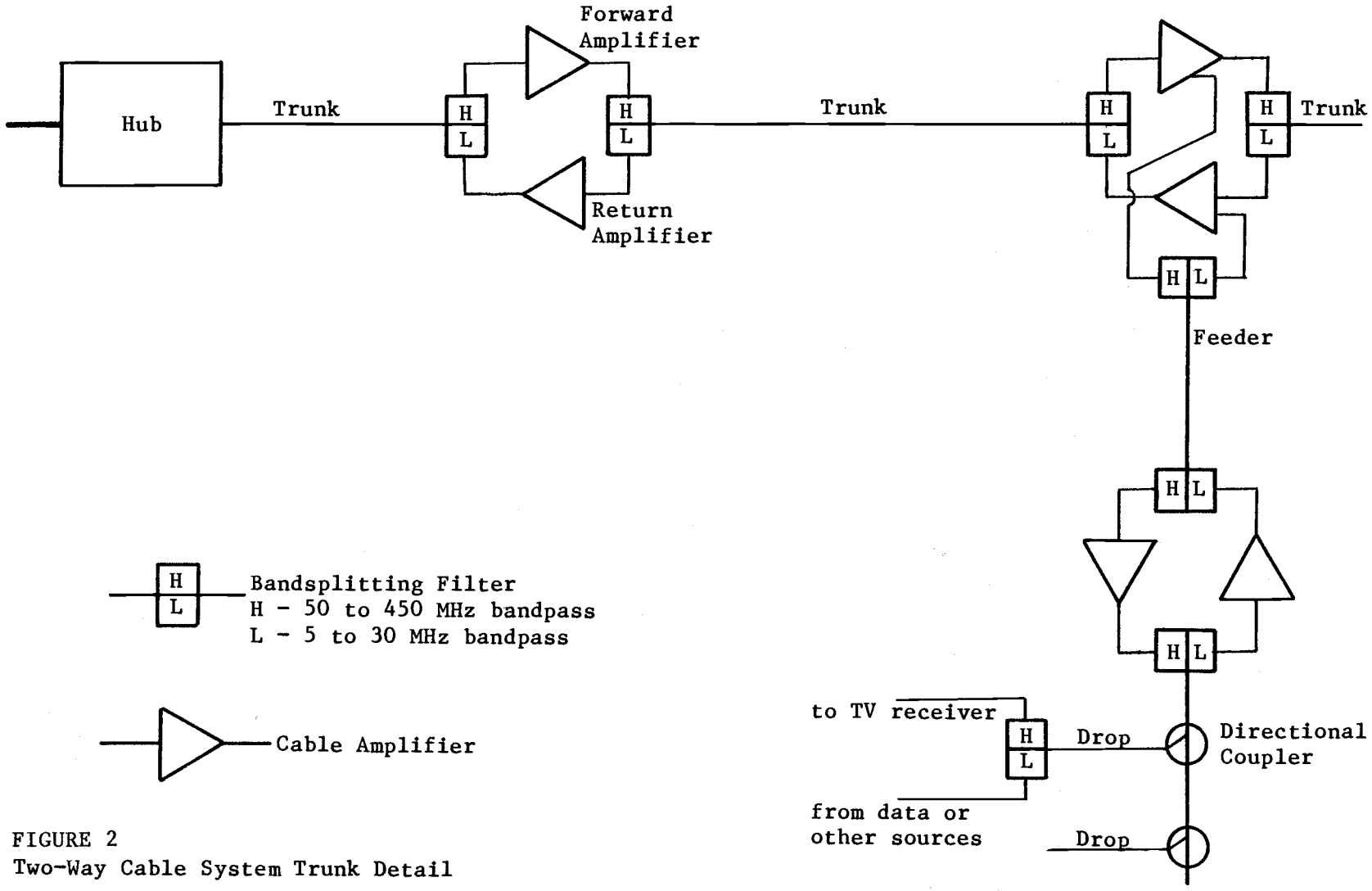

FIGURE 2
Two-Way Cable System Trunk Detail

Noise and Interference Environment of Cable Systems

Any signals which are carried on the cable system are subject to three primary sources of degradation which limit the utility of these signals. These are:

1. Amplifier noise
2. Intermodulation and other distortion products
3. Inadvertent and deliberate signal ingress

Each of these will be discussed in turn.

Amplifier Noise

Any system involving electrical circuitry will have some noise added to the signal caused by the random thermal motion of electrons in resistors and other components. This added noise is characterized as additive white noise with a gaussian-distributed amplitude probability density function (pdf). The amplifier is typically modelled as a ideal (noiseless) amplifier with an equivalent gaussian noise source, as well as the desired signal source, connected to the input. The mean square noise voltage is dependent on the temperature, resistance, and bandwidth, as given by the following formula:

$$\overline{V^2} = 4RkT_{eq}B$$

where R = resistance, k = Boltzmann's constant = 1.37×10^{-23} joule/deg. T_{eq} = temperature in Kelvin, and B = bandwidth in Hertz. The noise figure in dB for an amplifier is given by

$$F_{dB} = 10 \log_{10}\left(\frac{T_{eq}}{290} + 1\right)$$

The r.m.s. thermal noise voltage level at the input to the first amplifier out from the hub (the noise floor) in a 100 kHz bandwidth data channel at 75 ohm impedance is approximately -69 dBmV (decibels relative to 1 millivolt). The signal-to-noise ratio (SNR) at the output of the first amplifier is given by:

$$\text{SNR} = \text{Output level} - (-69 + F(\text{in dB}) + \text{amplifier gain})\ \text{dB}$$

The noise figure for these amplifiers is about 7 dB, the net gain is typically 22 dB, and with a data carrier output level of -15 dBmV, the resulting SNR is about 47 dB.

A detailed treatment of noise generation in the amplifiers is not the intention of this research. It is sufficient to view the noise on a system basis. The equivalent input noise source output is added to the amplifier noise figure and multiplied by the first amplifier gain. At the second amplifier, it is again multiplied by the second amplifier gain, along with the noise contribution of the second amplifier. As the amplifier cascade increases, the noise level increases. By performing the appropriate calculations, it can be shown that the noise power doubles (increases by 3 dB) each time the number of amplifiers doubles, assuming all the amplifiers are the same and the noise voltages are independent. In practice, noise builds up slightly faster than that due to imperfect coupling and impedance matching along the cable, and differences in individual amplifiers. However, the "doubling rule" is sufficiently accurate to be confidently applied.

The broadband trunk and feeder amplifiers normally operate as push-pull, Class AB amplifiers. The output levels are generally run as

high as possible so that the spacing to the next amplifier can be as long as possible. The output level limitation is governed by the degree of intermodulation distortion which is created as the amplifier is pushed into nonlinear operating regions. This distortion will be the subject of the next section. The important point here is that the amplifier output level, and hence the signal level on the cable, is limited. With a limited signal level, and an increasing noise level as the number of amplifiers increases, the signal-to-noise ratio is decreasing. Since the signal-to-noise ratio is a prime determinant of signal quality, this decreasing SNR effectively limits the number of amplifiers which can be cascaded. The noise from the signal generating equipment at the hub is controlled and generally such a low level that it can be ignored in the noise calculations.

The above discussion primarily dealt with noise buildup in forward amplifier cascades. Such cascade noise buildup also occurs in return amplifiers, but as Figure 2 shows, the noise from sources in the home add up in the feeder cable along with the noise from the feeder amplifiers. The situation is exacerbated at the trunk where all the feeders contribute their noise into the same 5 to 30 MHz bandwidth on the trunk cable. Depending on the individual noise inputs along the way, the noise in the return channel as it arrives at the hub can be a high level compared to the noise arriving at the home via the forward path. The forward cable path can thus be thought of as a tree-type distribution system, whereas the return cable path is a collection system in that signals, noise and interference are all funneled into the trunk cable for delivery to the hub.

The noise funneling problem on the return system has been addressed by two techniques: remotely switching the return feeder paths, and installation of separate return trunks for an individual or group of return feeder paths. Switching the feeder on and off, as signalling requires, at the point where it is connected to the trunk is effective at reducing noise on the trunk. However, such feeder switching is useless when signalling may originate from randomly located homes, as in an interactive data or security alarm system, because there is no efficient way to indicate which feeders should be switched on at any particular time.

The second technique involves a separate return system trunk back to the hubs for each return feeder (or group of feeders). While this also greatly reduces noise funneling, it substantially increases system cost since a whole set of additional return-only trunks must be added to the system architecture.

It should be noted that neither of these methods have been implemented to any great extent, primarily because the economic imperative for two-way services have not driven these problems to a solution, as already mentioned. While finding new methods for solving the noise funneling problem is a challenging engineering problem, the point of this discussion is to recognize that data communication on two-way cable systems will be corrupted by additive gaussian noise of predictable power levels, and that with current design practices, this noise degradation will generally be much worse on return paths than on forward paths. Additive gaussian noise is the first type of channel degradation which will be considered.

Intermodulation and Other Distortion Products

It was already mentioned that signal levels, and consequently signal-to-noise ratios, are limited by the linear operating region of the cable amplifiers. As the amplifier input level is increased, the output level increases to the point where the amplifier begins to distort the signal. The distortion produced is a function of the amplifier design, and generally falls into two categories:

1. Cross modulation, in which one signal amplitude-modulates another.
2. Intermodulation, in which the multiplying of two or more frequencies creates distortion products at new frequencies in spectrum space intended for other uses.

Amplifier distortion on cable TV systems has been studied in detail in the literature [1], [2], [3], [4]. Of the two types of distortion, intermodulation distortion is the limiting factor in most systems due to the large number of television channels which are carried in the 50 to 450 MHz forward path (50 to 60 television channels). The distortion usually takes the form of triple beats which are sums and differences involving three frequencies such as F1 $\pm$ F2 $\pm$ F3 or 2xF1 $\pm$ F2 or 3xF1. When 50 or more television carriers (and associated audio carriers at -13 to -20 dB levels relative to the video carriers) are run through an amplifier, the number of possible distortion products is enormous when all the conceivable combinations are considered. Computer calculations have shown that with a 53 channel system, the worst case channel has over 900 triple beat products falling in it. [5]

The intermodulation beat problem has been dealt with by using harmonically related carriers (HRC) or interval related carriers (IRC). With HRC and IRC systems, all the intermodulation products fall on other carrier frequencies rather than in the message (video) spectrum. While this considerably reduces the perceptibility of the beat products, it must be remembered that each of the input television signals to the amplifier is itself amplitude modulated (with the attendent sidebands) so that each intermodulation product is also accompanied by sidebands.

The input level of the amplifiers is usually controlled so that at the output the resulting intermodulation carrier products are 60 dB or more below desired carrier levels. With fewer channels, the operating levels can be increased since fewer products are created. Composite triple beat (CTB) in the forward path of modern cable systems is a prime design criterion which is often specified both in the trunk and at the home drop.

In the worst case, interference from intermodulation products shows up in television pictures as undesired artifacts of other signals. Forward data transmission would occur in unoccupied TV channels on the system, usually with several such data carriers packed into a single 6 MHz TV channel (depending on the data rate). In order not to exacerbate the CTB problem for TV viewers, the data carriers are typically set at levels 10 to 15 dB below the video carrier levels. The data channels will then be contending with multiple interference (CTB) carriers with predictable (but probably unknown) amplitude and phase characteristics. The effects of such intermodulation products is the second type of channel degradation which will be modelled in this

study.

Since the number of coincident carriers and the number of amplifiers in the return path is less than for the forward path, intermodulation distortion in the return system is not presently considered to be a significant problem. This may change if two-way data signalling does ultimately come into wide use.

Inadvertent and Deliberate Signal Ingress

A community cable system is installed throughout a city and may include a thousand or more miles of aerial cable strung between utility poles. It is therefore susceptible to interference from electromagnetic radiation sources randomly located throughout the service area. These sources include broadcast, amateur, citizen band and other transmitters, power line interference, and interference from large industrial machines. Normally a well-constructed, well-maintained coaxial cable will have low susceptibility to such interference ingress. However, where the interfering signals are strong or the state of the cable system is less than ideal with loose or corroded connections and damaged or faulty shielding, interference ingress can be a significant problem. The converse of this is also true; that is, radiation of energy from the cable through faulty shields or connectors can cause interference to other communications. Such cable radiation is controlled by FCC technical regulations on cable systems [6].

Another point of interference ingress is the drop cable into the home itself. Maintaining these cables represents the most significant maintenance problem for the cable operator. The termination of the drop cable at the television receiver or convertor box has been identified as a point of interference ingress. A TV set normally designed for off-air reception, and enclosed in a plastic or wooden cabinet, can function as a substantial antenna with some portion of the received signals ending up in the return spectrum of the drop cable where they are funneled up to the hub along with the noise and desired signals. An inadvertently unterminated or disconnected coax connector is another source of interference ingress.

A third source of interference which may also occur in the home is deliberate or malicious interference caused by someone intentially trying to disrupt the system or use it for illegal or unintended purposes. Although such cases can be regarded as highly improbable, a few efforts by knowledgeable individuals could cause more serious problems than random, unintentionally interference from other sources.

The interference ingress problem can be viewed as the potential for a large number of sources of varying frequencies, amplitudes, phases, transmission times, and transmission time durations. Because of the funneling effect, and because most offending transmitting sources (AM broadcast, amateur, shortwave, CB, and power line) are located in or below the return channel spectrum of 5 to 30 MHz, the interference ingress problem is much more significant on the return path than it is on the forward path. The susceptibility of interference from the home drop is also greatest in the return path since it was specifically designed to amplify and transmit all signals in

the 5 to 30 MHz band which originate at the home drop.

Some field studies have been done of the frequency and magnitude of return path interference and noise for a typical cable system. Figure 3 taken from Reference [7] shows a plot of amplitudes versus frequency in the 0 to 30 MHz band as recorded off the trunk cable at the hub. The peaks occur at frequencies corresponding to the transmitting sources. The plot also shows the noise floor. Although this data indicates the rough magnitude of the problem and which return frequency slots appear most interference-free, it does not give instantaneous amplitudes over all time nor does it provide an indication of the statistics of the interfering signal duration. Also, the plot was taken over a 24 hour period. Daily and seasonal variations in propagation conditions, especially on the shortwave frequencies, could cause substantial changes in the interference amplitudes. Because of this, and because little other field data of this type is available, it can be assumed that no specific and accurate characterization of the interference ingress problem in cable systems is currently available.

Summary of the Noise and Interference Environment

The noise and interference environment on cable systems can be summarized as follows:

1. Forward Path

    a) Additive gaussian noise from the amplifiers which builds up as the number of amplifiers in cascade increases.

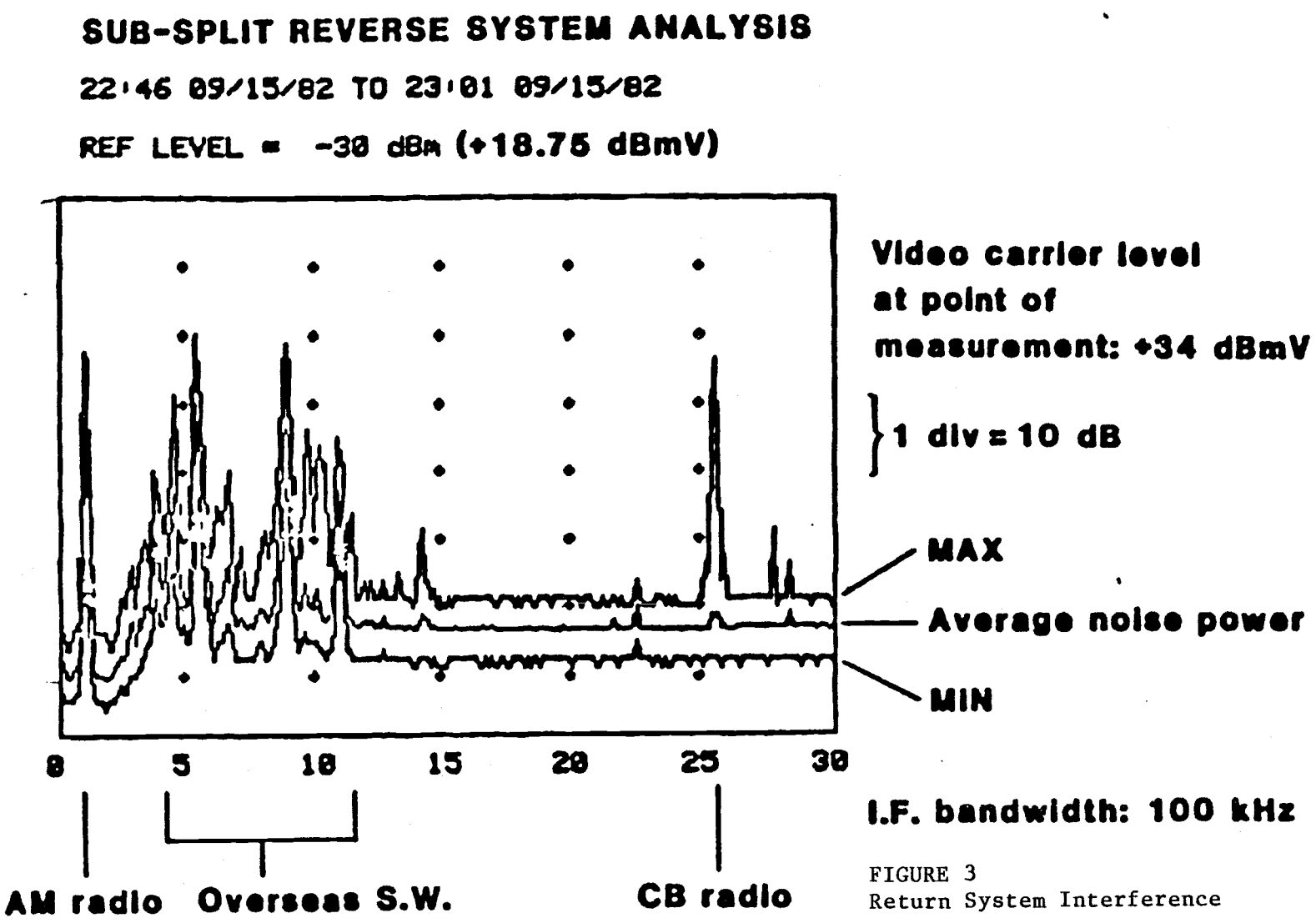

FIGURE 3
Return System Interference

b) Intermodulation distortion products manifest as multiple sinewave interference signals throughout the cable spectrum.

c) Interference ingress from random sources.

2. Return Path

a) Additive gaussian noise from amplifiers which builds up due to amplifier cascading and system funneling.

b) Intermodulation distortion in the return amplifiers

c) Interference ingress due to randomly distributed transmitting sources or unintentional and intentional undesired signal input at the home drop cable.

The limiting effects for forward transmission are the noise and intermodulation interference. Interference ingress is of minor importance, as already explained, because most of the offending sources are located at lower frequencies, and because the interference is not funneled up though the system.

The limiting effects for return transmission are once again amplifier noise, which will be more substantial than on the forward path, and interference ingress, both of which will be funneled back to the hub. Intermodulation interference is of minor importance here because the number of coincident carrier signals and the number of amplifiers on the return path is less than for the forward path.

A Model of Cable System Noise and Interference Environment

Except for the gaussian noise, it is difficult to model the other characteristics of the cable system environment since little measurement information is available. A conservative approach, then, is to model the system in a way which provides typical or worst case performance levels. In this way the identifiable on-off interference effects can be modelled as constantly on, and large numbers of randomly-distributed interferers can be modelled as additional gaussian noise in the channel.

To sort out amoung the possible system noise and interference models, the following three channel degradation situations were selected for study:

1. Additive gaussian noise of different amplitudes as bandlimited by the frontend bandpass filters of the FSK receiver. This is intended to model amplifier noise and large numbers of randomly distributed interference sources.

2. Single sinewave interference of different amplitudes and frequencies in the FSK data transmission spectrum, but without gaussian noise added. This is intended to model intermodulation distortion products in the forward path and individual interference sources in the return path.

3. Situation 2, but with low level gaussian noise added.

Situation 3 is intended as the most appropriate overall view of the transmission environment. Because the data channel noise floor is low (-69 dBmV in 100 kHz) the signal-to-noise ratio for the data signal at the most distant drop is still quite high. Assuming a cascade of 30 trunk amplifiers and 3 feeder amplifiers, and a destination data carrier amplitude of -15 dBmV (15 dB below the nominal design amplitude of the video carriers at the home drop), the

signal-to-noise ratio is almost 32 dB. With no interference and ideal equipment, in theory this signal-to-noise ratio should yield essentially unmeasurable error rates. In practice, however, this has not been found to be the case, indicating that interference mechanisms of some sort, and timing and synchronization errors in real hardware, are limiting the performance. The cable transmission environment can be regarded as one with high signal-to-noise ratios and the possibility of relatively low signal-to-interference ratios. Unlike radio data channels where fading causes randomly changing signal levels and hence randomly changing signal-to-noise ratios, the cable environment preserves essentially constant signal amplitudes through the use of temperature compensation and automatic gain control (AGC) in the amplifiers. The signal-to-noise ratios are therefore similarly constant over time.

The model presented in Section 2 of this thesis is intended for such situations where the SNR is high and constant, and the signal-to-interference ratio is variable and may be quite low.

SECTION 2 - THEORETICAL PERFORMANCE OF FSK MODULATION WITH FREQUENCY DISCRIMINATOR DETECTION

FSK Modulation

Frequency shift keying (FSK) is one of the oldest forms of digital modulation. It conveys information by the use of a discrete frequency to represent a single or sequence of data bits. In the binary case, two frequencies are used corresponding to a binary "one" and "zero." Use of multiple discrete frequencies can represent longer bit sequences (i.e., four frequencies can represent sequences "00", "01", "10" , and "11").

Early forms of FSK modulation used step switching between frequencies in response to the data stream. Recent modifications to FSK include continuous phase FSK (CP FSK) [8], in which the phase of the carrier wave is adjusted at the switching instant to provide a smooth phase transition, and tamed FSK (TFM), in which the data stream is lowpass filtered (or otherwise subjected to an operation to lenghten bit-to-bit transition times) so as to provide smooth rather than abrupt frequency transitions [9]. These more sophisticated methods primarily provide decreased spectrum occupancy as compared to hard switched FSK [10]. Since the focus of this research is on FSK performance in noise and interference, occupied bandwidth is of secondary concern. Consequently, this thesis will deal only with binary, hard-switched, non-CP FSK.

FSK Frequency Spacing

With binary FSK, one of the main parameters available to the system designer is the spacing between the frequency tones representing "one" and "zero." To make the task of distinguishing between a one and zero as easy as possible for the receiver, and thus achieve the best possible error rate, it is desireable to make the transmitted signals corresponding to one and zero as different as possible. This can be done by minimizing the product of the two signals over one bit period, T. Let the two frequencies corresponding to one and zero be

$$S_1 = A\cos(\omega_c + \frac{\Delta\omega}{2})t$$

$$S_2 = A\cos((\omega_c - \frac{\Delta\omega}{2})t + \theta)$$

where $\Delta\omega$ is the frequency difference in radians between the two tones. The angle θ is the phase difference between S1 and S2; when the frequency transition is made it is unlikely that the other carrier will be at zero phase.

The product integrated over T is

$$E = \int_0^T S_1 S_2 dt$$

$$E = A^2 \int_0^T \cos(\omega_c + \frac{\Delta\omega}{2})t \cos((\omega_c - \frac{\Delta\omega}{2})t + \theta)\, dt$$

$$E = \frac{A^2}{2}\int_0^T \cos(\Delta\omega t - \theta)dt + \frac{A^2}{2}\int_0^T \cos(2\omega_c t + \theta)dt \qquad (1)$$

If the carrier frequency ω_c is much larger than the data rate, then the term $2\omega_c T$ is much larger than 1 and the result of the second

integral in equation (1) is small enough to be ignored.

Evaluating the first integral in (1) yields

$$E = \frac{A^2}{2}\int_0^T \cos(\Delta\omega t - \theta)\,dt$$

$$E = \frac{A^2}{2}\int_0^T \cos\Delta\omega t\cos\theta - \sin\Delta\omega t\sin\theta\,dt$$

$$E = \frac{A^2}{2}\cos\theta\int_0^T \cos\Delta\omega t\,dt - \frac{A^2}{2}\sin\theta\int_0^T \sin\Delta\omega t\,dt$$

$$E = \frac{A^2T}{2}\cos\theta\left(\frac{\sin\Delta\omega T}{\Delta\omega T}\right) + \frac{A^2T}{2}\sin\theta\left(\frac{\cos\Delta\omega T - 1}{\Delta\omega T}\right) \qquad (1a)$$

For $\Delta\omega T = 2\pi n$, E = 0 regardless of the value of θ.

For $\Delta\omega T = .715\cdot(2\pi)$, the expression assumes its minimum value of -.217 if the transition phase θ is zero. This explains one virtue of continuous phase FSK. For $\theta \neq 0$, E is not -.217 but can be actually greater than zero. Since setting the frequency spacing at $\Delta f T = 1$, always yields E = 0, $\Delta f T = 1$ is often used.

Assuming $\theta = 0$, the first term takes on the familiar shape shown in Figure 4, plotted as a function of $\Delta f T$. Orthogonality of the two signals occurs when $2\Delta f T = n$, n = 1,2,3...

When the tone spacings is set so that $\Delta f T = 0.5$, it is known as miminum shift keying (MSK). When combined with continuous phase techniques at the switching time, CP MSK takes on a narrow, rapidly decaying occupied spectrum, and hence improved efficiency in terms of transmitted bits per occupied Hertz of bandwidth. It can be shown that

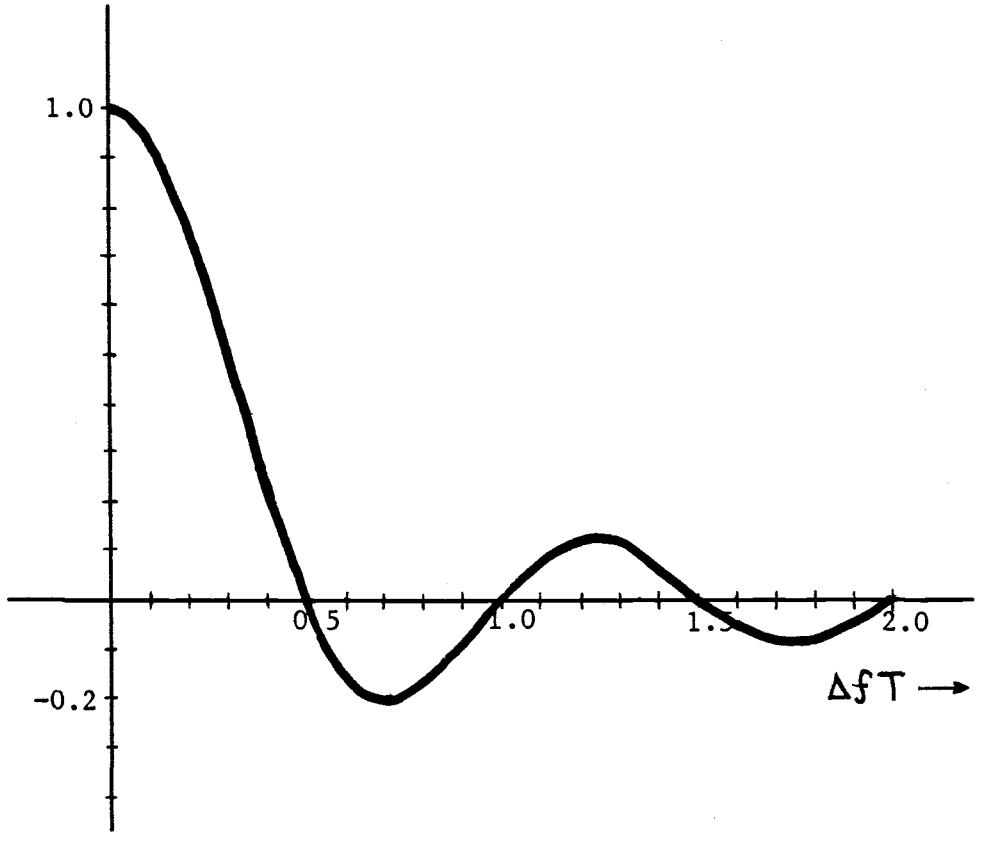

FIGURE 4
Plot of the first term of
equation 1a, normalized to 1.0

by averaging over 2 bit periods (2T), the error rate performance of CP MSK is superior to FSK and identical to binary coherent PSK [11].

It can be shown that using increased tone spacings in the presence of gaussian noise for hard-switched FSK does not improve the error rate performance [12]. This is because widening the channel bandwidth to accommodate wider tone spacings also increases the noise presented to the detector. Reexamining this conclusion about the value of increased tone spacing in the presence of gaussian noise and interference is one goal of this research.

FSK Demodulation

There are three main methods of detecting FSK modulation: 1) noncoherent with envelope detection, 2) coherent matched filter or correlation detection, and 3) frequency discriminator detection. The noncoherent method is shown in Figure 5 . It consists of two bandpass filters with (ideally) responses matched to the transmitted data signals centered at ω_a for a binary 1 and ω_b for a binary 0, followed by envelope detectors and a summation device which produces the difference between the output of the two envelope detectors. The decision device produces a binary one or zero depending on which filter has the greater output at sample time nT, n=1,2,3...

The noncoherent method is suggested by decision theory, and it has been extensively analyzed in the literature with both gaussian noise and interference added to the input signal [12], [13], [14]. The properties of the envelope detector when subjected to an input of noise and sinewave interference is also well known, making the analy-

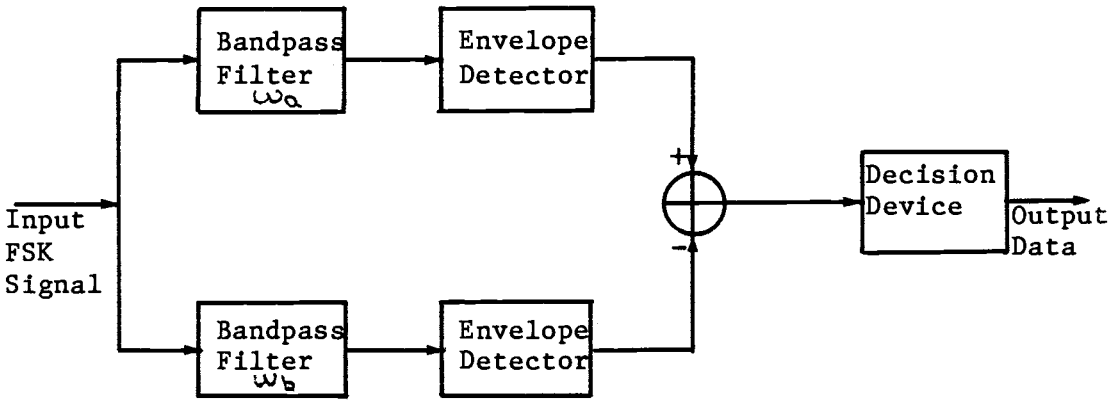

FIGURE 5
Noncoherent Demodulator

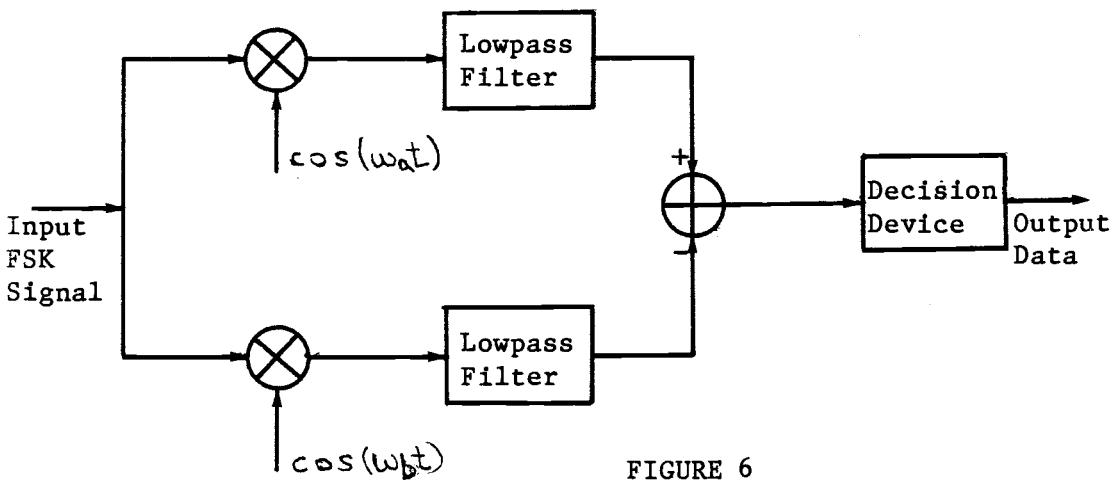

FIGURE 6
Coherent Demodulator

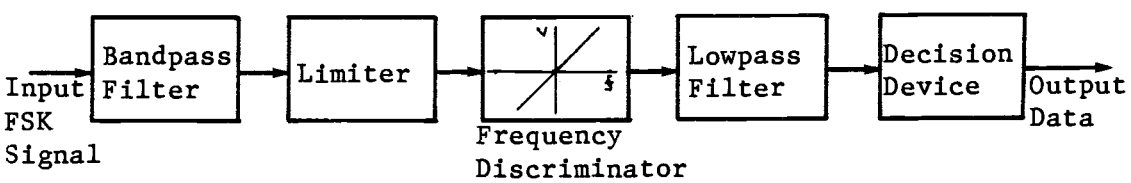

FIGURE 7
Frequency Discriminator Demodulator

sis of the noncoherent filter error rate performance straightforward. The problem with the noncoherent filter method is that it is not widely used in low cost commercial communication devices, such as would be used on a cable system, due to the difficulty of manufacturing the bandpass filters to appropriate tolerances.

The second matched filter or correlation detection method is illustrated in Figure 6. It consists of two multipliers which multiply the incoming signal by ω_a and ω_b, thus shifting the spectrums centered around ω_a and ω_b to baseband. The multipliers are followed by lowpass filters which remove the higher order product $(\omega_a + \omega_a)$ and limit the output spectrum to only that which is necessary to convey the data pulse without excessive intersymbol interference. This type of receiver has found little use in practice since it requires two phase-synchronized oscillators and, as has been shown [15], for high signal-to-noise ratios, its performance is only slightly better than the noncoherernt detector previously described.

The third detection method, the frequency discriminator, is shown in Figure 7. This is much more widely used in practice because of the availability of inexpensive integrated circuit phase lock loop (PLL) devices which serves as a quite linear detector with low detection threshold levels [16]. Because of its commercial viability, the PLL detector with input bandpass filter and output lowpass filter is the detector most likely to be employed in inexpensive data demodulation equipment used on cable systems. Therefore, it is the method chosen for analysis in this research.

It will be assumed that the bandwidth of the input filter is sufficiently wide so that delay distortion effects are negligible and

no intersymbol interference is present. The limiter provides a constant amplitude signal of varying phase in response to the transmitted data signal and whatever noise and interference is added on the channel. For simplicity, the analysis will consider the impact of the noise and interference when a binary one is being transmitted, corresponding to frequency ω_a. Figure 8 shows a vector diagram of the signal as it is presented to the frequency discriminator. The notation is as follows:

$$SP = R\cos\omega_a t \qquad (2a)$$

$$SQ = R\sin\omega_a t \qquad (2b)$$

Signal Components

$$IP = \sum_{n=1}^{N} I_n \cos(\omega_n t + \theta_n) \qquad (3a)$$

$$IQ = \sum_{n=1}^{N} I_n \sin(\omega_n t + \theta_n) \qquad (3b)$$

Interference Components

θ_n = random variable uniformly distributed over 2π.

NP = gaussian noise

NQ = gaussian noise independent of NP

The actual feedback loop operation of the PLL will be disregarded, rather it will be assumed to produce a voltage which is linearly related to the instantaneous frequency of the input signal. The instantaneous frequency is the time derivative of the instantanteous phase, ϕ.

$$\phi = \tan^{-1}\left[\frac{SQ + IQ + NQ}{SP + IP + NP}\right] \qquad (4)$$

$$\frac{d\phi}{dt} = \dot{\phi} = \frac{d}{dt}\tan^{-1}\left[\frac{SQ+IQ+NQ}{SP+IP+NP}\right] \qquad (5)$$

$$\dot{\phi} = \frac{(SP+IP+NP)(\dot{SQ}+\dot{IQ}+\dot{NQ}) - (\dot{SP}+\dot{IP}+\dot{NP})(SQ+IQ+NQ)}{(SP+IP+NP)^2 + (SQ+IQ+NQ)^2} \qquad (6)$$

The dot over a variable indicates differentiation with respect to time. The output voltage of the discriminator is proportional to $\dot{\phi}$.

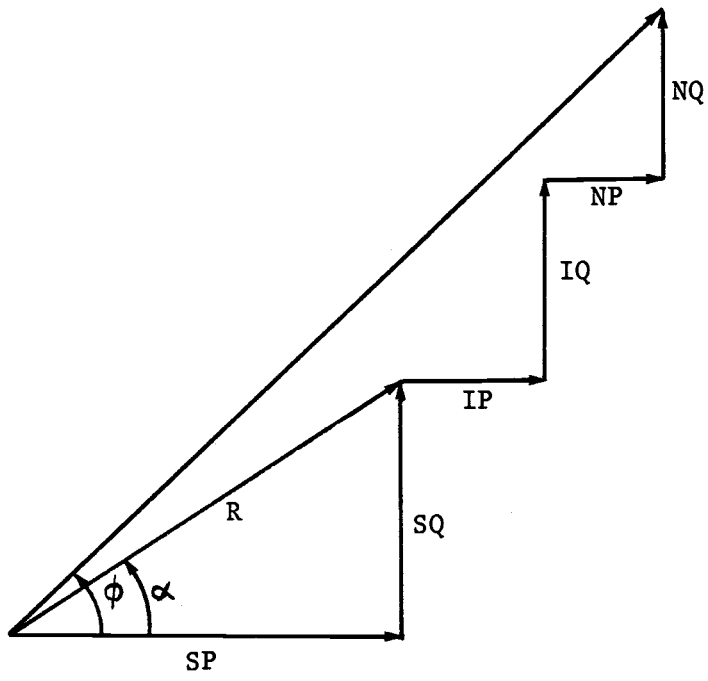

SP and SQ are the signal vectors

IP and IQ are the interference vectors

NP and NQ are the noise vectors

FIGURE 8

Vector Diagram of Signal
at Input to Limiter

For the moment the effect of the final low pass filter will be ignored. The analysis to follow will instead explore the probability density function of the detector output as given by equation (6).

Discriminator Output with Additive Gaussian Noise

With gaussian noise only added to the input signal (no interference), equation (6) reduces to

$$\dot{\phi} = \frac{(SP+NP)(\dot{S}Q+\dot{N}Q)-(\dot{S}P+\dot{N}P)(SQ+NQ)}{(SP+NP)^2+(SQ+NQ)^2} \qquad (7)$$

An error will occur whenever a binary one is transmitted and $\dot{\phi} < 0$, or a binary zero is transmitted and $\dot{\phi} > 0$. The denominator of (7) is the sum of the squares of two real quantities and therefore will always be positive. To determine when $\dot{\phi} > 0$ or $\dot{\phi} < 0$, only the numerator of (7) needs to be examined.

Let $$x = SP+NP \qquad \dot{x} = \dot{S}P+\dot{N}P \qquad (8a)$$

$$y = SQ+NQ \qquad \dot{y} = \dot{S}Q+\dot{N}Q \qquad (8b)$$

$$z = x\dot{y} - y\dot{x} \qquad (8c)$$

The probability density for z conditioned on x and y is given by

$$p(z|x,y) = \frac{1}{\sigma_z\sqrt{2\pi}} \exp\left[\frac{-(z-z_m)^2}{2\sigma_z^2}\right] \qquad (9)$$

where z_m is the mean of z, given x and y.

$$z_m = E[x\dot{y}] - E[y\dot{x}] = xE[\dot{y}] - yE[\dot{x}]$$

$$E[\dot{y}] = E[\dot{S}Q+\dot{N}Q] = E[\dot{S}Q] = \dot{S}Q$$

$$E[\dot{x}] = E[\dot{S}P+\dot{N}P] = E[\dot{S}P] = \dot{S}P$$

$\dot{N}Q$ and $\dot{N}P$ are the derivatives of zero mean gaussian processes . The mean of the derivative is also zero, and the distribution of the

derivative is gaussian [17]. Thus

$$z_m = x\dot{S}Q - y\dot{S}P \tag{10}$$

The variance of z is σ_z^2 and is equal to the sum of the variances of $x\dot{y}$ and $(-y\dot{x})$.

$$\sigma_z^2 = (x^2+y^2)\sigma_1^2 \tag{11}$$

where σ_1^2 is the variance of the derivative of a gaussian process, x(t) or y(t), given by

$$\sigma_1^2 = \int_{-\infty}^{\infty} X_{\dot{x}}(\omega)\,d\omega = 2\cdot\int_{-\infty}^{\infty} \omega^2 X(\omega_c+\omega)\,d\omega \tag{12}$$

For noise spectrum $X(\omega)$ or $Y(\omega)$ symmetrical around ω_c.

To find p(z), the probability density of z, the conditional density $p(z|x,y)$ is multiplied by the joint density $p(x,y)$ and then integrated over all x and y.

$$p(z) = \int_{-\infty}^{\infty}\int_{-\infty}^{\infty} p(z|x,y)\,p(x,y)\,dx\,dy \tag{13}$$

Since x and y are independent gaussian random variables,

$$p(x,y) = p(x)\,p(y)$$

$$p(x,y) = \frac{1}{2\pi\sigma_o^2}\exp\left[\frac{-(x-SP)^2-(y-SQ)^2}{2\sigma_o^2}\right] \tag{14}$$

Evaluating the error region when a binary zero is sent (i.e. p(z>0)) equation (13) is

$$P_e = \int_0^{\infty} dz \int_{-\infty}^{\infty}\int_{-\infty}^{\infty} p(-z|x,y)\,p(x,y)\,dx\,dy \tag{15}$$

$$P_e = \int_0^{\infty} dz \int_{-\infty}^{\infty}\int_{-\infty}^{\infty} \frac{1}{\sqrt{2\pi}\sigma_z}\exp\left[\frac{-(z-z_m)^2}{2\sigma_z^2}\right]\frac{1}{2\pi\sigma_o^2}\exp\left[\frac{-(x-SP)^2-(y-SQ)^2}{2\sigma_o^2}\right]dx\,dy \tag{16}$$

Performing the integration with respect to z, and using equations (10) and (11), yields the result in terms of the error function

$$P_e = \frac{1}{2}\frac{1}{4\pi\sigma_o^2}\int_{-\infty}^{\infty}\int_{-\infty}^{\infty} \operatorname{erf}\left[\frac{x\dot{S}Q - y\dot{S}P}{\sigma_1\sqrt{2}(x^2+y^2)^{1/2}}\right] \exp\left[\frac{-(x-SP)^2-(y-SQ)^2}{2\sigma_o^2}\right] dx\,dy \quad (17)$$

The solution of this integral is quite lengthy and involves transforming to polar coordinates and taking advantage of the odd symmetry properties of the error function around zero. The form of the integral is identical to that contained in Appendix A of Reference [18]. Since nothing is to be gained by repeating the solution here, only the final result is presented.

$$P_e = \frac{1}{2}\operatorname{erfc}\frac{R}{\sqrt{2}\sigma_o} + \frac{R}{2\sigma_o\sqrt{2\pi}}\int_{-1}^{1}\exp\left(\frac{-R^2x^2}{2\sigma_o^2}\right)\operatorname{erfc}\left[\frac{R\dot{\alpha}(1-x^2)^{1/2} - \dot{R}x}{\sqrt{2}\,\sigma_1}\right] dx \quad (18)$$

where $R = (SP^2 + SQ^2)^{1/2}$, $\dot{R} = dR/dt$

and $\alpha = \tan^{-1}(SP/SQ)$ is the transmitted phase so that

$$\dot{\alpha} = \frac{d\alpha}{dt} = \frac{SP\dot{S}Q - SQ\dot{S}P}{R^2}$$

The term $\dot{R}$ is the rate of change of the envelope of the signal. For an ideal FM system with wide bandwidth, the variations in the amplitude is very small (0 if BW $=\infty$). For practical systems, it is reasonable to design channel filters so that the amplitude variation is small enough to be neglected. Hence, assuming $\dot{R} = 0$ is reasonable. This condition is also a lower bound on error rate since it can be shown that P_e is minimum when and only when $\dot{R} = 0$ [18].

By rearranging terms and defining some new parameters, equation (18) can be put in a more useful form

$$P_e = \frac{1}{2}\operatorname{erfc}(\rho) + \frac{\rho}{2\sqrt{\pi}}\int_{-1}^{+1} e^{-\rho^2 x^2} \operatorname{erfc}\left[a\rho(1-x^2)^{1/2} - bx\right] dx \quad (19)$$

where

$$\rho^2 = \frac{R^2}{2\sigma_o^2}, \quad a^2 = \frac{\sigma_o^2 \dot{\alpha}^2}{\sigma_1^2}, \quad b^2 = \frac{\dot{R}^2}{2\sigma_1^2}$$

It will be assumed that $\dot{R} = 0$ and thus $b = 0$.

It will be noticed that the first term of equation (19) is the error rate for coherent FSK detection with matched filters [19]. This detection method translates the frequency spectrum of the noise around each tone frequency to baseband without any nonlinear modification in an envelope detector. The second term in equation (19) is therefore some additional degradation of the error rate resulting from the use of frequency discriminator detection rather than coherent detection. This additional probability of error has been attributed to "spike" or "click" phenomenon and is studied in detail in [16]. Rather than dwell on the phenomenological model for the existence of the spike -created errors, it is more useful here to evaluate the magnitude of this second term and its importance in the error rate calculations for real systems, especially those with high carrier-to-noise ratio (CNR) as would be expected on cable systems.

Equation (19) was evaluated numerically with and without the second term and for several values of CNR (R/σ), $b = 0$, and $a = 1$ and 2. The results are given in Tables 1 and 2. It is clear that for high CNR typical of cable systems, the contribution of the second term of equation (19) to the error rate does not change the probability of error to an extent that is significant to the data communications

TABLE 1

Probability of Error Calculations Based on Equation (19)
With and Without Term 2, and With a = 1

CNR(dB)	ρ	P_e Without Term 2	P_e With Term 2
1	0.7933	1.309 E -1	2.665 E -1
2	0.8902	1.224 E -1	2.264 E -1
3	0.9988	7.889 E -2	1.844 E -1
4	1.1207	5.649 E -2	1.425 E -1
5	1.2574	3.768 E -2	1.029 E -1
6	1.4109	2.300 E -2	6.836 E -2
7	1.5830	1.259 E -2	4.083 E -2
8	1.7762	6.004 E -3	2.134 E -2
9	1.9929	2.413 E -3	9.434 E -3
10	2.2361	7.827 E -4	3.375 E -3
11	2.5089	1.940 E -4	9.251 E -4
12	2.8150	3.432 E -5	1.814 E -4
13	3.1585	3.973 E -6	2.333 E -5
14	3.5439	2.699 E -7	1.764 E -6
15	3.9766	9.386 E -9	6.836 E -8
16	4.4615	1.405 E -10	1.142 E -9
17	5.0059	7.285 E -13	6.613 E -12
18	5.6167	9.943 E -16	1.009 E -14
19	6.3021	2.530 E -19	2.871 E -18
20	7.0711	7.770 E -24	9.867 E -23

TABLE 2

Probability of Error Calculations Based on Equation (19)
With and Without Term 2, and With a = 2

CNR(dB)	ρ	P_e Without Term 2	P_e With Term 2
1	0.7933	1.309 E -1	1.675 E -1
2	0.8902	1.224 E -1	1.314 E -1
3	0.9988	7.889 E -2	9.824 E -2
4	1.1207	5.649 E -2	6.940 E -2
5	1.2574	3.768 E -2	4.575 E -2
6	1.4109	2.300 E -2	2.768 E -2
7	1.5830	1.259 E -2	1.504 E -2
8	1.7762	6.004 E -3	7.148 E -3
9	1.9929	2.413 E -3	2.869 E -3
10	2.2361	7.827 E -4	9.296 E -4
11	2.5089	1.940 E -4	2.308 E -4
12	2.8150	3.432 E -5	4.101 E -5
13	3.1585	3.973 E -6	4.781 E -6
14	3.5439	2.699 E -7	3.284 E -7
15	3.9766	9.386 E -9	1.160 E -8
16	4.4615	1.405 E -10	1.775 E -10
17	5.0059	7.285 E -13	9.472 E -13
18	5.6167	9.943 E -16	1.343 E -15
19	6.3021	2.530 E -19	3.589 E -19
20	7.0711	7.770 E -24	1.172 E -23

design process. The random noise decision variable at the output of the frequency discriminator with high CNR can therefore be reasonably represented as a gaussian random variable with mean value equal to the output voltage resulting from the transmitted FSK tones. This approximation will be the basis for the simplified model of the frequency discriminator detector when both noise and interference are present at the input.

The parameter "a" in equation (19) can be thought of as the ratio of the frequency deviation , Δf, to the "rms frequency" of the noise, σ_1 , as given by equation (12). As the numbers in Tables 1 and 2 show, as "a" increases, the gaussian approximation becomes more accurate. However, for $a > 1$, $\Delta f > \frac{\sigma_1}{\sigma_0}$, and the transmitted Δf would be greater than the rms frequency of the noise. The rms frequency of the noise is determined by the bandpass characteristics of the input filter. For $\Delta f > \frac{\sigma_1}{\sigma_0}$, the tone spacing would be greater than the bandwidth of the filter. While this is permissible, it will result in amplitude modulation of the envelope of R, or $\dot{R} \neq 0$. The parameter "b" would therefore not be zero and the argument of the erfc function inside the integral changes. Systems are often designed such that the relationship of the filter bandwidth (and skirt slopes) and tone spacing Δf results in a value for "a" of one or greater. For the special circumstance when a = 1, the error rate is given by Montgomery's classic formula

$$P_e = \frac{1}{2} \exp\left[-\rho/2\right]$$

Derivation of this result can be found in reference [12]. A further discussion of the relationship between the input filter characteristics and the gaussian noise which will be "patched in" to the simpli-

fied linear discriminator model can be found later in this Section.

Discriminator Output with Sinewave Interference

With no noise and with a single sinewave interference present when a binary one, frequency ω_a, is transmitted, equation (6) reduces to

$$\dot{\phi} = \frac{(SP+IP)(\dot{SQ}+\dot{IQ})-(\dot{SP}+\dot{IP})(SQ+IQ)}{(SP+IP)^2+(SQ+IQ)^2} \qquad (20)$$

where

$$SP = S\cos\omega_a t \qquad \dot{SP} = -\omega_a S\sin\omega_a t$$

$$SQ = S\sin\omega_a t \qquad \dot{SQ} = \omega_a S\cos\omega_a t \qquad \text{Eqns (21)}$$

$$IP = I_n\cos(\omega_n t+\theta_n) \qquad \dot{IP} = -\omega_n I_n\sin(\omega_n t+\theta_n)$$

$$IQ = I_n\sin(\omega_n t+\theta_n) \qquad \dot{IQ} = \omega_n I_n\cos(\omega_n t+\theta_n)$$

and In = interference amplitude, ω_n = interference frequency , and θ_n = phase angle of the interference, a random variable uniformly distributed over 0 to 2π.

By plugging the variable definitions in equations (21) into the expression in (20), performing the appropriate multiplications, and noting that

$$\cos^2(\omega_a t) + \sin^2(\omega_a t) = 1$$

$$\cos^2(\omega_n t+\theta_n)+\sin^2(\omega_n t+\theta_n) = 1 \qquad \text{Eqns (22)}$$

$$\cos\omega_a t\cos(\omega_n t+\theta_n)+\sin\omega_a t\sin(\omega_n t+\theta_n)=\cos(\omega_a t-\omega_n t-\theta_n)$$

the resulting expression is

$$\dot{\phi} = \frac{S^2\omega_a + I_n^2\omega_n + SI_n(\omega_a+\omega_n)\cos((\omega_a-\omega_n)t-\theta_n)}{S^2+I_n^2+2SI_n\cos((\omega_a-\omega_n)t-\theta_n)} \qquad (23)$$

This expression for the output voltage of the discriminator includes a voltage due to the signal frequency tone, ω_a, and an error term due to the presence of the interference. The error term is the portion of the output signal of interest here since it, along with the noise to be added later, will lead to errors in data detection. The error voltage term is given by

Error voltage = Ve = $\dot{\phi} - \omega_a$

$$Ve = \frac{S^2\omega_a - I_n^2\omega_n + SI_n(\omega_a+\omega_n)\cos((\omega_a-\omega_n)t-\theta_n)}{S^2 + I_n^2 + 2SI_n\cos((\omega_a-\omega_n)t-\theta_n)} - \omega_a \quad (24)$$

By cross multiplying the denominator of the first term of (24) with ω_a, combining the numerators, and noting that $\cos(\alpha) = \cos(-\alpha)$, the following expression is obtained

$$Ve = \frac{I_n^2(\omega_n-\omega_a) + SI_n(\omega_n-\omega_a)\cos((\omega_n-\omega_a)t+\theta_n)}{S^2+I_n^2+2SI_n\cos((\omega_n-\omega_a)t+\theta_n)} \quad (25)$$

Before evaluating the pdf of this error term over the possible values of θ_n, it is useful to study its time and frequency domain properties. The expression in (25) was used in a computer program to plot the error voltage for various signal carrier-to-interference ratios (CIR), interfering frequencies, and using an FSK tone spacing of $\Delta f T = 1$. The results of this analysis are shown in Figures 9 through 12.

These figures show a demodulated data waveform consisting of two binary ones (positive voltage) followed by two binary zeros (negative voltage), with a binary one corresponding to frequency f_a = 4.5280 MHz and binary zero corresponding to frequency f_b = 4.4720 MHz. These frequencies were chosen to correspond to those which will be used

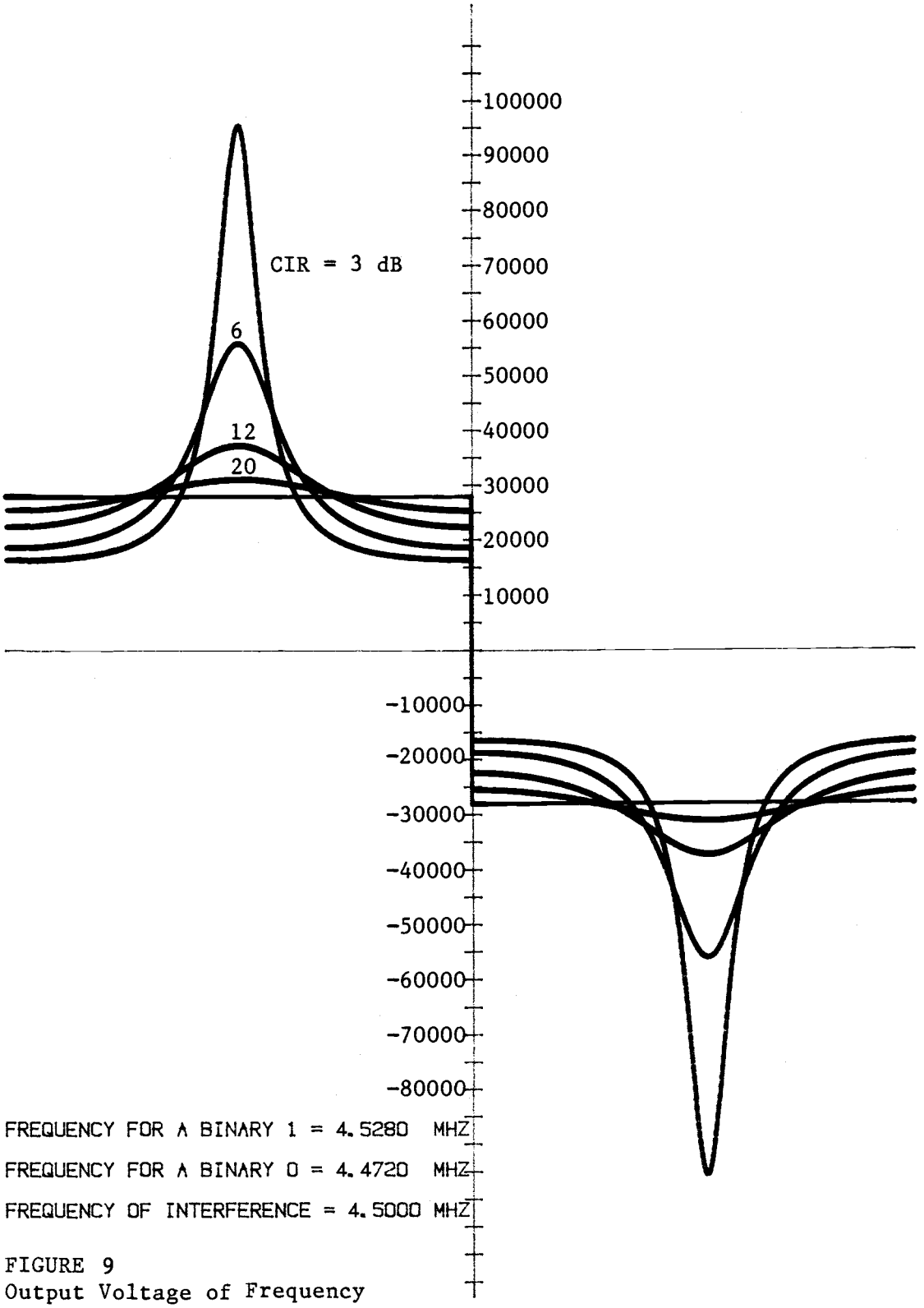

FIGURE 9
Output Voltage of Frequency
Discriminator with Sinewave Interference

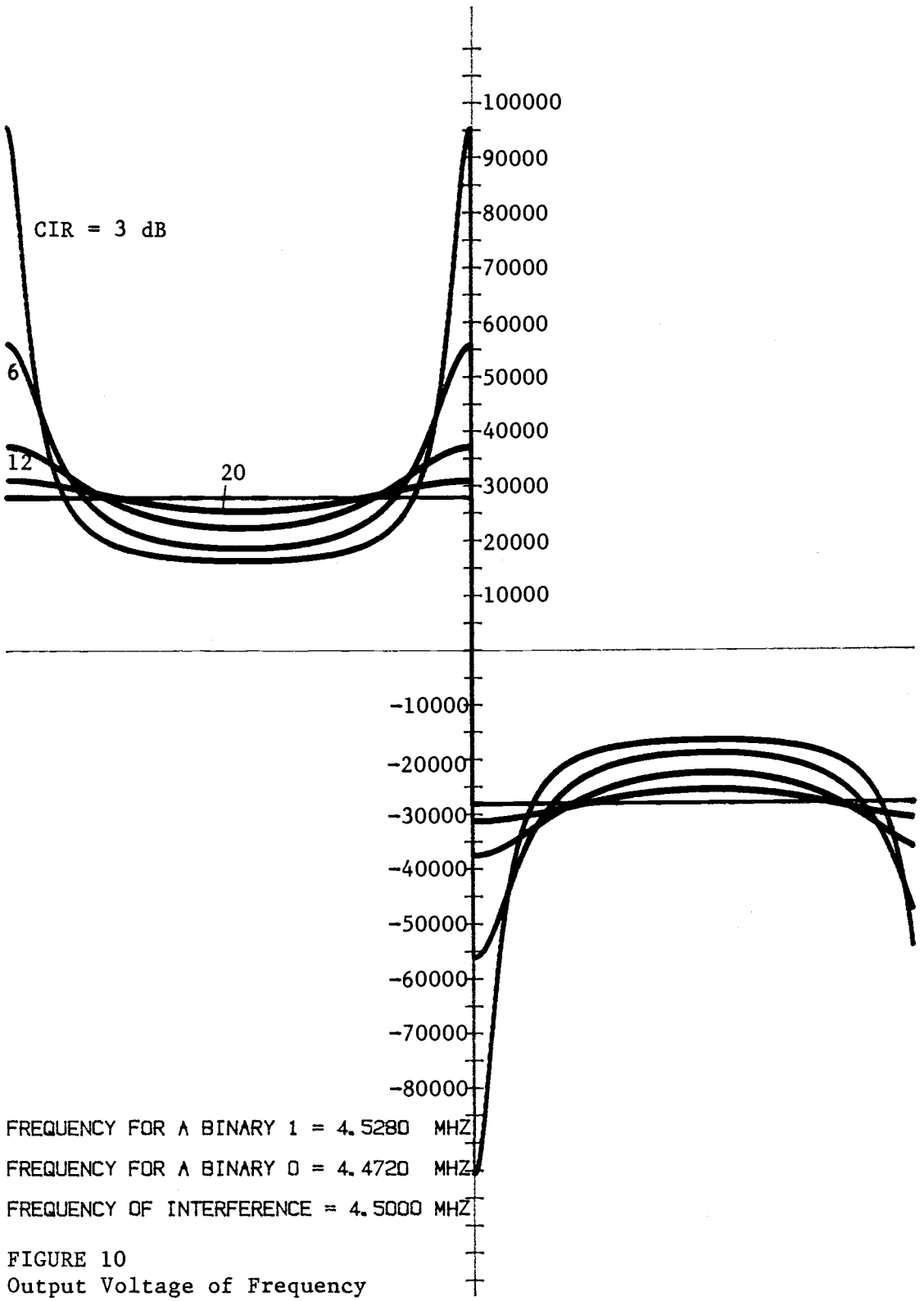

FIGURE 10
Output Voltage of Frequency Discriminator with Sinewave Interference
Θ_n = 180 degrees

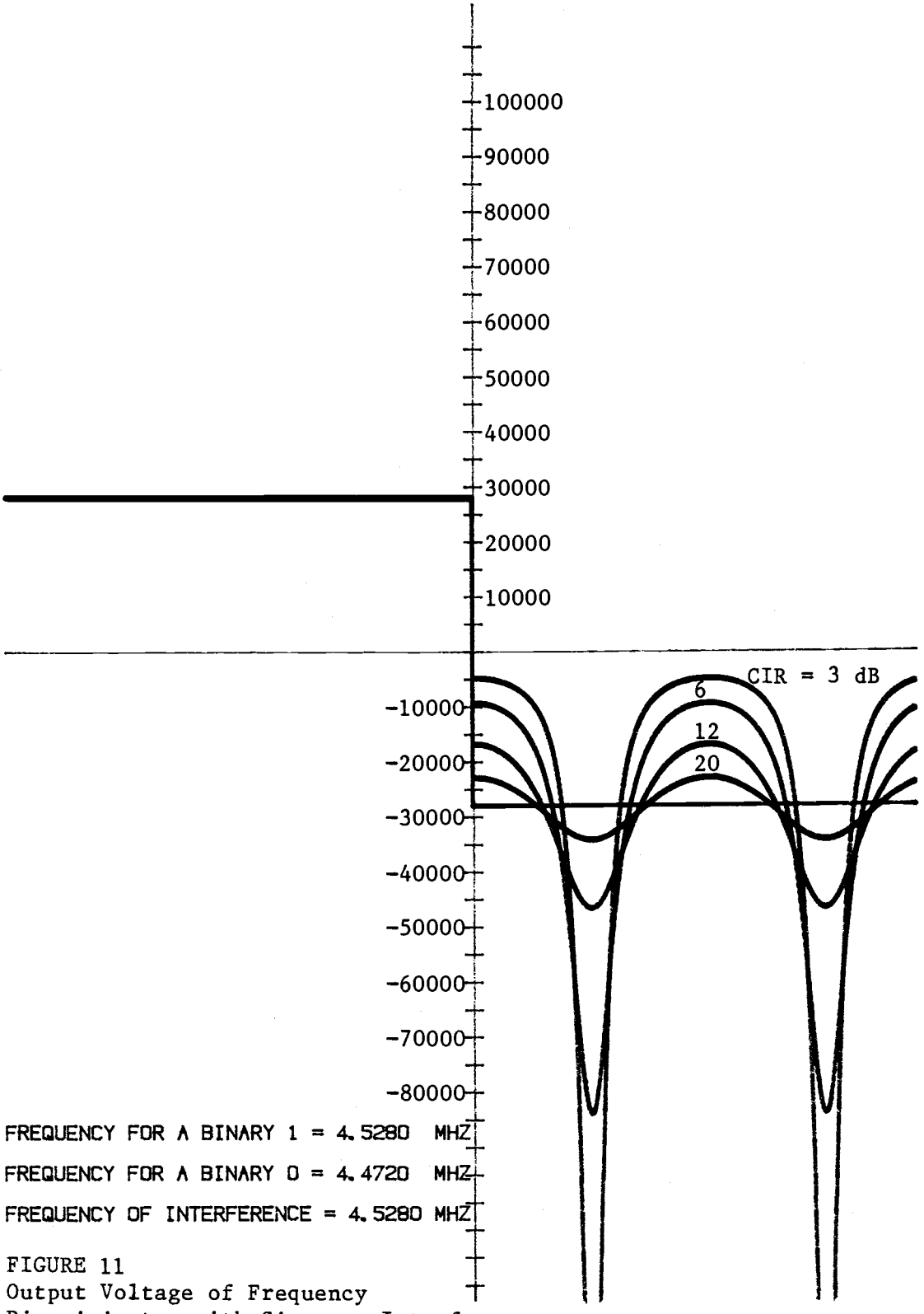

FIGURE 11
Output Voltage of Frequency Discriminator with Sinewave Interference

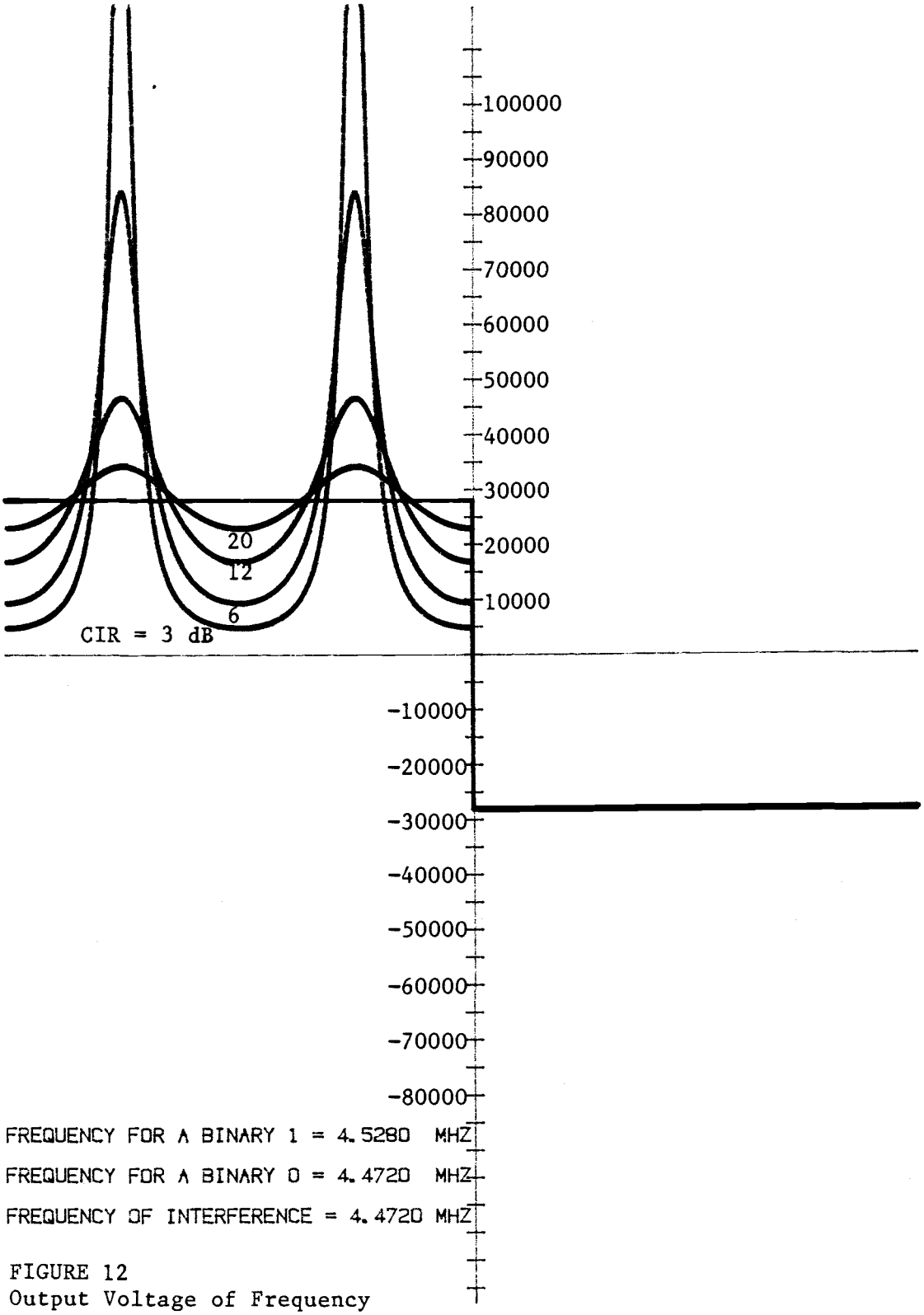

FIGURE 12
Output Voltage of Frequency
Discriminator with Sinewave Interference

later in experimental tests. The two bit sequence length for a one and zero was chosen so that a complete period of the error voltage could be illustrated during the transmission time of both f_a and f_b. Since Θ_n is random, any value in the illustrated error voltage range may occur at the decision instant.

The vertical scale in these figures is plotted in volts assuming a frequency discriminator conversion gain of 1 volt per Hertz. Clearly, the conversion gain of an actual detection circuit would be much less than this - the frequency detector used in the experiments described later has a conversion gain of about 1 volt output for a frequency deviation of 150 kHz. However, the 1 volt per Hertz gain will be used throughout this theoretical section so that the plot scales showing output voltage and pdf's can be directly related to the frequencies of the FSK tone and the interference.

The interfering frequency in Figure 9 was chosen at f_n= 4.5 MHz, or halfway between the one and zero frequencies. The frequency of the error voltage is $f_a - f_n$ or 28 kHz. The error voltage shows increasing harmonic distortion as CIR is reduced.

Figure 10 is the same as 9 except that Θ_n = 180 degrees. The result is the expected time shift in the error voltage.

Figures 11 and 12 show the same recovered data signal except that $f_n = f_a$ and $f_n = f_b$, respectively. As expected, the error voltage frequency is doubled to 56 kHz and its peak amplitude is also doubled as the numerator of (25) suggests. The peaks in the error voltage have been truncated in these plots to permit a more useful display scale for the rest of the data.

Because the error voltage contains harmonic distortion, it is useful to do a Fourier analysis to determine where the energy in the error signal occurs. A 512 point FFT computer algorithm was used on the first half of the error signal (that occuring during f_a) as shown in Figure 9 . The results of the Fourier analysis are shown in Figure 13 for the four error voltages corresponding to the four values of CIR used in Figure 9. The error term has increasing harmonic distortion as the CIR level is reduced. The error voltage can be represented by a Fourier series as follows

$$V_e = (\omega_n - \omega_a) \sum_{m=1}^{\infty} (-1)^{m+1} (I_n/S)^m \cos(m(\omega_n - \omega_a)t + m\theta_n) \quad (26)$$

The virtue of the lowpass filter (LPF) on the output of the discriminator is now evident. This LPF will ideally be designed to just pass the data pulse with no intersymbol interference (ISI). Such a filter will have a cutoff frequency of about one half the data rate with perhaps 12 dB per octave rolloff at higher frequencies. A filter with characteristics similar to this will be employed in the experimental work to be described in Section 3. The important point here is that only the first spectral component of the error voltage will pass through the filter with little or no attenuation, while the second component will experience about 12 dB of attenuation, and the higher order components will be reduced to the point where their contribution to the output error voltage is negligible. This sort of attenuation applies to the situation of Figure 9 where the interference frequency is halfway between the FSK tone frequencies so that the fundamental frequency is $f_a - f_n$, or half the data rate if the tone spacing is $\Delta f T = 1$.

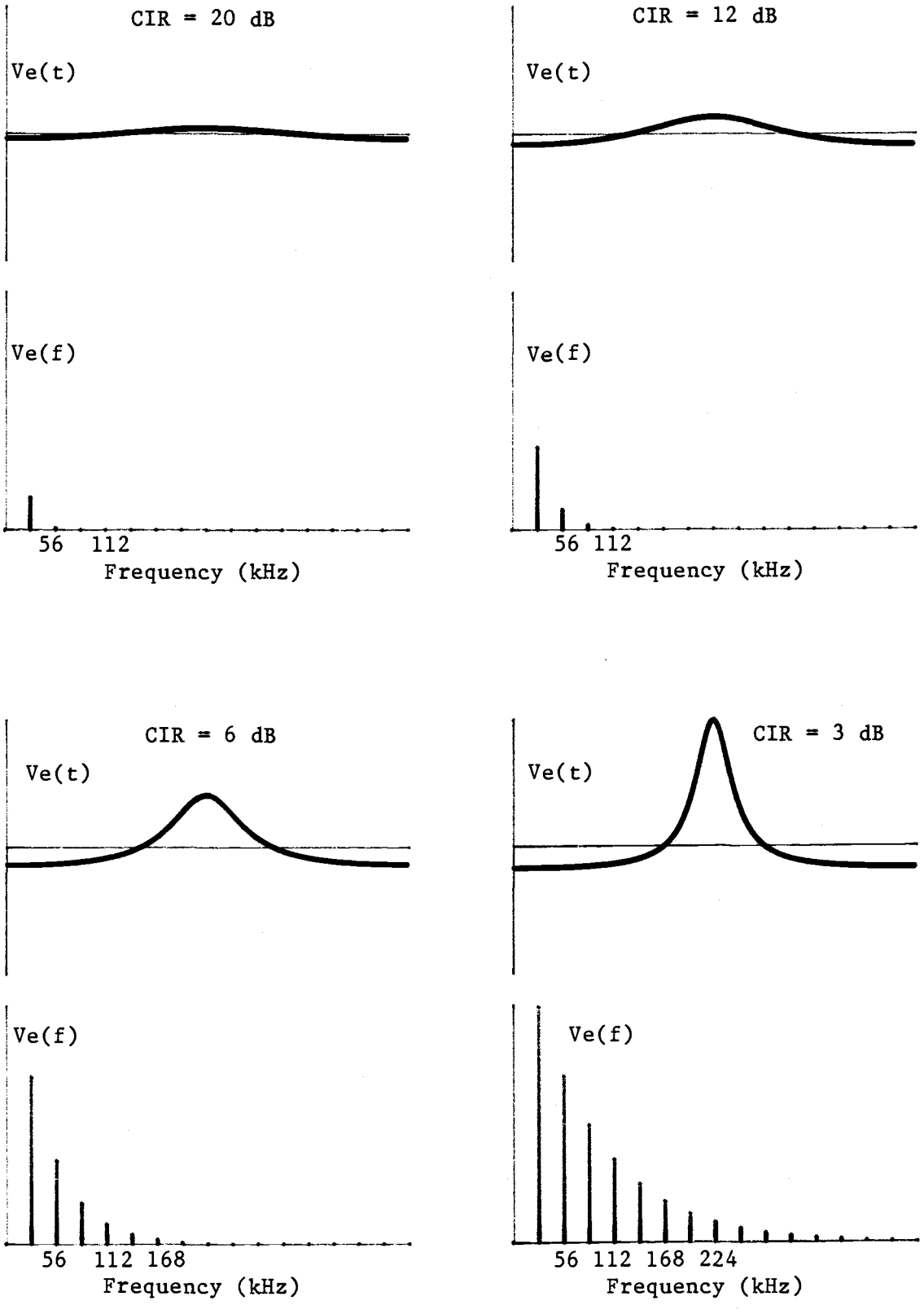

FIGURE 13- Spectral Analysis of Error Voltage

If only the first two components of the error voltage are significant, equation (26) can be reduced to

$$Ve \cong (\omega_n - \omega_a)\left[(I_n/S)H(\omega_n - \omega_a)\cos((\omega_n - \omega_a)t + \theta_n) - (I_n/S)^2 H(2(\omega_n - \omega_a))\cos(2(\omega_n - \omega_a)t + 2\theta_n)\right] \quad (27)$$

In this equation $H(\omega)$ is the response of the lowpass filter.

For an interfering frequency not midway between f_a and f_b, the difference frequency between f_n and one tone (say f_a) decreases, resulting in more harmonic energy inside the LPF passband, while the difference frequency between f_n and other (f_b) will be increased, resulting in less energy inside the LPF passband. This effect is offset by the fact that the overall amplitude of the error term varies directly with the difference frequency. Also, for f_n not halfway between f_a and f_b, the error voltage will be unsymmetrical and the probability of error for a transmitted one and a transmitted zero will be different. The question then arises, is there a worst case interference frequency in terms of the amount of error energy appearing at the output of the LPF? This question is addressed by calculating the total error energy for the two situations:

$f_n = f_a - 0.5\cdot(f_a - f_b)$ and $f_n = f_a - 0.25\cdot(f_a - f_b)$

Using equation (27), $f_a = 4.528$ MHz, $f_b = 4.472$ MHz, $\theta_n = 0$, CIR = 3 dB, a discriminator conversion gain of 1 volt per Hertz, and an LPF response of $H(\omega) = 1$ for $\omega < \frac{1}{2}|(\omega_a - \omega_b)|$

$H(\omega) = -12$ dB per octave for $\omega > \frac{1}{2}|(\omega_a - \omega_b)|$

When $f_n = f_a - 0.5\cdot(f_a - f_b)$

Error energy $= \left[(28000 \cdot .707 \cdot 1)^2 + (-28000 \cdot .5 \cdot .25)^2\right] \times 2 \cong 4.04 \times 10^8$

When $f_n = f_a - 0.25\,(f_a - f_b)$

Error energy $= (14000 \cdot .707 \cdot 1)^2 + (-14000 \cdot .5 \cdot 1)^2$
$+ (42000 \cdot .707 \cdot .5)^2 + (-42000 \cdot .5 \cdot .125)^2 \cong 2.268 \times 10^8$

The total error energy for $f_n = f_a - 0.5 \cdot (f_a - f_b)$ is greater than for the case when $f_n = f_a - 0.25 \cdot (f_a - f_b)$. This result can be intuitively generalized to other interfering frequencies inside the receiver RF passband, thus leading to the conclusion that greatest error energy for the stated LPF response occurs when $f_n = f_a - 0.5 \cdot (f_a - f_b)$. Since the LPF is designed for zero ISI (and indeed this is closely realizable), the time delay through it is constant and phase shift is essentially linear. This means that the relative time positions of the harmonics of the error voltage will be preserved so that the peak excursions will remain unchanged for a particular level of interference. Since these excursions of the error voltage, when added to the noise, will determine when data sampling errors occur, it is maintained that the single sinewave interference situation with the greatest error energy at the output of the LPF will also be the interference situation which will cause the highest data error rate. Therefore, the situation with $f_n = f_a - 0.5 \cdot (f_a - f_b)$ is the worst case from an error probability standpoint. The pdf of the error voltage for this interference frequency will now be studied.

As already shown, only the first two terms of the error series in equation (26) contribute significantly to the output. These two terms are given in Equation (27). If it is assumed that the LPF response is such that $H(\omega_a - \omega_n) = 1$ and $H(2 \cdot (\omega_a - \omega_n)) = 0.25$, then

$$V_e \cong (\omega_n - \omega_a)\left[(I_n/s)\cos((\omega_n - \omega_a)t + \theta_n) - (I_n/s)^2 (.25)\cos(2(\omega_n - \omega_a)t + 2\theta_n)\right] \quad (28)$$

This voltage has been plotted over one period of the fundamental frequency (ω_a-ω_n), and for the four values of CIR used previously. This information is plotted in Figure 14. The pdf's for each error voltage curve are plotted in Figure 15. These pdf's were determined numerically by evaluating the slope of the voltage function. As expected, for low interference amplitudes, the pdf is essentially that of a sinewave. As the interference level increases, the output becomes more distorted and the pdf shifts so that it is no longer symmetrical around the voltage corresponding to the transmitted data pulse.

The pdf's given in Figure 15 are actually pdf's of Ve given CIR and ω_n, or $p(V_e \backslash I_n, \omega_n)$. If a distribution for the interference amplitude, $p(I_n)$, and a distribution for the probability of a given interfering frequency occuring, $p(\omega_n)$, were known, the unconditional pdf, $p(V_e)$, could be found.

$$p(V_e) = \int_{-\infty}^{\infty}\int_{-\infty}^{\infty} p(V_e|I_n,\omega_n)\, p(I_n)p(\omega_n)\, dI_n d\omega_n \qquad (29)$$

Some reasonable assumptions could be made, however. In a given narrow band on a cable system, the interference due to ingress may likely be uniformly distributed in the passband of the data receiver, the pdf for ω_n would then be

$$p(\omega_n) = P_{\omega_n} \cdot BW$$

where P_{ω_n} is the probability of a given interferer appearing at a given frequency at a given time.

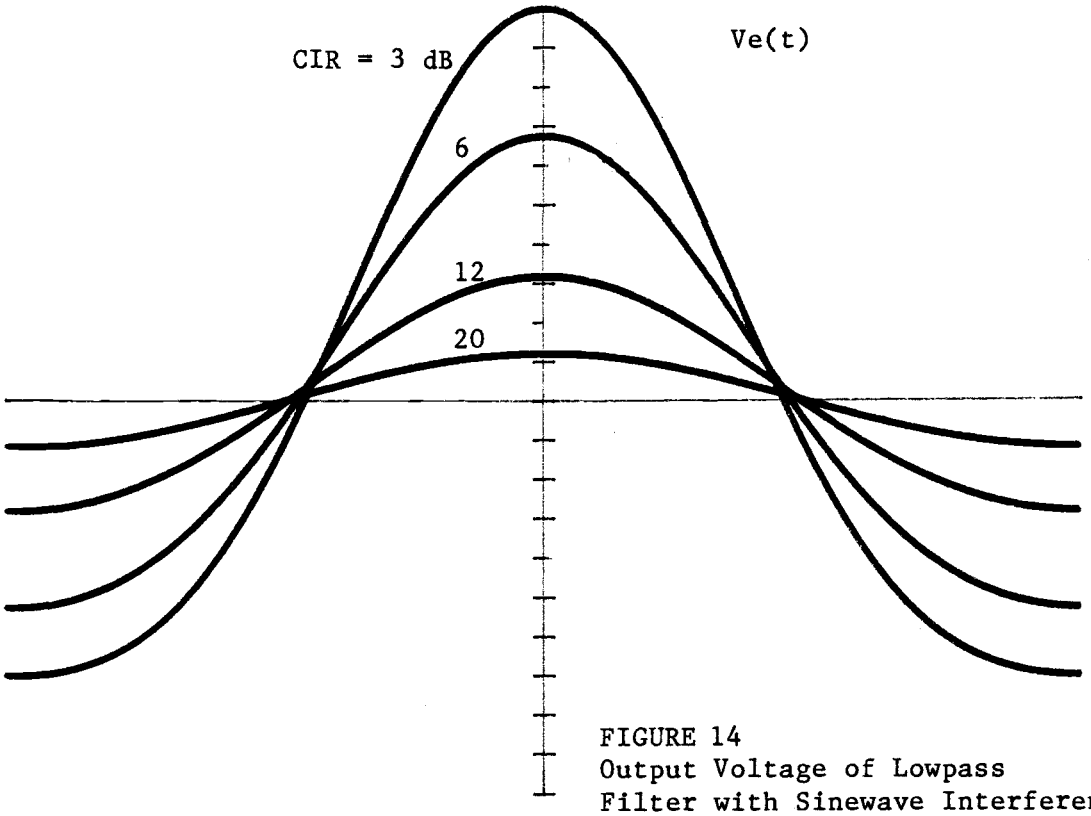

FIGURE 14
Output Voltage of Lowpass
Filter with Sinewave Interference

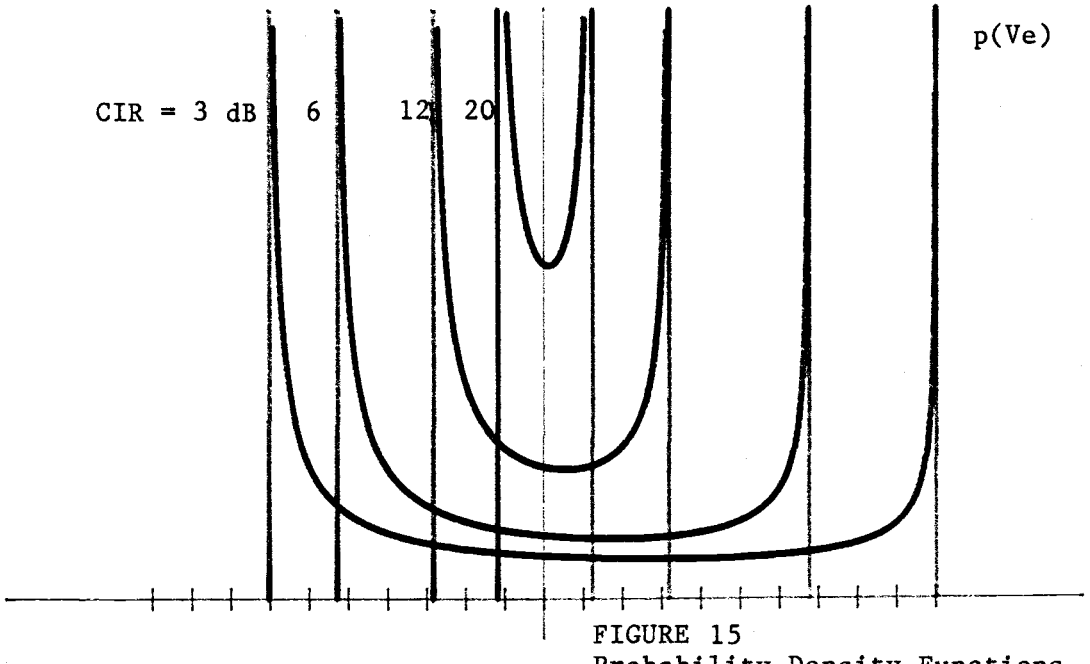

FIGURE 15
Probability Density Functions
for Ve(t) in Figure 14

Amplitudes of unknown signals are often described by a Rayleigh-distributed random variable

$$p(I_n) = \frac{2I_n}{A} \exp\left[\frac{-I_n^2}{A}\right] \qquad I_n > 0$$

where A is some constant (A > 0) which characterizes the distribution. Equation (29) then becomes

$$p(V_e) = \int_{-BW/2}^{BW/2} \int_{0}^{\infty} p(V_e | I_n, \omega_n) \left(\frac{2I_n}{A} \exp\left[\frac{-I_n^2}{A}\right]\right) p_{\omega_n} \, dI_n \, d\omega_n \qquad (30)$$

Equation (30) could possibly be evaluated if an analytical expression for $p(V_e|I_n,\omega_n)$ were available, rather than just the numerical representations for a few values of CIR and $\omega_n = \omega_a - \frac{1}{2}(\omega_a - \omega_b)$. Alternately, $p(V_e|I_n,\omega_n)$ could be evaluated for many values of I_n and the integral in equation (30) evaluated numerically.

It is clear from Figure 9 that if only interference (no noise) were present, no errors would ever occur since the error voltage never crosses over the decision threshold. It is only when the gaussian noise is added to the interference that errors will occur. This combination is addressed in the next subsection.

Performance of FSK Transmission with Sinewave Interference and High Carrier-to-Noise Ratios - A Simplified Linear Model

The proposed model for the error voltage from the frequency discriminator with noise and interference corrupting the FSK signal consists of a linear combination of a gaussian noise error voltage with the error voltage resulting from the non-linear transfer of the interference, as presented in the previous section.

It was seen before that the error voltage with noise only was essentially gaussian at high CNR. Based on error rate formula in equation (19), the detected CNR ratio is the same as the input CNR; that is, the FSK carrier-to-noise ratio at the input to the detector and the data pulse amplitude-to-noise ratio at the output of the detector are the same. The model adds some noise error voltage to the data pulse. The data pulse amplitude is a function of the FSK frequency tone spacing; the noise power (variance) is a function of the input CNR.

The interference is handled as if it were passed through the detector, lowpass filtered, and added to the noise. A block diagram of the resulting model is shown in Figure 16.

The gaussian noise and interference error voltage are independent random variables. The pdf of their sum, z , is given by the convolution of the individual pdf's,

$$p(z) = p(\text{noise}) * p(\text{interference})$$
$$p(z) = p(x) * p(Y_e) \qquad (31)$$

The pdf's for the interference error voltages shown in Figure 15 are represented by 256 point sequences, p(m), extending from the lower amplitude limit to the upper amplitude limit. The gaussian pdf is a well known function. Since the interference error pdf is given by a sequence rather than an analytic expression, the convolution was performed numerically using the general equation,

$$p(n) = \sum_{m=1}^{256} p_{noise}(n-m)\, p_{int.}(m) \qquad (32)$$

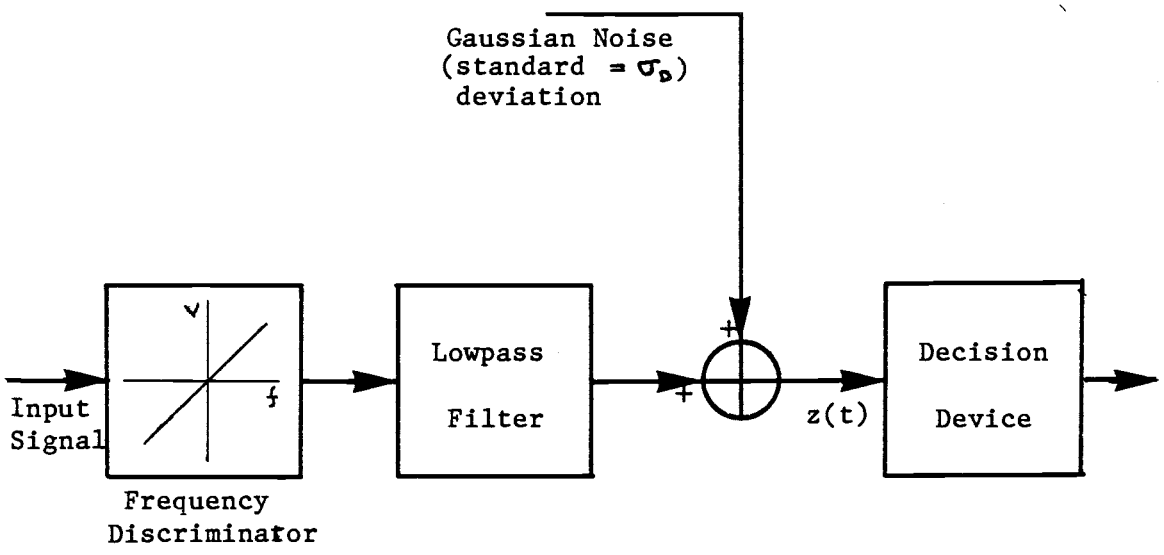

$$\sigma_D = \frac{\text{Detected Data Pulse Amplitude}}{\text{Input CNR}}$$

Input Signal = FSK signal + interference (no noise)

FIGURE 16
Simplified Linear Model of Frequency Discriminator Operation on FSK Signals with Interference and Additive Gaussian Noise

A computer program was written to perform the convolution for n = 1 to 256. The resulting pdf's for the output voltage of the detector model of Figure 16 are shown in Figure 17 through 21 for the values of CIR used before, and for CNR values of 25, 20, 15, 10, and 5 dB. The plots are two-sided in that they show the total error voltage distribution around the voltage corresponding to a binary one (+ 28000) and around the voltage corresponding to binary zero (-28000). This was done to better illustrate that the pdf's are not symmetrical around the data pulse voltages, and that the pdf's are weighted toward the decision threshold at zero volts.

During the convolution process, the area under the resulting pdf curves were summed and the error rate calculated as the ratio of the area under the pdf curve for $p(z < 0 \mid \text{one sent})$ to the total area under the pdf curve around the binary one detected voltage (+28000) which is equal to 0.5 if the probabilities of a one or zero being transmitted are equal. The error probabilities for the plotted combinations of CIR and CNR are given in Table 3. Figure 22 is a plot showing the same information. As expected the error rate increases with decreasing CIR and decreasing CNR. For high CNR and CIR the calculated probability of error shown in the table is zero. These values result because the area of the error region under the pdf curve was smaller than the smallest number representable on the computer which is approximately 1 E -38.

The question posed earlier as to the value of increased FSK frequency spacing in the presence of noise and interference can now be addressed. Clearly, for $\Delta ST = 2$ instead of 1, the voltages corresponding to a binary one and binary zero of the pdf's in Figure 11 would

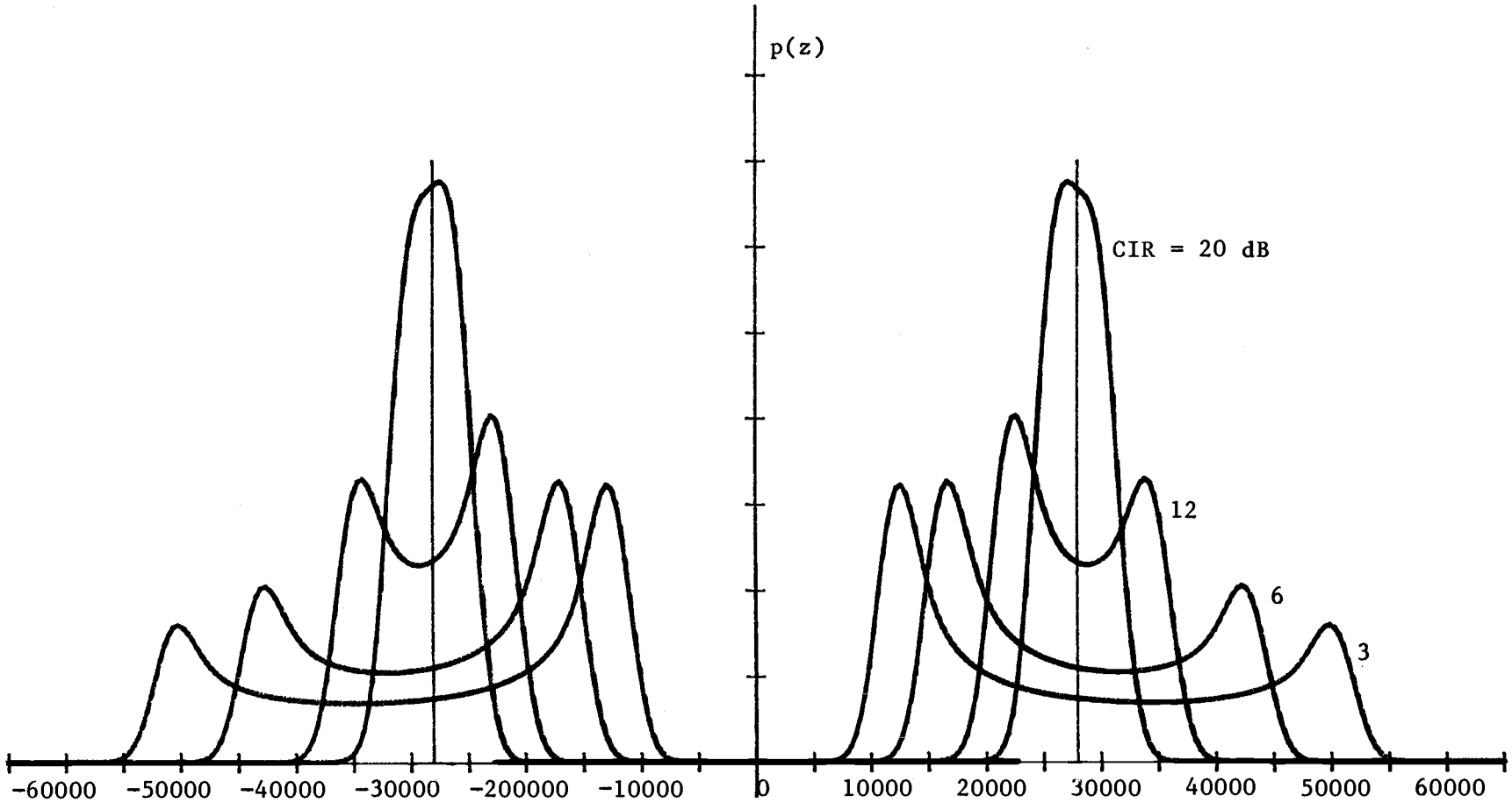

FIGURE 17 - Probability Density Function of Detector Output Voltage With Noise and Interference
CNR = 25 dB Vertical Scale = 1.0 E -5 per division

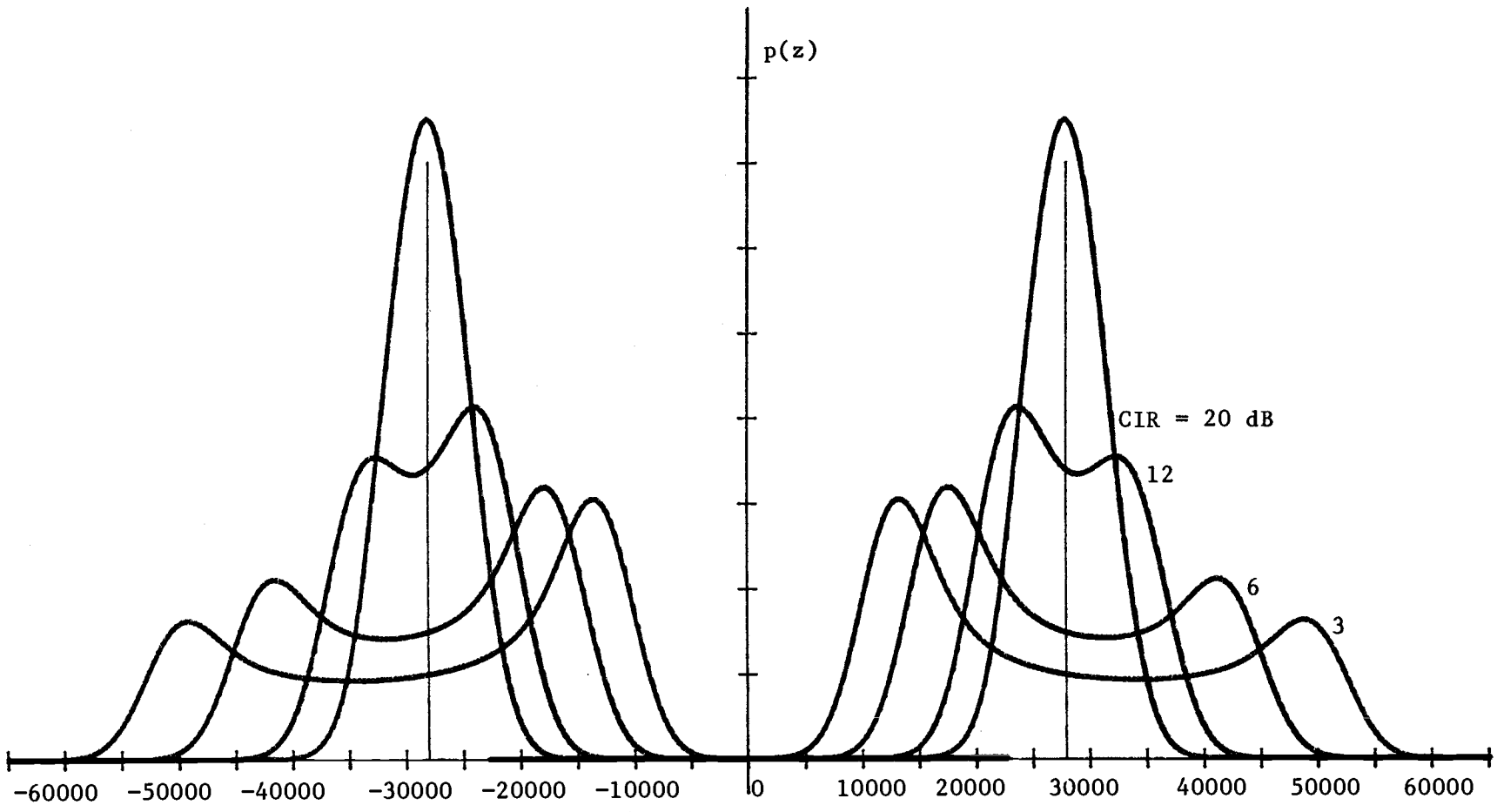

FIGURE 18 - Probability Density Function of Detector Output Voltage With Noise and Interference
CNR = 20 dB Vertical Scale = 0.75 E -5 per division

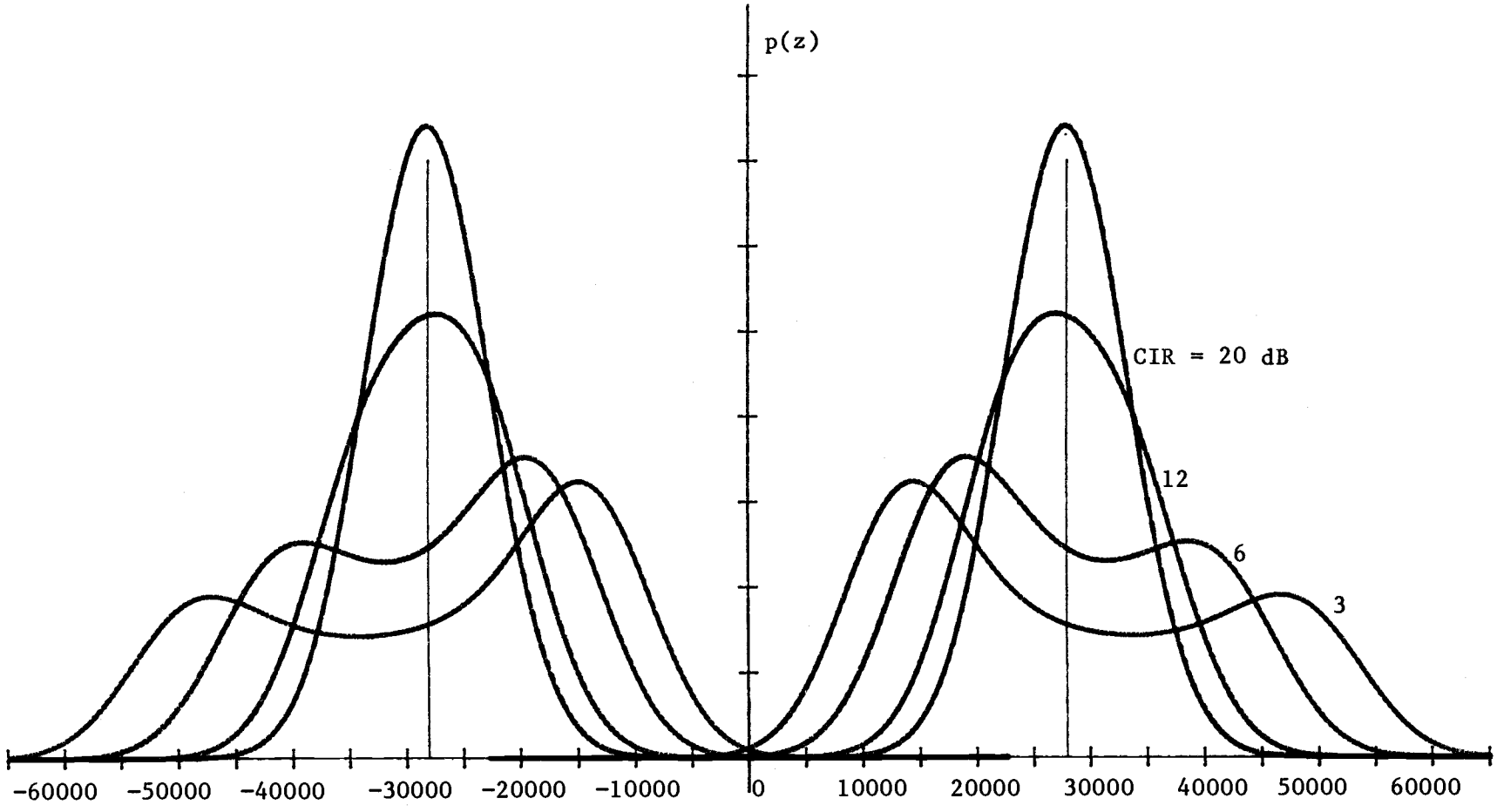

FIGURE 19 - Probability Density Function of Detector Output Voltage With Noise and Interference
CNR = 15 dB Vertical Scale = 0.5 E -5 per division

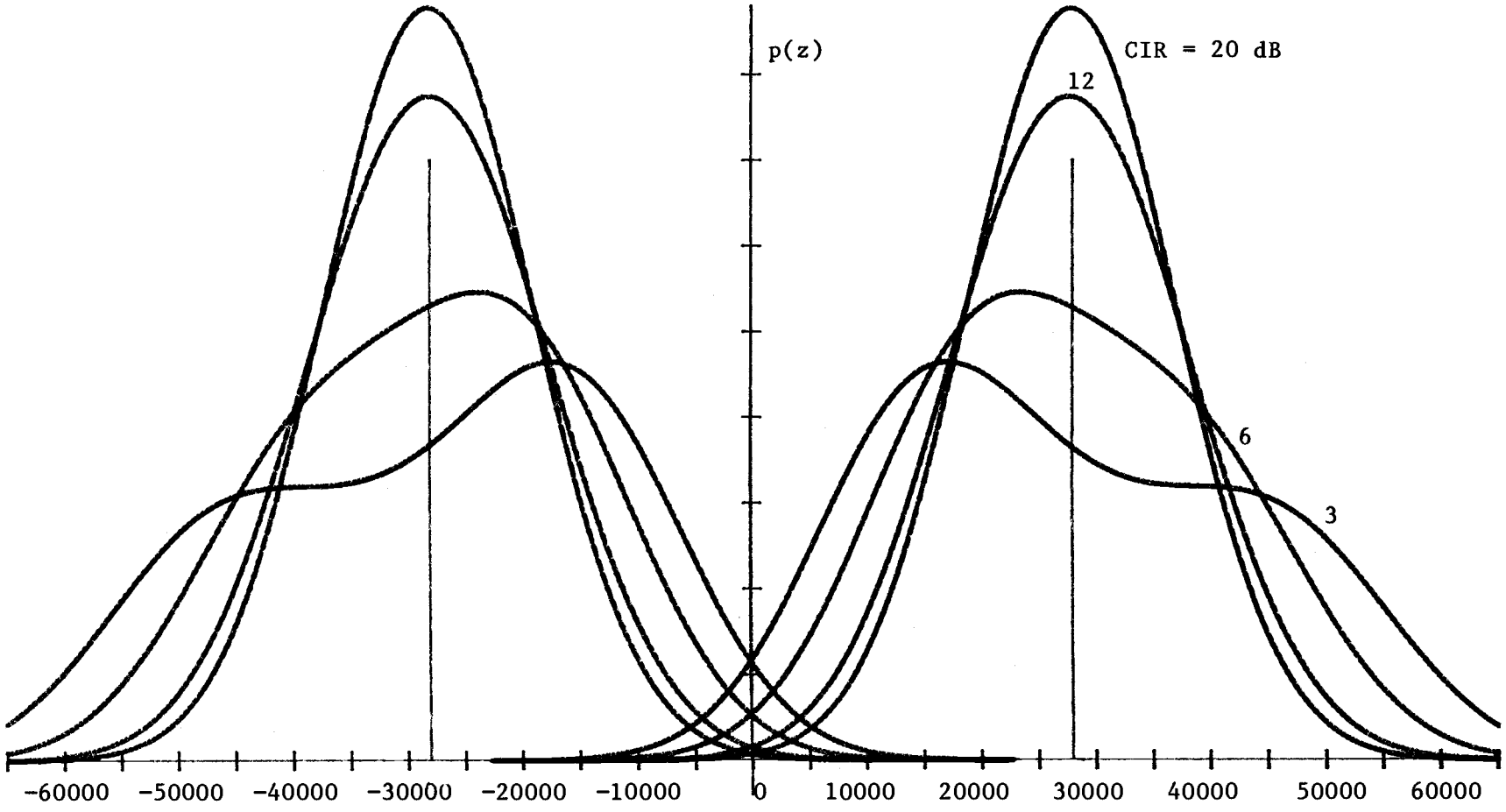

FIGURE 20 - Probability Density Function of Detector Output Voltage With Noise and Interference
CNR = 10 dB Vertical Scale = 0.25 E -5 per division

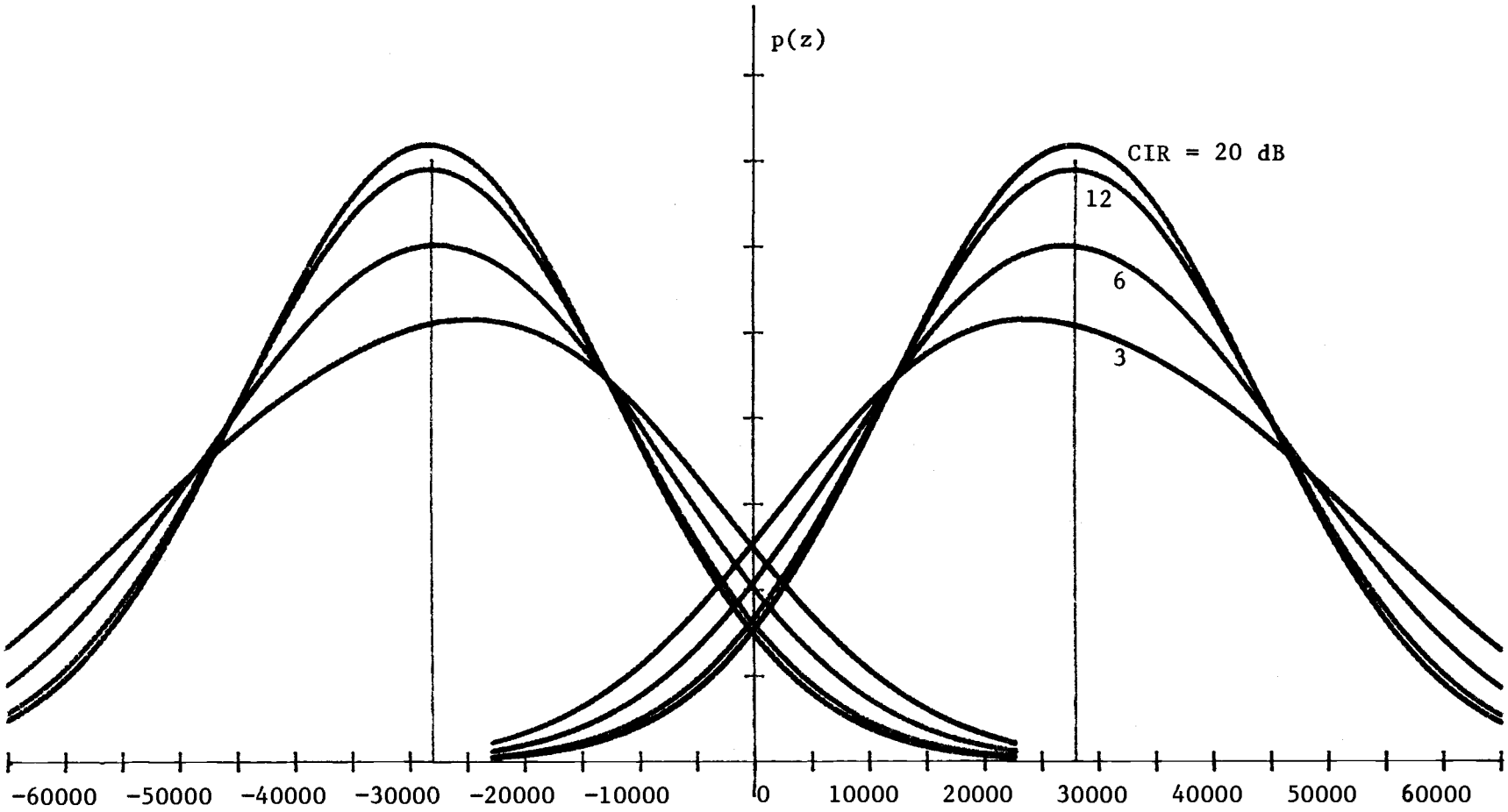

FIGURE 21 - Probability Density Function of Detector Output Voltage With Noise and Interference
CNR = 5 dB Vertical Scale = 0.175 E -5 per division

TABLE 3

Probability of Error Results For Simplified Linear Model of Frequency Discriminator Detector With Noise and Interference

CNR(dB)	CIR(dB)	Calculated Probability of Error
25	20	0
	12	0
	6	1.149 E -24
	3	8.411 E -15
20	20	2.235 E -20
	12	1.163 E -15
	6	1.380 E -09
	3	2.387 E -06
15	20	5.957 E -08
	12	1.787 E -06
	6	1.520 E -04
	3	2.008 E -03
10	20	1.077 E -03
	12	2.530 E -03
	6	1.072 E -02
	3	2.750 E -02
5	20	3.920 E -02
	12	4.510 E -02
	6	6.490 E -02
	3	8.950 E -02

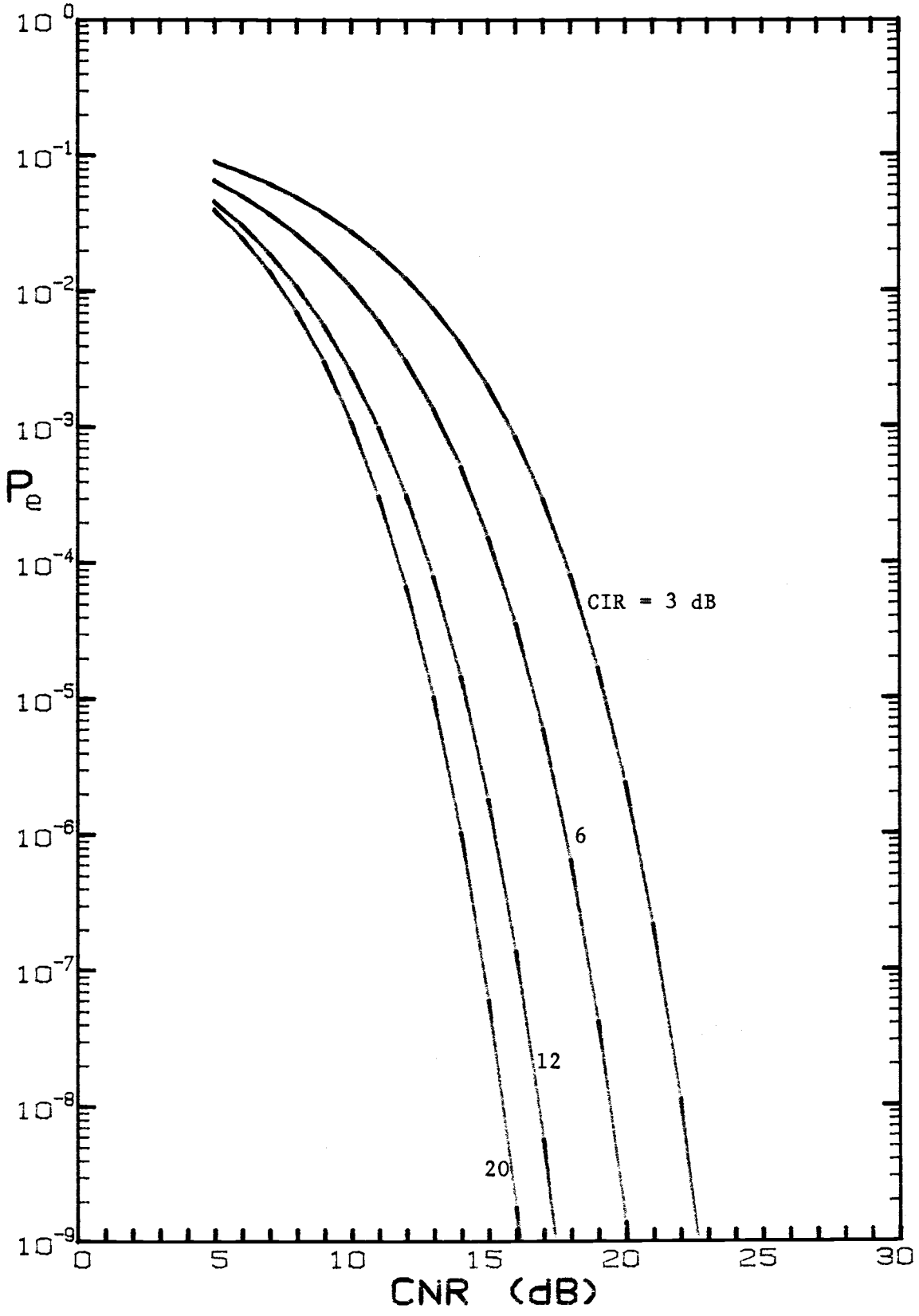

FIGURE 22 - Probability of Error With Noise and Interference

move twice as far away from the 0 volt decision threshold. The pdf's of the interference would change since an interferer centered at $f_n = f_a - 0.5\cdot(f_a - f_b)$ would be twice as far away from either transmitted frequency, resulting in an error voltage with higher amplitude and half the period (See Figure 11). The noise power would essentially double since a broader input filter would be required to accommodate the wider tone spacing. For the same carrier amplitude the CNR would the reduced. This would be offset by the increase in the detected pulse amplitudes.

The increased amplitude and frequency of the interference is largely mitigated by the lowpass filter. A calculation of interference error energy, as previously done, for the case when $\Delta f T = 2$ and $f_n = f_a - 0.5\cdot(f_a - f_b)$ would show less error energy than for the $\Delta f T = 1$ case, indicating that improved performance may be obtained by the wider tone spacing.

This conclusion is complicated when multiple interferers at random frequencies are considered (but fewer than would permit a gaussian approximation.) Certainly, if the possible interferers are uniformly distributed in the bandwidth, as suggested before, increasing the tone spacing and hence the bandwidth of the receiver would correspondingly increase the probability of a random interferer showing up in the passband. To properly address this question would require evaluation of equations (29) and (30) for multiple interference sinewaves. Such an analysis is one level more precise than the cable system interference and noise environment model laid out in Section 1 of this thesis. Given some worthwhile data describing the statistics of the potential interferers, the refined analysis suggested in this para-

graph would provide a logical extension of this research.

The model presented here has used additive gaussian noise as the random decision variable added to the interference-caused error voltage at the output of the discriminator. By doing this, it is not maintained that the discriminator necessarily functions so as to produce this effect; but rather that this composite interference error plus gaussian error represents a useful approximation for predicting the resulting error rate. Some distribution other than gaussian, such as lognormal, could have also been chosen, but this would also be an approximation with its own particular limitations. Recent research specific to PLL performance has used the little known Meyr distribution to characterize the random noise decision variable at the output of the PLL [20]. The gaussian distribution was selected because its properties are well known, the convolution with the interference-caused error voltage is straighforward, and as will be shown in Section 3, it does lead to useful predictions of FSK error rate performance when both noise and interference are present.

SECTION 3 - EXPERIMENTAL PERFORMANCE OF FSK DATA TRANSMISSION WITH FREQUENCY DISCRIMINATOR DETECTION

The model of the discriminator performance set forth in Section 2 was tested using a hardware implementation of an FSK data generator, receiver, and appropriate noise and sinewave generators to serve as channel degradation sources. A hardware implementation was chosen instead of a computer simulation because the number of samples necessary to reliably predict error rates of 1.0 E-8 or lower results in excessively long computation times, especially if the basic speed of the computer is slow. Running a hardware experiment at a data rate of 56 kbit/sec or higher is straightforward, allowing low error rates to be counted in a matter of minutes of transmission time. A hardware implementation also is less of an approximation than a simulation; real rather than idealized filters and other components are used leading to results which more accurately predict field performance of actual data communications equipment.

Description of FSK Data Transmission and Detection Circuitry

A block diagram of the experimental setup is shown in Figure 23. The 56 kbit data signal consisted of alternating ones and zeros (a squarewave) derived from a 14.318 MHz crystal oscillator. The data signal feeds a FM signal generator which switches between 4.528 MHz and 4.472 MHz according to the one or zero data pulses.

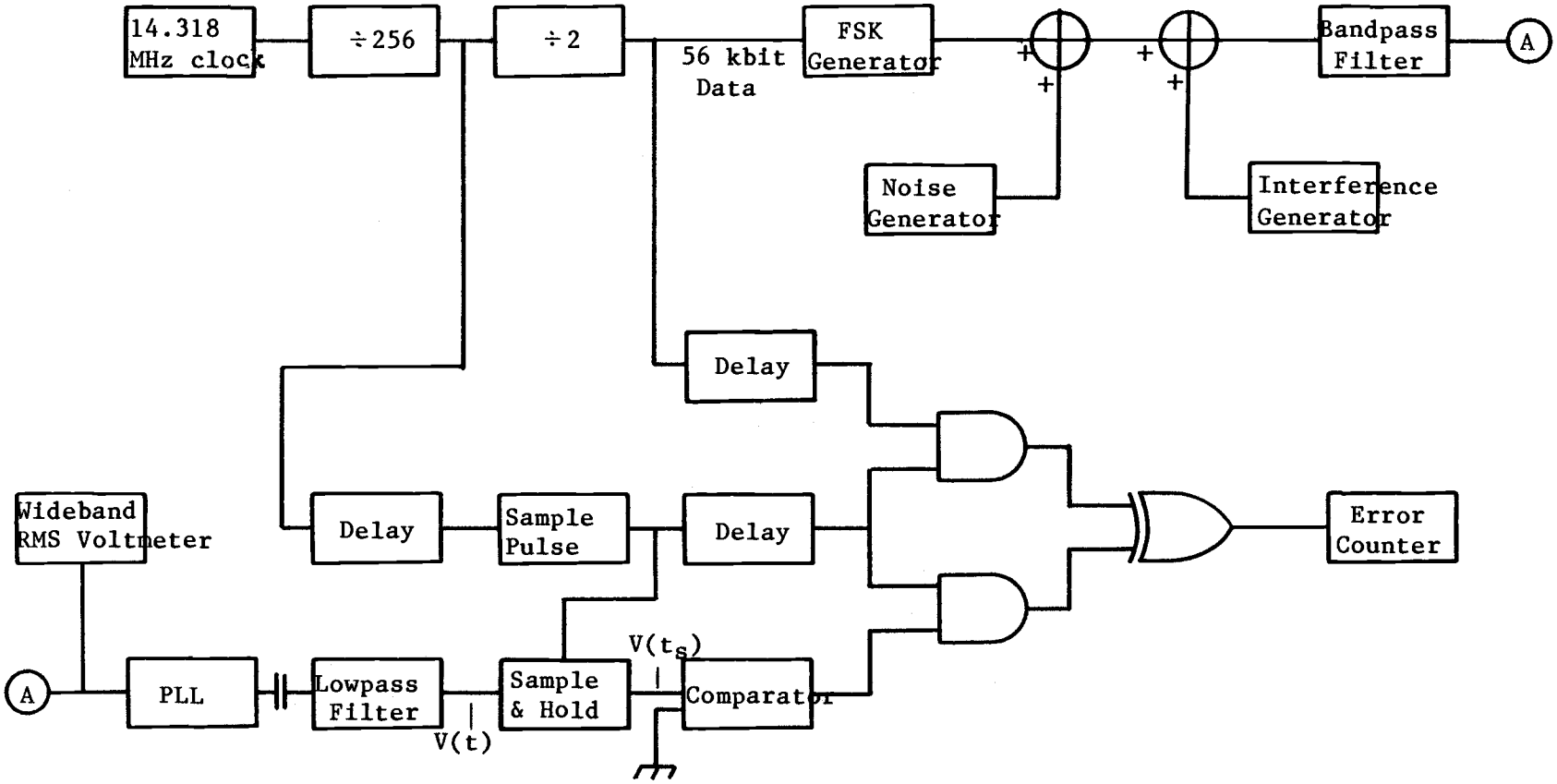

FIGURE 23 - Block Diagram of Equipment Connections for FSK Transmission Experiments

The FSK signal is summed with noise and interference sources and the combination fed to a bandpass filter centered at 4.5 MHz. The output of the bandpass filter is routed to a phase locked loop detector which serves as a limiter/frequency discriminator. The parameters of the loop response were set so that its voltage-to-frequency response curve was essentially linear from 4.0 to 5.0 MHz. The control voltage of the PLL was fed to a lowpass filter. The output of the filter was directed to digital circuitry which made the decision as to whether a one or a zero had been received.

The critical element in the decision circuitry is timing. The output of the LPF is fed to a sample-and-hold (SAH) circuit. For best error performance, the SAH must "hold" the input signal at exactly the point where the output pulse of the lowpass filter reaches its maximum value. This is accomplished by using a 2 X the data rate signal (which has a rising edge in the center of the desired data pulse), delaying this edge by 14.3 uSec to compensate for the propagation delay through the modulator-channel-demodulator-LPF sequence, and using it to trigger a narrow pulse generator which opens and closes the SAH. The 14.3 uSec pulse delay was adjustable to allow precise positioning of the sampling - a luxury of a laboratory experiment which real equipment separated by miles of cable would not have. In an actual data channel, sample timing would be derived from the received signal which suffers noise and interference degradation and results in poorer error rates than an experiment such as this with ideal sample timing.

The output of the SAH is fed to a comparator which compares it against a zero volt reference threshold. If the output of the SAH $V(t_s)$ is positive, the comparator rapidly switches to a positive

voltage equal to a positive power supply voltage; for $V(t_s)$ less than zero, the comparator output voltage switches to the negative supply voltage level.

The output of the comparator is fed to an AND gate which puts out a positive pulse if $V(t_s)$ is positive, zero otherwise. A second delay is used on a gate pulse so that the output of the AND gate reflects the comparator output after transients and ringing from the SAH and comparator have died out. This delayed gate pulse is also fed to another AND gate which has as its second input a delayed version of the original transmitted data. This delay also compensates for the channel propagation delay.

The output of the two AND gates should be identical (either a positive pulse or no pulse) if the received data is the same as the transmitted data. The output of the two AND gates is fed to an exclusive OR (XOR) gate which produces a positive pulse whenever the two inputs are different. By design, these inputs will only be different when the received data pulse does not match the transmitted data pulse; i.e. when a transmission error has occurred. The output of the XOR gate is fed directly to the input of a totalizing counter which counts the number of events (pulses) which occur during a manually (user) set time interval. The interval can be set from seconds to minutes to hours to days depending on how many samples are desired. By counting error events in a set time period equal to a set number of transmitted pulses at 56 kbit per second, the error rate can be directly calculated.

A considerable amount of effort was devoted to developing the

described circuitry. Only the FSK generator, noise generator, interference sinewave generator, and error event counter are commercial units. The rest is custom circuitry developed for this project. The details of the designs are not relevant to the thread of this discussion; however, all the information including detailed schematics and filter response curves are given in Appendix B. To verify proper operation of the test set up, some initial tests of baseband transmission with noise only were run. These tests are described in the next subsection.

Test Results of Baseband Data Transmission With Additive Gaussian Noise - A Benchmark Test

To check the limitations of the test set up in Figure 23, the FSK-PLL portion of the sequence was bypassed. The 56 kbit data was added to gaussian noise and fed directly into the lowpass filter. The signal and noise levels were measured at the output of the lowpass filter and adjusted to various values to allow measurement of the error rate. It should be noted that the propagation delays of Figure 23 on the sampling pulses were all shorten for this test since the delays associated with the modulation-demodulation process were not present.

The results of the baseband tests are shown in Figure 24, along with those predicted by theory. The measured results show reasonably close agreement with theory - within 1.5 dB out to an error rate of about 1.0E-9. The discrepancies could result from several sources:

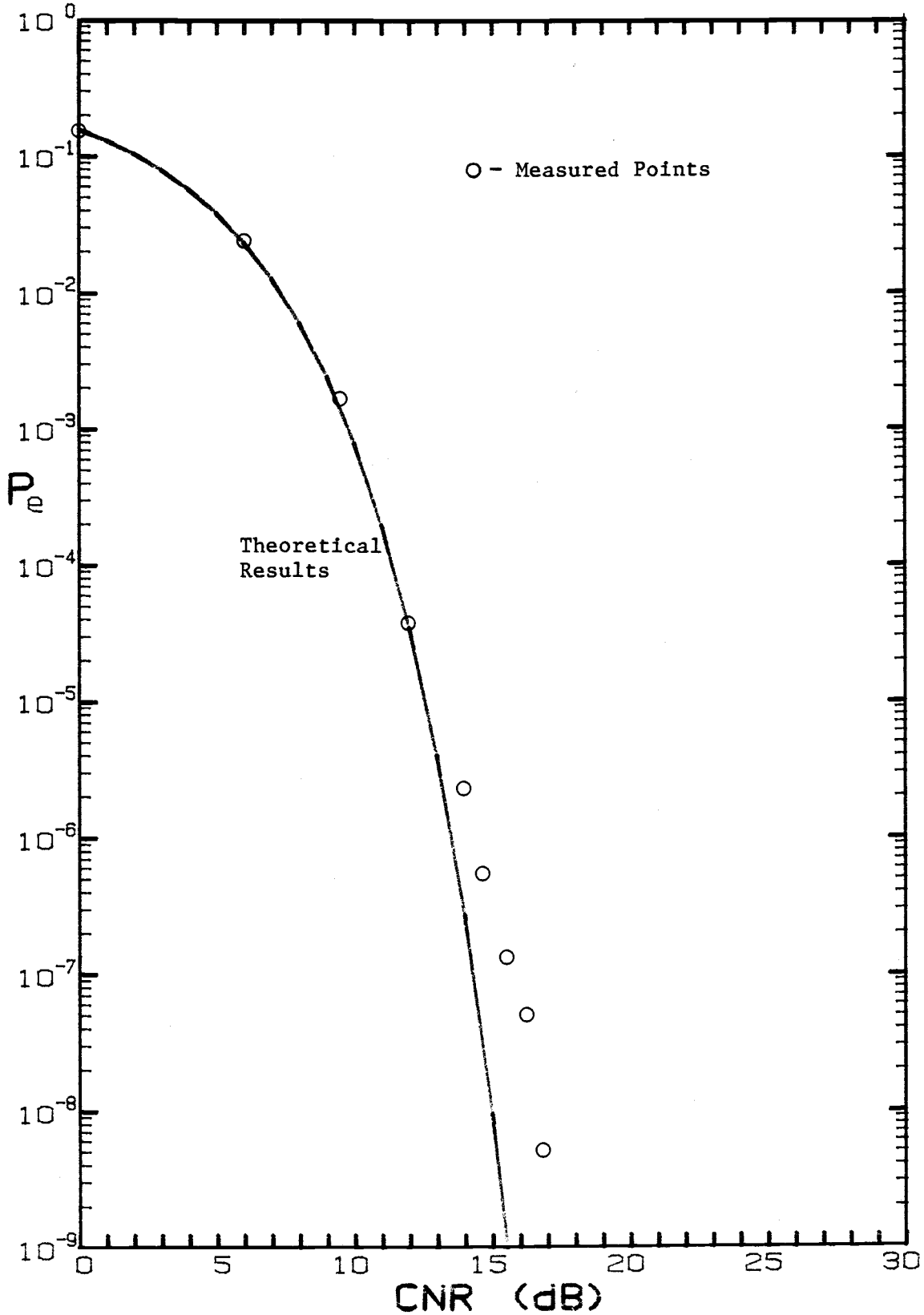

FIGURE 24 - Baseband Data Transmission Performance

1. A not quite gaussian noise generator which, by observation, did not produce a symmetrical gaussian distribution.
2. Small deadbands of a few millivolts around 0 volts for both the sample and hold and comparator circuits.
3. Inaccuracies (about $\pm$ 0.3 dB) in setting the input signal-to-noise ratios.

In spite of the minor inadequacies, the test shows that the timing and decision circuitry basically functions as intended.

Measured Performance of FSK Transmission With Additive Gaussian Noise

For the tests with additive gaussian noise and no interference, the system was fully configured as shown in Figure 23 except the interference amplitude was set to zero volts.

The response of the bandpass filter constructed for these tests is shown in Figure 25. Its characteristics are not very close to the rectangular response of a multiple pole, multiple stage intermediate frequency (IF) filter which would likely be employed in an FSK data receiver. As a simple high Q single tuned circuit, it lacks the flat 100 kHz passband and steep skirts of a well-designed IF filter which was assumed when the model of Section 2 was formulated. Because it is wider than the well-designed filter, it admits more noise at frequencies which are farther removed from the center (0 output volts) frequency of the frequency detector. In order to compare the measured error rates with the error rate predictions based on using a proper IF filter, it is necessary to rationalize the impact the constructed bandpass filter will have on the measured results.

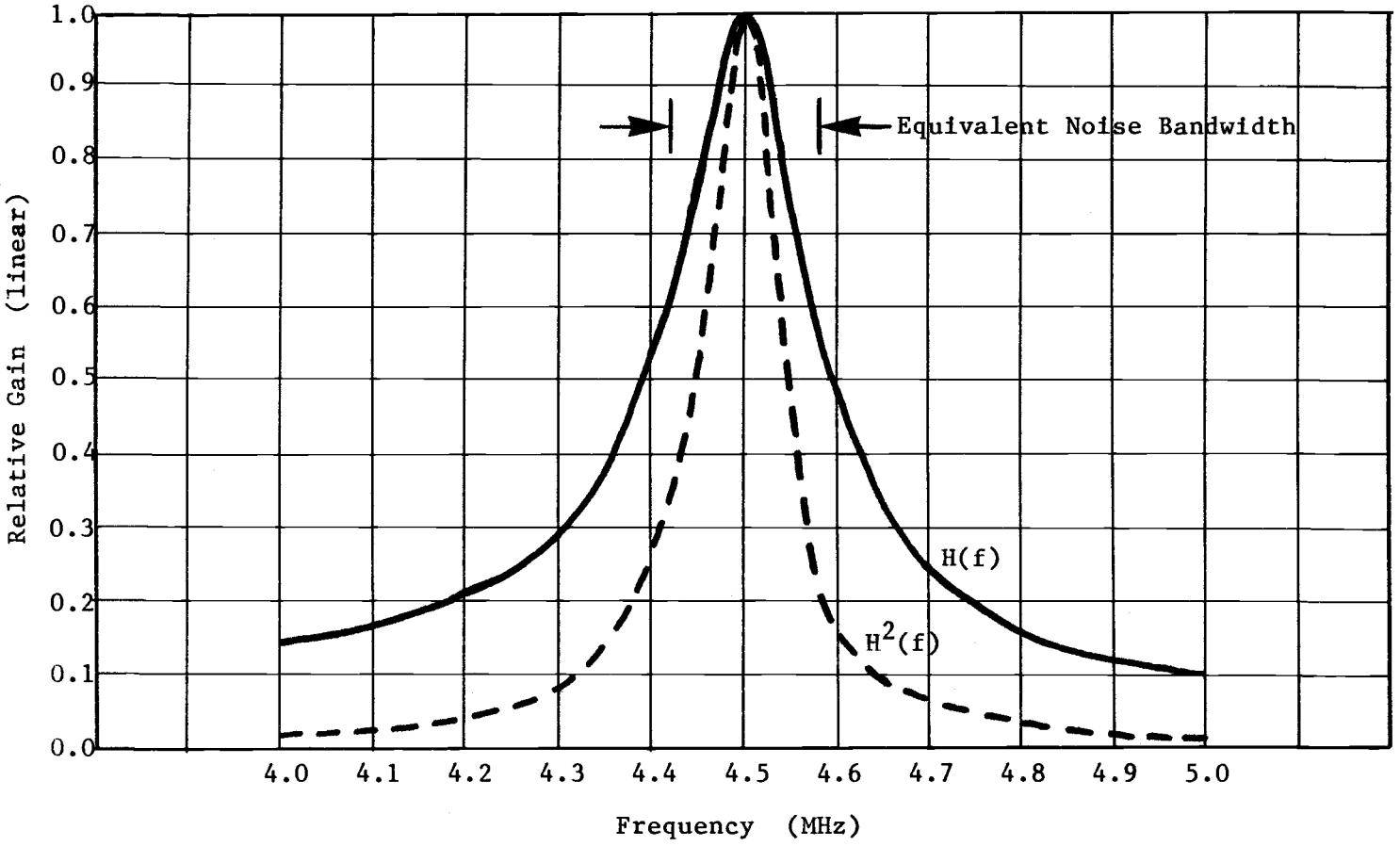

FIGURE 25 - Measured Response of Bandpass Filter

The difference in noise output of the two filters was determined by computing the equivalent noise bandwidth of the test filter and comparing it with a 100 kHz noise bandwidth. The plotted response of the bandpass filter H(f) in Figure 25 was squared to produce H^2(f). The area under this curve was determined using a polar planimeter. The equivalent noise bandwidth was calculated from this area and found to be approximately 160 kHz. The measured CNR set at the input to the detector was therefore adjusted by the ratio 160/100 or about 2 dB.

With this factor in mind, the error rate was measured for several values of input CNR. The results are shown in Figure 26. The measured points show reasonably good agreement with the theoretical no interference case given by term 1 of Equation (19), as the model assumes. The discrepancy from the theoretical curve for low error rates shows the same characteristics as the baseband case with gaussian noise. Interestingly, for lower CNR (below about 8 or 10 dB), the error rates rise well above the prediction, indicating the gaussian noise assumption is increasingly inaccurate. The 10 dB point is classically thought of as the threshold point in analog FM and the point where the click-created output distortion becomes significant [21]. The measured results for FSK transmission given here seem to reflect the same phenomenon.

Measured Performance of FSK Transmission With Sinewave Interference and Additive Gaussian Noise

Using the sinewave generator shown in Figure 23, various amounts of interference were added to the FSK carrier along with the gaussian

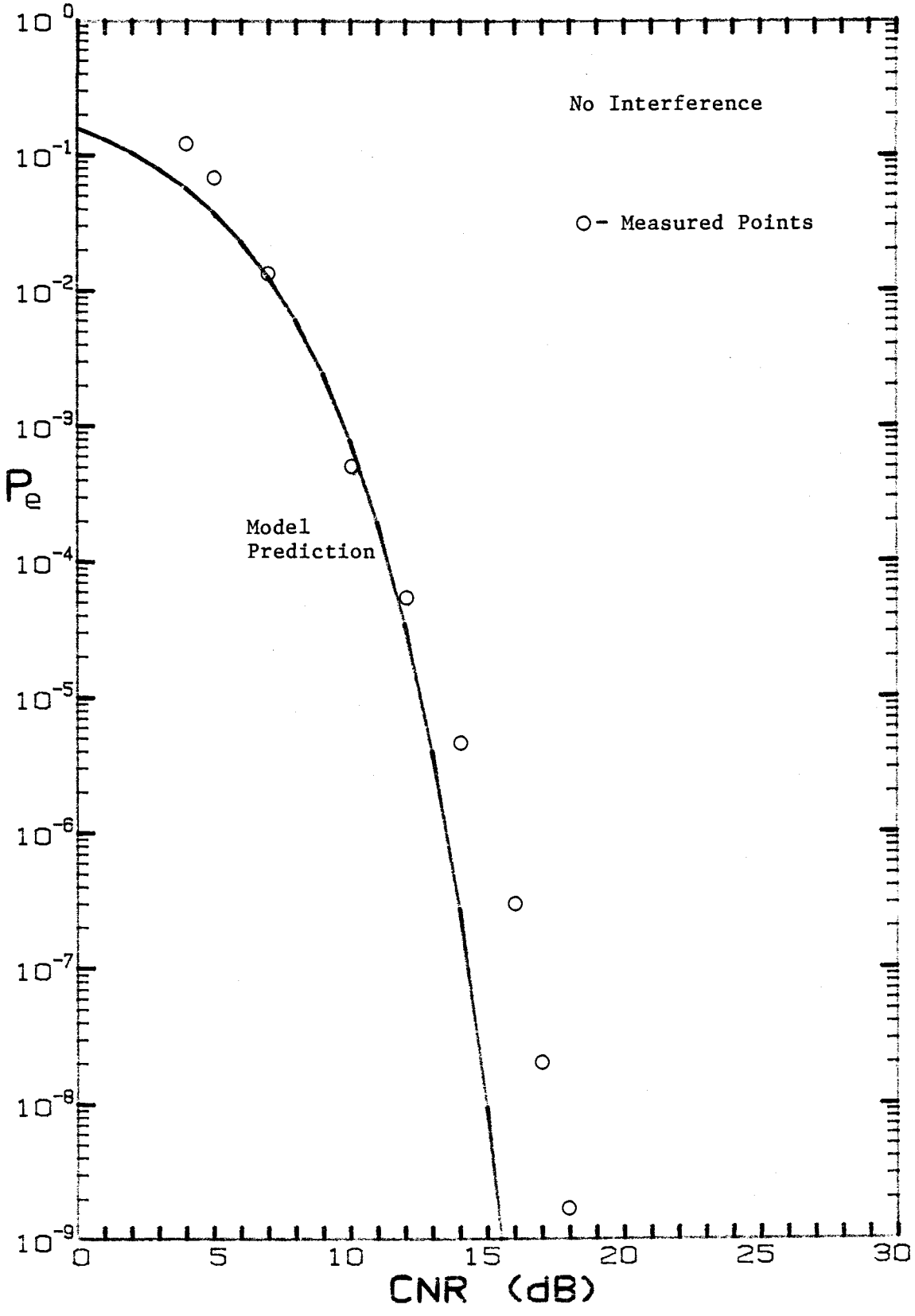

FIGURE 26 - FSK Data Transmission Performance, No Interference

noise. In all cases the interfering frequency was set at 4.5 MHz, or midway between the FSK frequencies corresponding to a binary one and zero. In Section 2 this was judged to be the worst case error situation.

Conducting the tests and measurements proved to be reasonably straightforward. The only problems encountered were equipment drift during the long test periods needed for measuring very low error rates. It was found that the amplitude of the noise generator could drift by 1 dB, and that the frequency of the interference generator could drift by $\pm$ 5 kHz over a 24 hour period. The bandpass filter was also sensitve to temperature changes. A slight change in its center frequency would cause amplitude variations in the envelope of the FSK carrier signal, a circumstance which violates earlier assumptions about the time variation of the envelope of the FSK signal. By exploring this filter misadjustment problem, it was found that the error rate performance did indeed worsen as amplitude variations increased, although no systematic measurements of this effect were made.

After recognizing and compensating for these equipment problems, the measurement or error rates proceeded with no other difficulties. The measured results, along with the predicted curves based on the model presented in Section 2, are shown in Figures 27 through 30 for CIR values of 20, 12, 6 and 3 dB. As expected, measured error performance degrades with decreasing CNR and decreasing CIR. This relationship was consistent for all the measured points.

The actual measured numbers show reasonably close agreement with the predictions made using the model of Section 2. For high CNR and

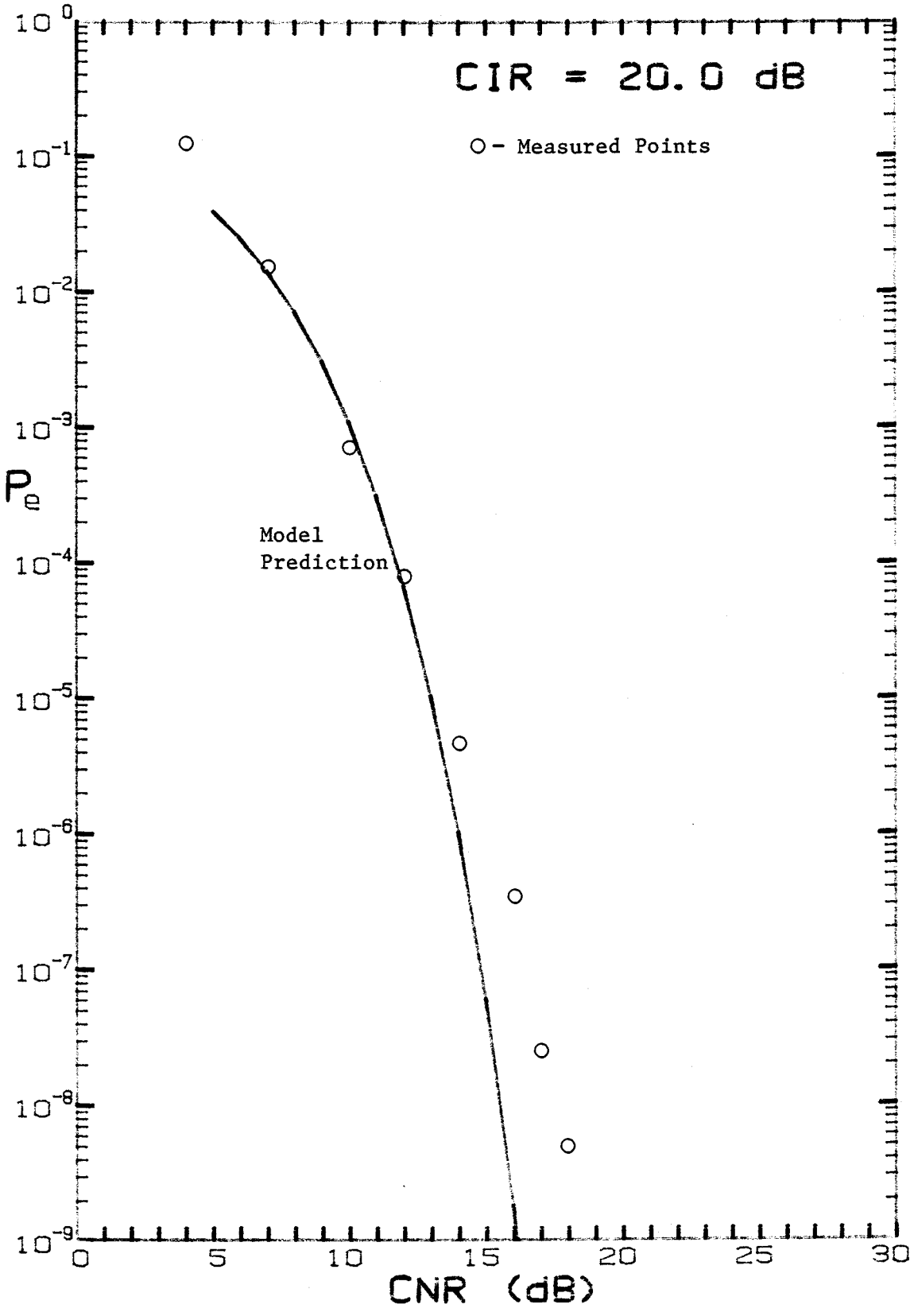

FIGURE 27 - FSK Data Transmission Performance, CIR = 20 dB

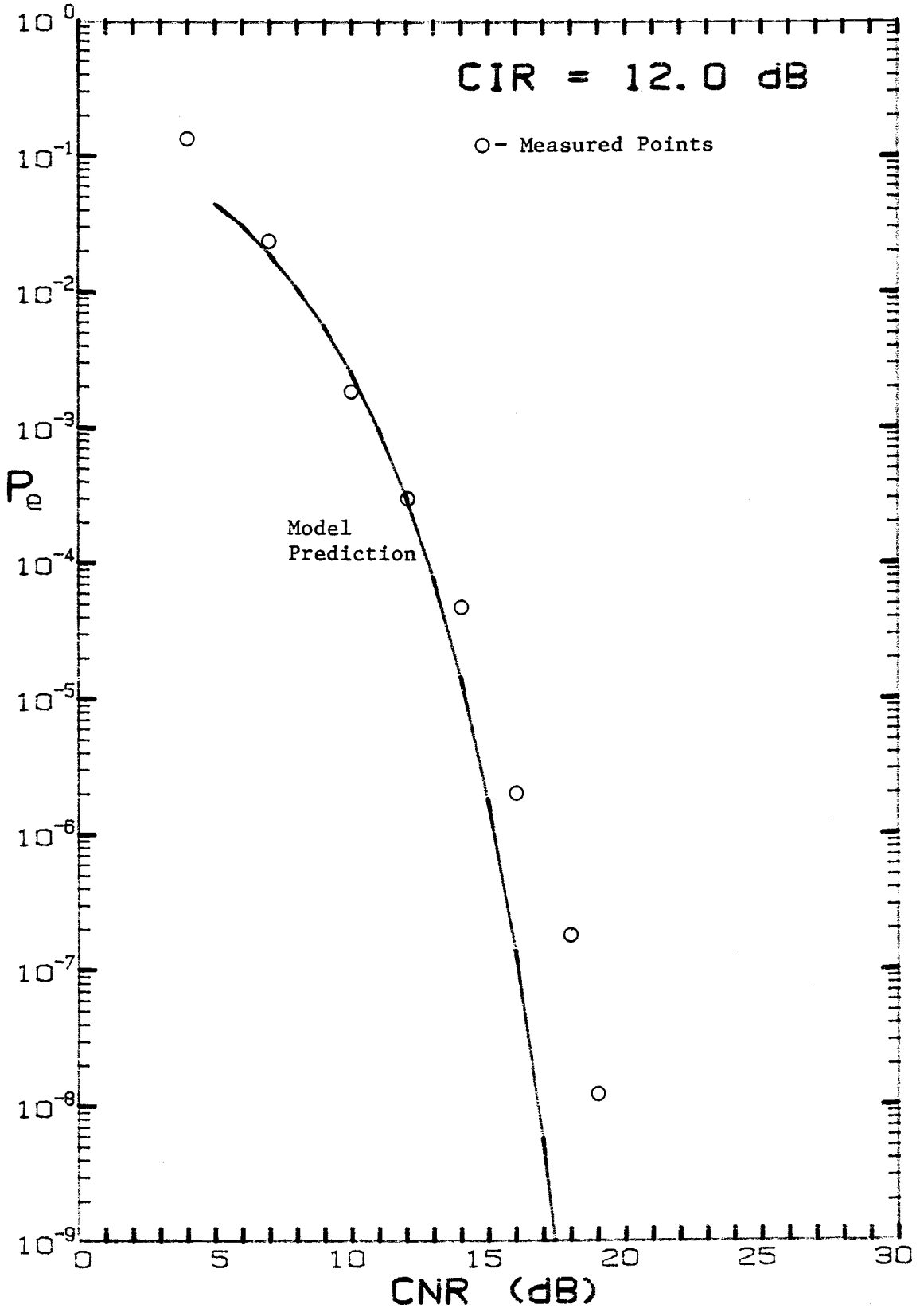

FIGURE 28 - FSK Data Transmission Performance, CIR = 12 dB

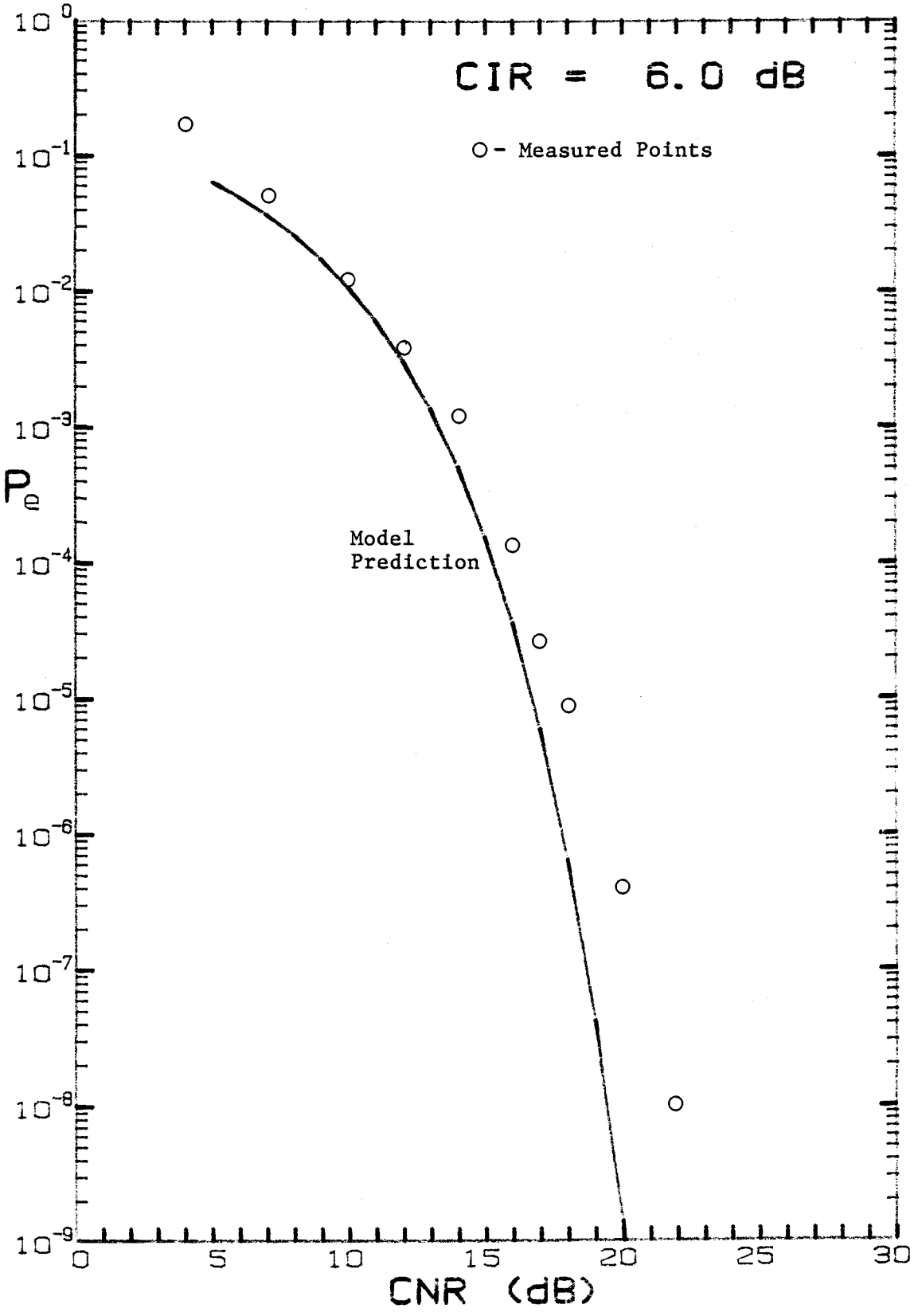

FIGURE 29 - FSK Data Transmission Performance, CIR = 6 dB

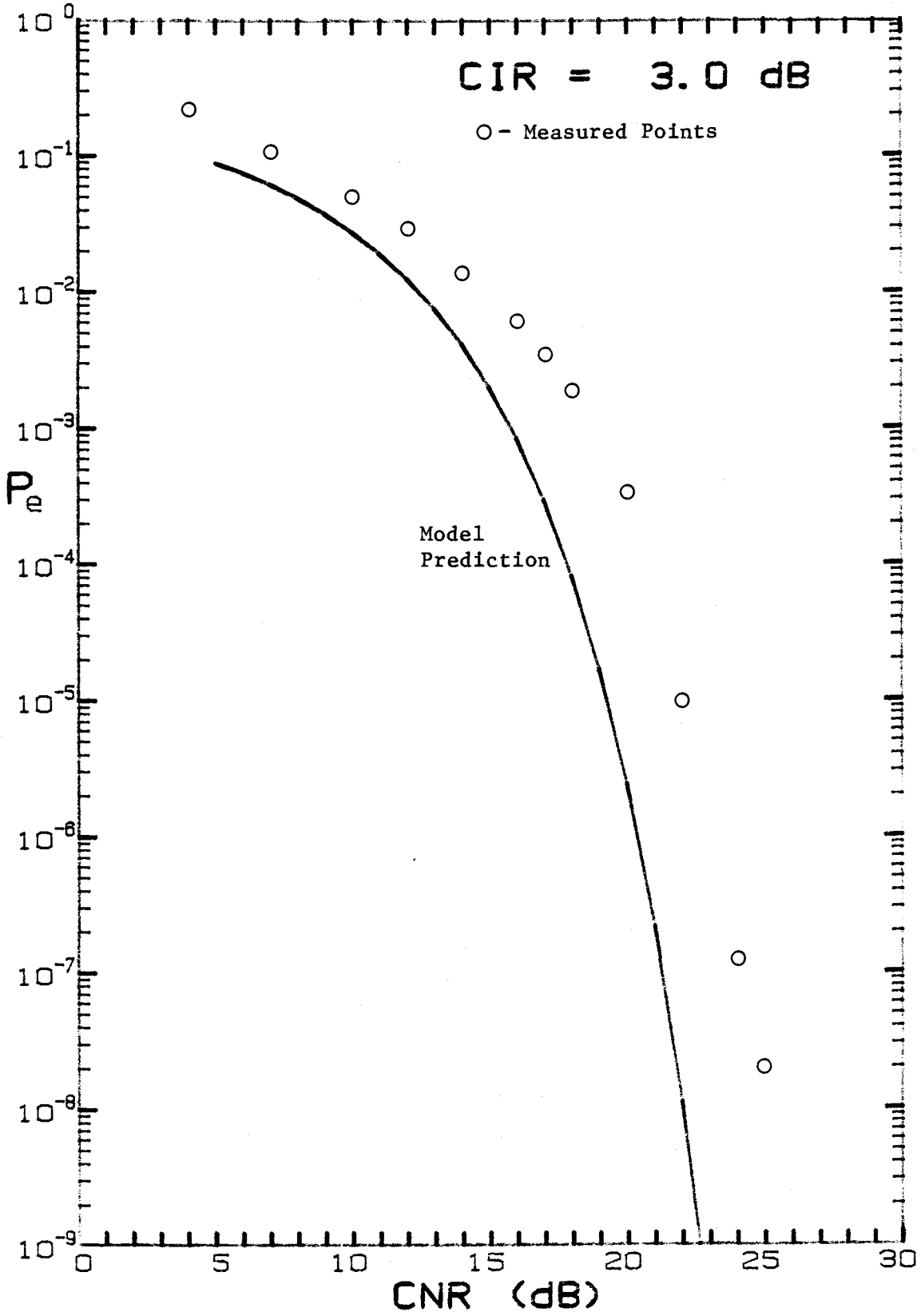

FIGURE 30 - FSK Data Transmission Performance, CIR = 3 dB

low error rates, the measured error rates deviate from the predicted curve by about the same amount as for the baseband gaussian noise only measurements, indicating that these deviations are likely the result of the test setup or nongaussian nature of the noise, as explained before, rather than a failure of the validity of the model. For low CNR and higher error rates, the measured error rates are higher than the values predicted by the model. As discussed before, this region is below what is regarded as the FM threshold where click-related distortion begins to dominate the error rate.

Comparison of Model Predictions and Experimental Results

The validity of the model of FSK transmission performance with noise and interference can be judged from the relationship between the model predictions and the experimental results. For carrier-to-noise ratios above about 10 dB, the model predicts error rates which are comparable to the measured values. Deviations between the predicted and measured error rates can largely be explained by the inherent limitation of the experimental test set up. The model therefore appears to provide useful results for CNR values above 10 dB.

The validity of the model is also limited to a certain range of carrier-to-interference ratios. Figure 30 with results for CIR = 3 dB shows measured results which deviate from the model predictions throughout the range of CNR values, whereas for CIR = 6 dB, the results are much closer to the predictions. It consequently appears that for very high interference levels (CIR = 3 dB), the validity of the model is questionable.

There are two likely causes for the model's lack of validity for the high CIR levels. As the interference level increases, the opportunity for the interference plus noise to exceed the carrier level increases. When this happens, the detector cannot tell which is the intended signal and which is the interference. The normal FM capture mechanism which tends to suppress the interference breaks down when the interference is within a few decibels of the desired carrier level [22].

The second factor is the assumption used in Section 2 that because of the lowpass filter, only the first two harmonics of the error voltage are significant. While this is substantially the case, it becomes less and less valid as the CIR decreases and the harmonic content of the error voltage increases. It's possible, then, that for CIR = 3 dB the third harmonic is also contributing to the error voltage thus causing the measured error rates to be higher than the model predicts.

SECTION 4 - CONCLUSIONS

Usefulness of Results for Predicting Cable System Data Communications Performance With Noise and Interference

The model for FSK data detection with additive gaussian noise and single sinewave interference presented and tested in this thesis has been shown to provide useable results for situations in which the FSK carrier-to-noise ratios are greater than about 10 dB and the FSK carrier-to-interference ratios of greater than about 3 dB. As explained in Section 1, the forward path of a cable system is so designed to provide CNR values of between 20 and 30 dB in a 100 kHz data channel. This falls within the range where the model is valid. The CNR values for the return path are more difficult to assess because they depend on the number of feeders funneling noise into a given trunk line. However, measurements of return path noise at the hub show that return path CNR values of from 10 to 30 dB can be provided for in the system design without feeder switching or segmented return trunks. The model will therefore offer useable results for return path transmission in noise.

The applicability of the model when interference is also considered is less well-defined. As explained in Section 1, the forward path interference is primarily due to intermodulation distortion and can therefore be reasonably well controlled to CIR levels which are much greater than 3 dB. The return path, however, may be subject to interference which is actually greater than the FSK signal amplitude itself. If such interference occurred in the passband of receiver, the

detector would take the interference as the desired signal and vice versa. Detection errors would then occur with greatly increased probability. The relevant question, then, is what sort of probability distribution applies to the amplitude of the return path interference? Equation (29) sets forth the relationship for finding the probability distribution of the error term given a pdf for the amplitude of the interference. A Rayleigh pdf was also postulated as one possible form of the interference amplitude distribution. However, without some measured field data, the actual characteristics of the interference can only be roughly estimated. The model presented here does give useable error rate predictions over a range of CIR levels below 3 dB, so that if a pdf for the interference were found, it most likely could be used in this model.

Design of the return path may ultimately provide some upper bounds on the interference levels. Since an FSK signal envelope ideally has no amplitude variations, a limiter could be installed at every home drop so that any interference entering the system there would not be any greater in amplitude than the FSK signal amplitude. Prefiltering (ahead of the FSK signal insertion) frequency bands where return path FSK transmission takes place is another method of mitigating the impact of random interference ingress from the home drop.

As explained in Section 3, the measured results presented in this thesis are artificially optimistic in that perfect sample and hold timing on received data was possible. In a normal FSK receiver, the sample and hold operation would be derived from the received signal, usually occurring one half bit time after a detected zero crossing. If

the zero crossings are corrupted by noise and interference, the sample timing will be imperfect and the error rate will be higher.

Suggestions for Further Research

As stated, the main deterrent to fully utilizing the model presented in this thesis is the lack of empirical data describing return path interference. Consequently, the next step to further refining the model is to obtain statistically worthwhile information on return path interference from existing cable systems.

Such a measurement program should be structured to derive a reasonably accurate probability density function for the interference. It would be most effective, then, to use an actual FSK data receiver with a 100 kHz passband and continuously record the voltage which is presented to the frequency detector circuit. With long time span recordings on tape, statistical evaluation could be conducted at some later time, rather than attempting the analysis in real time. Recordings done in this way would provide a much more complete picture of the interference and noise characteristics than simply counting errors over a long period of time.

A simplified analysis would be possible if only a worst case assessment of error performance was desired. By knowing only the maximum (Im) and r.m.s. (σ_I) values of the channel degradation, a worst case interference pdf is given by

$$p(x) = \left[1 - \left(\frac{\sigma_I}{I_m}\right)^2\right]\delta(x) + \frac{1}{2}\left(\frac{\sigma_I}{I_m}\right)^2\delta(x-I_m) + \frac{1}{2}\left(\frac{\sigma_I}{I_m}\right)^2\delta(x+I_m) \quad (33)$$

This equation was taken from Reference [23]. Determining peak and r.m.s. values of the interference would be a much easier task than recording the entire signal.

The situation for FSK transmission is complicated because not only the amplitude but the frequency of the interference is relevant to the error voltage produced at the output of the detector. For this reason, it may be better to measure the peak and r.m.s. error voltage excursions at the output of the detector, and construct a worst case pdf using equation (33). Such a method would be mathematically tractable and provide a means for incorporating empirical data from existing cable systems.

With a viable error rate prediction technique, cable system design parameters to allow reliable data transmission can be determined. For example, given the noise and interference on the return path, perhaps there is an upper limit to the number of feeders which can be routed back into a given trunk in order to achieve a specified level of data integrity. By using empirical noise and interference information, and the techniques set forth in this thesis, design limits of this type could be calculated, thus resolving some of the technical questions which are currently inhibiting the growth of two-way data transmission on community-wide cable systems.

REFERENCES

[1] K.A. Simons, "The Decibel Relationships Between Amplifier Distortion Products," Proceedings of the IEEE, Vol. 58, No. 7, July 1970, pp. 1071 - 1086.

[2] A. Prochazka, "Cascading of Distortion in CATV Trunk Line," IEEE Transactions on Broadcasting, Vol. BC-20, No. 2, June 1976, pp. 25 - 32.

[3] A. Prochazka, "Multichannel Cross Modulation in CATV Amplifier," IEEE Transactions on Broadcasting, Vol. BC-20, No. 3, September 1976, pp. 33 - 35.

[4] B. Arnold, "Third Order Intermodulation Products In A CATV System," IEEE Transactions on Cable Television, Vol. CATV-2, No. 2, April 1977, pp. 67 - 80.

[5] "Sylvannia Pathmaker CATV DATA," CATV Division, GTE Products Corporation, No date, page 42.

[6] Code of Federal Regulations, Telecommunications, Sections 76.610, 76.611, and 76.613, 1982, pp. 556 - 558.

[7] R. E. Pidgeon and D. H. Slim, "Frequency Allocation For Data and Video," Technical Papers, National Cable Television Association Convention, June 1983, pp. 64 - 68.

[8] W. P. Osborne and M. B. Luntz, "Coherent and Noncoherent Detection of CPFSK," IEEE Transactions on Communications, Vol. COM-22, August 1974, pp. 1023 - 1036.

[9] F. deJaeger and C. B. Dekker, "Tamed Frequency Modulation - A Novel Method to Achieve Spectrum Economy in Digital Transmission," IEEE Transactions on Communications, Vol. COM-26, May 1978, pp. 534 - 542.

[10] J. D. Oetting, "A Comparison of Modulation Techniques for Digital Radio," IEEE Transactions on Communications, Vol. COM-27, December 1979, pp. 1752 - 1762.

[11] B. P. Lathi, Modern Digital and Analog Communication Systems, New York: Holt, Reinhart and Winston, 1983, pp. 517-518

[12] M. Schwartz, W. Bennett, and S. Stein, Communication Systems and Techniques, New York: McGraw-Hill, 1966.

[13] L. Wang, "Error Probability of a Binary Noncoherent FSK System in the Presence of Two CW Tone Interferers," IEEE Transactions on Communications, Vol. COM-22, December 1974, pp. 1948 - 1949.

[14] J. Jones, "FSK and DPSK Performance in a Mixture of CW Tone and Random Noise Interference," Correspondence, IEEE Transactions on Communications, Vol. COM-18, October 1970, pp. 693 - 695.

[15] A. B. Carlson, Communication Systems: An Introduction to Signals and Noise in Electrical Communication, New York: McGraw-Hill, 1968, pp. 387 - 388.

[16] D. L. Schilling, E. Hoffman, E. A. Nelson, "Error Rates for Digital Signals Demodulated by an FM Discriminator," IEEE Transactions on Communications Technology, Vol. COM-15, No. 4, August 1967, pp. 507 - 517.

[17] P. Beckmann, Elements of Applied Probability Theory, New York: Harcourt, Brace & World, Inc., 1968, page 47.

[18] W.R. Bennett and J. Salz, "Binary Data Transmission by FM over a Real Channel," Bell System Technical Journal, Vol. 42, 1963, pp. 2387 - 2426.

[19] See Reference [12], page 300.

[20] W. C. Lindsey and M. K. Simon, "Detection of Digital FSK and PSK Using a First-Order Phase-Locked Loop," IEEE Transactions on Communications, Vol. COM-25, No. 2, February 1977, pp. 200 - 214.

[21] See Reference [12], page 123.

[22] See Reference [11], page 318.

[23] J. H. Roberts, Angle Modulation, Stevenage, England: Peter Peregrinus Ltd., 1977, page 237.

APPENDICES

APPENDIX A - COMPUTER PROGRAMS USED FOR CALCULATIONS

This appendix contains listings for the major computer programs used in conducting the research described in this thesis. The programs are briefly described below in their order of appearance. All are written in Microsoft BASIC (MBASIC) for use with an 8 bit Z80-based computer with data output directed to either a printer or Hewlett-Packard 7470A plotter.

Program EQ19.BAS

This program calculates the value of terms 1 and 2 of equation (19) in the text for various carrier-to-noise ratios and values of the parameter a.

Program DER.BAS

This program computes and plots the interference error voltage term at the output of the frequency discriminator given the FSK signalling frequencies, and the amplitude and frequency of the interference.

Program FFT1.BAS

This program computes and plots the spectrum components of given input time sequence.

Program PDF.BAS

This program computes and plots time domain representations of the lowpass filtered interference error term for various levels of interference. It also computes and plots the probability density function (pdf) for the error terms.

Program CONV.BAS

This program performs a convolution of the pdf of the filtered interference error term with the pdf of gaussian noise for various noise variances. It also computes error rates and plots the double sided pdf of the results from the convolution.

Program PERTH.BAS

This program draws the probability of error curve figures and plots error rate curves from data contained in input files or generated internally by equations.

```
10 REM
20 REM PROGRAM EQ19.BAS TO COMPUTE TERM 1 AND TERM 2 OF EQUATION 19
30 REM
40 PI=3.14159
50 A=.5
60 FOR I=1 TO 30
70 REM
80 REM COMPUTER TERM 1
90 REM
100 SNR=10^(I/20)
110 RHO=SNR/SQR(2)
120 X1=RHO
130 GOSUB 320
140 TERM1=.5*ERFCX
150 REM
160 REM COMPUTE TERM 2
170 REM
180 TERM2=0
190 FOR N=1 TO 200
200 X=-1+.01*N
210 P1=EXP(-RHO*RHO*X*X)
220 X1=A*RHO*SQR(1-X*X)
230 GOSUB 320
240 TERM2=TERM2+P1*ERFCX*.01
250 NEXT N
260 TERM2=TERM2*(RHO/(2*SQR(PI)))
270 LPRINT
280 LPRINT I,SNR,RHO,TERM1,TERM2,TERM1+TERM2
290 LPRINT
300 NEXT I
310 END
320 REM
330 REM SUBROUTINE TO COMPUTE COMPLIMENTARY ERROR FUNCTION
340 REM
350 T=1/(1+.327591*X1)
360 T2=T*T
370 T3=T2*T
380 T4=T2*T2
390 T5=T2*T3
400 X2=X1*X1
410 ERFCX=.25482959#*T-.28449673#*T2+1.4214137#*T3-1.45315202#*T4+1.06140542#*T5
420 ERFCX=ERFCX*EXP(-X2)
430 RETURN
```

FIGURE 31 - Program EQ19.BAS

```
10 REM
20 REM PROGRAM DER.BAS TO CALCULATE AND PLOT ERROR TERM FOR FREQUENCY
30 REM DISCRIMINATOR WITH INTERFERENCE IN THE CHANNEL
40 REM
50 DIM ER(1025) , P(1025)
60 PRINT
70 INPUT "ENTER TONE SEPARATION MULTIPLE (1,2,3  ETC.): ",MX
80 PRINT
90 INPUT "ENTER FREQUENCY(HZ) AND PHASE SHIFT(DEGS.) OF INTERFERENCE: ",FK,TH
100 THETA=TH/57.2958
110 S=1
120 PI=3.14159
130 F1=4.5E+06+28000*MX
140 F2=4.5E+06-28000*MX
150 W1=F1*2*PI
160 W2=F2*2*PI
170 WK=FK*2*PI
180 DELTAT=2/56000!
190 DELTAT=DELTAT/512
200 PRINT
210 INPUT "DO PLOT(1) OR NO(2): ",KY1
220 IF(KY1=2) GOTO 530
230 LPRINT USING "&";CHR$(27);".Y"
240 LPRINT "DF"
250 LPRINT "IP 00,130,10100,7250"
260 LPRINT "SC 0,10,0,7"
270 LPRINT "SP 1"
280 LPRINT "PAPU",1!,3.5,"PD",9!,3.5,"PU",5!,.75,"PD",5!,6.4,"PU"
290 LPRINT "PU",2,6.4
300 ETX$=CHR$(3)
310 LPRINT USING "&";"DT";ETX$
320 LPRINT "SI";.13,.2
330 LPRINT "DI",0,-1
340 LPRINT "LBFREQUENCY FOR A BINARY 1 = ";
350 LPRINT USING "#.####";F1/1E+06;
360 LPRINT "  MHZ";ETX$
370 LPRINT "PU",1.75,6.4
380 LPRINT "LBFREQUENCY FOR A BINARY 0 = ";
390 LPRINT USING "#.#### ";F2/1E+06;
400 LPRINT " MHZ";ETX$
410 LPRINT "PU",1.5,6.4
420 LPRINT "LBFREQUENCY OF INTERFERENCE = ";
430 LPRINT USING "#.#### ";FK/1E+06;
440 LPRINT "MHZ";ETX$
450 PRINT
460 INPUT "HIT <CR> TO CONTINUE",YYY
470 PRINT
480 FOR I=1 TO 46
490 X=1.0909+(I-1)*.16996
500 LPRINT "PU",X,3.55,"PD",X,3.45
510 NEXT I
520 LPRINT "PU"
530 T=-DELTAT
540 FOR M=1 TO 4
550 IF(M=1) THEN I=.1
```

FIGURE 32 - Program DER.BAS

```
560 IF(M=2) THEN I=.25
570 IF(M=3) THEN I=.5
580 IF(M=4) THEN I=.707
590 WX=W1
600 FOR N=1 TO 1024
610 T=T+DELTAT
620 IF(N < 513) GOTO 660
630 IF(WX=W2) GOTO 660
640 T=-DELTAT
650 WX=W2
660 REM
670 CT=COS((WK-WX)*T-THETA)
680 ER(N)=I*I*(WK-WX)+S*I*(WK-WX)*CT
690 ER(N)=ER(N)/(S*S+I*I+2*S*I*CT)
700 NEXT N
710 GOTO 890
720 FOR N=2 TO 513
730 DIF=ABS(ER(N)-ER(N-1))
740 IF(DIF<.00001) THEN DIF=.00001
750 P(N)=1/DIF
760 SUM=SUM+P(N)
770 NEXT N
780 PRINT
790 PKY=2
800 IF(PKY=2) GOTO 890
810 FOR N=1 TO 513
820 X=1+N*.025
830 Y=500*P(N)/SUM
840 IF(Y>7) THEN Y=7
850 IF(N=1) THEN LPRINT "PU"
860 LPRINT X,Y
870 IF(N=1) THEN LPRINT "PD"
880 NEXT N
890 T=0
900 DX=((W1-W2)*5.41E-06)/2
910 DT=DX
920 IF(KY1=2) GOTO 950
930 LPRINT "PU",5!+DT,6.4,"PD",5!+DT,3.5,5!-DT,3.5,5!-DT,.75
940 LPRINT "SP 2"
950 PRINT
960 INPUT "DATA TO OUTPUT FILE(1) OR NO(2): ",KY
970 IF(KY=2) GOTO 1040
980 INPUT "NAME OF OUTPUT FILE: ",FL$
990 OPEN "O",#1,FL$
1000 FOR I=1 TO 512
1010 PRINT #1,ER(I),XII
1020 NEXT I
1030 CLOSE #1
1040 REM
1050 IF(KY1=2) GOTO 1170
1060 FOR I=1 TO 1024
1070 IF(I>512) THEN DT=-DX
1080 Y=6.4-I*.0056641
1090 X=5!+DT+ER(I)*5.41E-06
1100 IF(I=1) THEN LPRINT "PU"
```

FIGURE 32 continued

```
1110 IF(Y<.75) GOTO 1170
1120 IF(X<1) THEN X=1
1130 IF(X>9) THEN X=9
1140 LPRINT X,Y
1150 IF (I=1) THEN LPRINT "PD"
1160 NEXT I
1170 NEXT M
1180 IF(KY1=2) GOTO 1210
1190 LPRINT "SP 0"
1200 LPRINT USING "&";CHR$(27);".Z"
1210 END
```

FIGURE 32 continued

```
10 REM
20 REM
30 REM
40 REM PROGRAM FFT1.BAS TO DO FOURIER TRANSFORM OF INPUT FILE SEQUENCE
50 REM
60 DIM XR(1024),XI(1024),XNR(1024),XNI(1024)
70 PI=3.14159
80 REM
90 REM READ INPUT DATA SEQUENCE FROM INPUT FILE
100 REM
110 PRINT
120 INPUT "N (2 TO 1024): ",N
130 PRINT
140 INPUT "NAME OF INPUT DATA FILE: ",FL$
150 OPEN "I", #1, FL$
160 FOR I=1 TO N
170 INPUT #1,XR(I),XI(I)
180 IF(ABS(XR(I))>MAX) THEN MAX=ABS(XR(I))
190 NEXT I
200 PRINT
210 PRINT USING "MAXIMUM VALUE OF INPUT = ######.# , ";MAX
220 INPUT "ENTER SCALE FACTOR: ",SCALE
230 FOR I=1 TO N
240 XR(I)=XR(I)/SCALE
250 XI(I)=XI(I)/SCALE
260 NEXT I
270 REM
280 REM DATA READ IN AND NORMALIZED, START FFT ROUTINE
290 REM
300 FOR I=1 TO N
310 XNR(I)=XR(I)
320 XNI(I)=XI(I)
330 NEXT I
340 CLOSE #1
350 REM
360 REM SET UP CONSTANTS
370 REM
380 M=LOG(N)/.693147
390 NV2=N/2
400 NM1=N-1
410 REM
420 REM
430 REM DO FFT BY DECIMATION-IN-TIME METHOD
440 REM
450 REM DO BIT REVERSAL ON INPUT DATA
460 REM
470 PRINT "START"
480 J=1
490 FOR I=1 TO NM1
500 IF(I>J) GOTO 570
510 TR=XR(J)
520 TI=XI(J)
530 XR(J)=XR(I)
540 XI(J)=XI(I)
550 XR(I)=TR
```

FIGURE 33 - Program FFT1. BAS

```
560 XI(I)=TI
570 K=NV2
580 IF(K>=J) GOTO 620
590 J=J-K
600 K=K/2
610 GOTO 580
620 J=J+K
630 NEXT I
640 REM
650 REM  BIT REVERSAL DONE
660 REM NOW PROGRESS THROUGH "IN-PLACE" CALCULATIONS
670 REM
680 LE1=1
690 IF(LE1>=N) GOTO 920
700 LE=2*LE1
710 FOR J=1 TO LE1
720 THETA=PI*(-(J-1))/LE1
730 WR=COS(THETA)
740 WI=SIN(THETA)
750 FOR I=J TO N STEP LE
760 IP=I+LE1
770 TR=XR(IP)*WR - XI(IP)*WI
780 TI=XI(IP)*WR + XR(IP)*WI
790 XR(IP)=XR(I)-TR
800 XI(IP)=XI(I)-TI
810 XR(I)=XR(I)+TR
820 XI(I)=XI(I)+TI
830 NEXT I
840 NEXT J
850 LE1=LE
860 GOTO 690
870 LE1=LE
880 GOTO 690
890 REM
900 REM     FFT ROUTINE DONE. OUTPUT RESULTS.
910 REM
920 REM
930 REM FFT CALCULATED RESULTS ARE IN XR(I) AND XI(I)
940 REM PRINT OR PLOT OUTPUT VALUES
950 REM
960 PRINT
970 PRINT "STOP"
980 PRINT
990 INPUT "OUTPUT TO PRINTER(1) OR PLOTTER(2): ",MKY
1000 IF(MKY=2) GOTO 1190
1010 PRINT
1020 INPUT "PREPARE PRINTER, THEN HIT <CR>",T
1030 LPRINT "   K        MAGNITUDE       PHASE"
1040 LPRINT "-------     ---------     --------"
1050 FOR I=1 TO N
1060 MAG=SQR(XR(I)*XR(I)+XI(I)*XI(I))
1070 IF(XR(I)=0) THEN XR(I)=.000001
1080 ANG=ATN(XI(I)/XR(I))
1090 IF(XR(I)<0) THEN ANG=ANG-PI
1100 IF(ABS(XR(I))<.0001) AND (ABS(XI(I))<.0001) THEN ANG=-PI
```

FIGURE 33 continued

```
1110 LPRINT USING " ###        ###.####     ###.####";I-1;MAG;ANG;
1120 LPRINT "         ";
1130 LPRINT XR(I);XI(I)
1140 NEXT I
1150 GOTO 1750
1160 REM
1170 REM PLOT INPUT SEQUENCE, MAGNITUDE AND PHASE OF OUTPUT SPECTRUM
1180 REM
1190 PRINT
1200 INPUT "LINE(1) OR CONTINUOUS(2) AMPLITUDE SPECTRUM: ";SKY
1210 PRINT
1220 FOR I=1 TO N
1230 IF(ABS(XR(I))>MAXP) THEN MAXP=ABS(XR(I))
1240 NEXT I
1250 PRINT
1260 PRINT USING "MAX. SPECTRAL COMPONENT = #####.# ";MAXP
1270 INPUT "ENTER OUTPUT SCALE FACTOR: ",MAXP
1280 SC=1/MAXP
1290 INPUT "PREPARE PLOTTER, THEN HIT <CR>",T
1300 PRINT
1310 INPUT "PLOT POSITION (1,2,3 OR 4): ",PP
1320 XC=1
1330 IF(PP=1) OR (PP=2) THEN XC=5.5
1340 YC=6.15
1350 IF(PP=2) OR (PP=4) THEN YC=3!
1360 LPRINT USING "&";CHR$(27);".Y"
1370 LPRINT "DF"
1380 LPRINT "IP 00,130,10100,7250"
1390 LPRINT "IP"
1400 LPRINT "SC 0,10,0,7"
1410 LPRINT "SP 1"
1420 LPRINT "PU",XC+3.3,YC,"PD",XC+1.7,YC,XC+2.5,YC,XC+2.5,YC-2.5
1430 LPRINT "PU",XC+1.5,YC,"PD",XC,YC,XC,YC-2.5
1440 LPRINT "SP 2"
1450 FOR I=1 TO N
1460 Y=YC-(I-1)*.0048828
1470 X=XC+2.5+XNR(I)*.8
1480 IF(I=1) THEN LPRINT "PU",X,Y,"PD"
1490 IF(I=2) THEN LPRINT "PD"
1500 LPRINT X,Y
1510 NEXT I
1520 FOR I=1 TO 16
1530 MAG=SQR(XR(I)*XR(I)+XI(I)*XI(I))
1540 MAG=SC*MAG
1550 Y=YC-(I-1)*.15625
1560 X=XC+MAG*1.5
1570 IF(SKY=1) GOTO 1610
1580 IF(I=1) THEN LPRINT "PU",X,Y
1590 LPRINT "PD",X,Y
1600 GOTO 1620
1610 LPRINT "PU",XC,Y,"PD",X,Y
1620 NEXT I
1630 GOTO 1730
1640 FOR I=1 TO N/2+1
1650 IF(XR(I)=0) THEN XR(I)=.000001
```

FIGURE 33 continued

```
1660 ANG=ATN(XI(I)/XR(I))
1670 IF(XR(I)<0) THEN ANG=ANG-PI
1680 IF(ANG<-PI) THEN ANG=-PI
1690 Y=6.5-(I-1)*.05
1700 X=1.6+(ANG/PI)*1.5
1710 LPRINT "PU",1.6,Y,"PD",X,Y
1720 NEXT I
1730 LPRINT "PU",0,0
1740 LPRINT USING "&";CHR$(27);".Z"
1750 END
```

FIGURE 33 continued

```
10 REM
20 REM PROGRAM PDF.BAS TO CALCULATE VALUE OF TWO TERM ERROR VOLTAGE
30 REM AND COMPUTE AND PLOT PDF
40 REM
50 DIM ER1(1025), PDF(1025)
60 S=1
70 I=.707
80 MX=1
90 PI=3.14159
100 FA=4.5E+06+28000*MX
110 FB=4.5E+06-28000*MX
120 FK=4.5E+06
130 WA=FA*2*PI
140 WB=FB*2*PI
150 WK=FK*2*PI
160 DELTAT=2/56000!
170 DELTAT=DELTAT/512
180 T=-DELTAT
190 PRINT
200 INPUT "PLOT VOLTS(1) OR PDF(2) OR BOTH(3): ",KY
210 LPRINT USING "&";CHR$(27);".Y"
220 LPRINT "DF"
230 LPRINT "IP 00,130,10100,7250"
240 LPRINT "SC 0,10,0,7"
250 LPRINT "SP 1"
260 IF(KY=2) GOTO 320
270 LPRINT "PU",7,6.4,"PD"7,.9,"PU",5,3.65,"PD",9,3.65
280 FOR I=1 TO 21
290 X=5+(I-1)*.2
300 LPRINT "PU",X,3.7,"PD",X,3.6
310 NEXT I
320 LPRINT "PU",1.5,6.4,"PD",1.5,.9,"PU",1.3,3.65,"PD",4.5,3.65
330 FOR I=1 TO 21
340 Y=5.65-(I-1)*.2
350 LPRINT "PU",1.45,Y,"PD",1.55,Y
360 NEXT I
370 LPRINT "SP 2"
380 FOR M=1 TO 4
390 IF(M=1) THEN I=.1
400 IF(M=2) THEN I=.25
410 IF(M=3) THEN I=.5
420 IF(M=4) THEN I=.707
430 ER1(0)=0
440 PDF(0)=0
450 PDFT=0
460 FOR N=1 TO 512
470 T=T+DELTAT
480 ER= (WK-WA)*(I/S)*COS((WK-WA)*T+THETA)
490 ER1(N)=ER-(WK-WA)*(I/S)*(I/S)*.25*COS(2*(WK-WA)*T+THETA)
500 ER1(N)=ER1(N)/(2*PI)
510 DIF=ABS(ER1(N)-ER1(N-1))
520 IF(DIF<.00001) THEN DIF=.00001
530 PDF(N)=1/DIF
540 NEXT N
550 IF(KY=2) GOTO 630
```

FIGURE 34 - Program PDF.BAS

```
560 FOR N= 1 TO 512
570 Y=6.4-(N-1)*.0107422
580 X=7+ER1(N)/11618
590 IF(N=1) THEN LPRINT "PU",X,Y,"PD"
600 LPRINT X,Y
610 NEXT N
620 IF(KY=1) GOTO 920
630 REM
640 PRINT
650 INPUT "PDF DATA TO OUTPUT FILE(1) OR NO(2): ",KY1
660 IF(KY1=2) GOTO 700
670 PRINT
680 INPUT "NAME OF OUTPUT FILE: ",FL$
690 OPEN "O",#1,FL$
700 FOR N=1 TO 256
710 Y=3.65-ER1(N)/11618
720 X=1.5+15000*PDF(N)/256
730 IF(KY1=2) GOTO 780
740 PRINT #1,N,ER1(N),PDF(N)/256
750 AREA=(ER1(N)-ER1(N-1))*(PDF(N)+.5*(PDF(N-1)-PDF(N)))
760 AREA=AREA/256
770 PDFT=PDFT+AREA
780 IF(N=1) THEN LPRINT "PU",1.5,Y,"PD",4.5,Y,"PU"
790 IF(X>4.5) GOTO 840
800 IF(FLAG=1) THEN LPRINT "PU",X,Y
810 LPRINT "PD",X,Y
820 FLAG=0
830 GOTO 850
840 FLAG=1
850 NEXT N
860 CLOSE #1
870 PRINT
880 PRINT PDFT
890 LPRINT "PU",4.5,Y,"PD",1.5,Y,"PU"
900 NEXT M
910 REM
920 LPRINT "SP 0"
930 LPRINT USING "&";CHR$(27);".Z"
940 END
```

FIGURE 34 continued

```
10 REM
20 REM PROGRAM CONV.BAS TO DO NUMERICAL CONVOLUTION OF GAUSSIAN PDF
30 REM WITH UP TO 1024 POINT PDF TABULATED IN AN INPUT FILE
40 REM
50 DIM ER(1024),PDF(1024),CNV(1024),SCAL(1024)
60 REM
70 REM READ INPUT DATA
80 REM
90 PRINT
100 NT=256
110 INPUT "NUMBER OF POINTS IN PDF FILE: ",MT
120 PRINT
130 INPUT "NAME OF INPUT PDF FILE: ",FL$
140 OPEN "I",#1,FL$
150 FOR I=1 TO MT
160 INPUT #1,NQ,ER(I),PDF(I)
170 NEXT I
180 CLOSE #1
190 INC=(ER(MT)-ER(1))/MT
200 FOR I=2 TO MT
210 AREA=AREA+ABS(ER(I)-ER(I-1))*(PDF(I)+.5*(PDF(I)-PDF(I-1)))
220 SCAL(I)=(ER(I)-ER(I-1))/INC
230 NEXT I
240 PRINT
250 PRINT USING "AREA OF INPUT PDF = ###.#####";AREA
260 PRINT
270 INPUT "DO PLOT(1) OR NO(2): ",KY
280 IF (KY=2) GOTO 480
290 LPRINT USING "&";CHR$(27);".Y"
300 LPRINT "DF"
310 LPRINT "IP 00,130,10100,7250"
320 LPRINT "SC 0,10,0,7"
330 LPRINT "SP 1"
340 LPRINT "PU",.66667,2,"PD",9.3333,2,"PU",5,1.8,"PD,5,6.4
350 XINC=1/3
360 FOR I=1 TO 27
370 X=.66667+(I-1)*XINC
380 LPRINT "PU",X,1.95,"PD",X,2.05
390 NEXT I
400 LPRINT "PU",6.8666,1.9,"PD",6.8666,5.5
410 LPRINT "PU",3.1333,1.9,"PD",3.1333,5.5
420 FOR I=1 TO 8
430 Y=2+I*.5
440 LPRINT "PU",4.95,Y,"PD",5.05,Y
450 NEXT I
460 LPRINT "PU"
470 REM
480 REM COMPUTE CONVOLUTION OF GAUSSIAN R.V. AND INPUT PDF AT 1024 POINTS
490 REM AND PUT IN ARRAY CNV
500 REM
510 FOR L=16 TO 25
520 SIGMA=28000/(10^(L/20))
530 A1=.398942/SIGMA
540 A2=2*SIGMA*SIGMA
550 TAREA=0
```

FIGURE 35 - Program CONV.BAS

```
560 TERR=0
570 FOR N=1 TO NT
580 NR=-51200!+N*400*(256/NT)
590 CNV(N)=0
600 FOR M=1 TO MT
610 X=NR-ER(M)
620 G=A1*EXP(-(X*X)/A2)
630 CNV(N)=CNV(N)+G*PDF(M)*SCAL(M)
640 NEXT M
650 IF(NR<=-28000) THEN TERR=TERR+CNV(N)
660 TAREA=TAREA+CNV(N)
670 PRINT NR,CNV(N),TERR,TAREA
680 NEXT N
690 LPRINT
700 LPRINT USING "ERROR RATE FOR SNR = ##.### IS ";L;
710 LPRINT TERR/TAREA
720 LPRINT
730 MAX=0
740 PA=0
750 FOR I=1 TO NT
760 PA=PA+CNV(I)*400
770 NEXT I
780 ASCAL=.5/PA
790 FOR I=1 TO NT
800 CNV(I)=CNV(I)*ASCAL
810 IF(CNV(I)>MAX) THEN MAX=CNV(I)
820 NEXT I
830 IF(KY=2) GOTO 1090
840 PRINT
850 PRINT "MAX. PDF EXCURSION = ";MAX
860 INPUT "ENTER VERT. SCALE FACTOR (UNITS PER INCH): ",VSCAL
870 VSCAL=1/VSCAL
880 REM
890 REM
900 REM PLOT PDF RESULTING FROM CONVOLUTION
910 REM
920 LPRINT "SP 2"
930 FOR I=1 TO NT
940 NR=-51200!+I*400*(256/NT)
950 X=6.8666+NR*6.666E-05
960 Y=2+CNV(I)*VSCAL
970 IF(X>9.35) GOTO 1000
980 IF(I=1) THEN LPRINT "PU",X,Y,"PD"
990 LPRINT X,Y
1000 NEXT I
1010 FOR I=NT TO 1 STEP -1
1020 NR=-51200!+I*400*(256/NT)
1030 X=3.13333-NR*6.6666E-05
1040 Y=2+CNV(I)*VSCAL
1050 IF(I=NT) THEN LPRINT "PU",X,Y,"PD"
1060 IF(X<.6666) THEN GOTO 1080
1070 LPRINT X,Y
1080 NEXT I
1090 NEXT L
1100 REM
```

FIGURE 35 continued

```
1110 LPRINT "SP 0"
1120 LPRINT USING "&";CHR$(27);".Z"
1130 END
```

FIGURE 35 continued

```
10 REM
20 REM PROGRAM  PERTH.BAS TO COMPUTE AND PLOT ERROR RATE PERFORMANCE
30 REM VERSUS C/N RATIO FOR BINARY PSK AND FSK DATA TRANSMISSION
40 REM
50 PXX=.177828
60 DIM CNR(31),A(31),PE(40),DB(40)
70 DEF FNLG10(X)=LOG(X)/2.30259
80 FOR I=1 TO 37
90 PE(I)=PXX/1.77828
100 PXX=PE(I)
110 READ DB(I)
120 NEXT I
130 DATA -.65,.19,.95,1.67,2.31,2.95,3.52,4.06,4.5,4.96,5.36,5.71,6.04,6.41
140 DATA 6.68,6.98,7.25,7.51,7.74,7.97,8.2,8.42,8.62,8.81,8.99,9.17,9.35,9.53
150 DATA 9.7,9.85,10.0,10.14,10.27,10.42,10.57,10.71,10.84
160 PRINT
170 INPUT "CURVE FROM EQUATIONS(1) OR DATA FILE(2): ";CRVKEY
180 PRINT
190 INPUT "ADD ATMOSPHERIC NOISE CORRECTION(1) OR NO(2): ";ATMOS
200 PRINT
210 IF(CRVKEY=1) GOTO 330
220 XNN=31
230 INPUT "NAME OF DATA FILE: ";FL$
240 OPEN "I",1,FL$
250 PRINT
260 INPUT "CIR: ";CIR
270 PRINT
280 FOR I=1 TO 31
290 INPUT #1, CNR(I),A(I)
300 NEXT I
310 CLOSE #1
320 GOTO 390
330 INPUT "FSK(1) OR PSK(2) MODULATION: ";MTYP
340 PRINT
350 INPUT "CORRELATION COEFICIENT: ";RHO
360 PRINT
370 INPUT "FIXED CIR LEVEL (DB) : ";FXCIR
380 PRINT
390 INPUT "PLOT SCALES(1) OR NO(2): ";SCAL
400 PRINT
410 PRINT
420 REM
430 REM SET UP SCALES, THEN DO CALCULATIONS AND PLOTS
440 REM
450 LPRINT USING "&";CHR$(27);".Y"
460 LPRINT "DF"
470 LPRINT "IP 1000,200,9750,6450"
480 LPRINT "SC 0,10,0,7.3"
490 IF (SCAL=2) GOTO 1440
500 LPRINT "SP 2"
510 LPRINT "PAPU 9.5,6.8"
520 LPRINT "PD 0.5,6.8,0.5,0.8,9.5,0.8,9.5,6.8"
530 FOR N=1 TO 30
540 Y=.8+(N-1)*.2
550 LPRINT "PU",.5,Y
```

FIGURE 36 - Program PERTH.BAS

```
560 LPRINT "PD",.6,Y
570 NEXT N
580 FOR N=1 TO 30
590 Y=.8+(N-1)*.2
600 LPRINT "PU",9.5,Y
610 LPRINT "PD",9.4,Y
620 NEXT N
630 FOR N=1 TO 8
640 X=.5+N*1
650 LPRINT "PU",X,6.8
660 LPRINT "PD",X,6.675
670 NEXT N
680 LPRINT "SP 1"
690 FOR NB=1 TO 9
700 XB=.5+(NB-1)
710 FOR N=2 TO 9
720 X=XB+1*LOG(N)/2.30259
730 LPRINT "PU",X,6.8
740 LPRINT "PD",X,6.73
750 NEXT N
760 NEXT NB
770 LPRINT "SP 2"
780 FOR N=1 TO 8
790 X=.5+N
800 LPRINT "PU",X,.8
810 LPRINT "PD",X,.925
820 NEXT N
830 LPRINT "SP 1"
840 FOR NB=1 TO 9
850 XB=.5+(NB-1)
860 FOR N=2 TO 9
870 X=XB+LOG(N)/2.30259
880 LPRINT "PU",X,.8
890 LPRINT "PD",X,.87
900 NEXT N
910 NEXT NB
920 REM
930 REM WRITE SCALE LABELS
940 REM
950 ETX$=CHR$(3)
960 LPRINT "DI",0,-1
970 LPRINT "SP 1"
980 LPRINT "SI .2214,.25"
990 LABEL =10
1000 FOR N=1 TO 10
1010 X=9.65-(N-1)
1020 LPRINT "PU",X,7.25
1030 LPRINT "LB"
1040 LPRINT USING "##";LABEL
1050 LPRINT ETX$
1060 NEXT N
1070 LPRINT "SI 0.12,0.20"
1080 FOR N =1 TO 10
1090 X=9.7-(N-1)
1100 LPRINT "PU",X,7.05
```

FIGURE 36 continued

```
1110 LABEL=-(N-1)
1120 LPRINT "LB"
1130 LPRINT USING "###";LABEL
1140 LPRINT ETX$
1150 NEXT N
1160 LPRINT "SI .2214,.25"
1170 FOR N=1 TO 7
1180 LABEL=(N-1)*5
1190 Y=6.97-((N-1)*1!)
1200 LPRINT "PU",.55,Y
1210 LPRINT "LB"
1220 LPRINT USING "##";LABEL
1230 LPRINT ETX$
1240 NEXT N
1250 LPRINT "SP 2"
1260 LPRINT "SI .35,.5"
1270 LPRINT "PU",5.95,7.3
1280 LPRINT "LBP";ETX$
1290 LPRINT "PU",5.9,7.17
1300 LPRINT "SI",.2,.35
1310 LPRINT "SP 1"
1320 LPRINT "LBe";ETX$
1330 LPRINT "SI .3,.4"
1340 LPRINT "PU",.05,4.5
1350 LPRINT "SP 2"
1360 LPRINT "LBCNR (dB)";ETX$
1370 LPRINT "PU 9.,4.0"
1380 LPRINT "LBCIR = ";
1390 LPRINT USING "##.#";CIR;
1400 LPRINT " dB";ETX$
1410 REM
1420 REM NOW COMPUTE ERROR PERFORMANCE EVERY 1.0 DB.
1430 REM USING FORMULAS IN RODEN (PG. 282 AND PG. 304)
1440 REM
1450 LPRINT "SP 2"
1460 FLAG2=1
1470 FOR N=1 TO 31
1480 IF(CRVKEY=2) GOTO 1640
1490 EOVRNDB=(N-1)
1500 IF(EOVRNDB=0) THEN EOVRNDB=.01
1510 EOVRN=10!^(EOVRNDB/10)
1520 NCIR=10!^(FXCIR/10!)
1530 X=SQR((1!-RHO)*(1!/((1!/EOVRN+1!/NCIR)*2!)))
1540 T=1/(1+.327591*X)
1550 T2=T*T
1560 T3=T2*T
1570 T4=T2*T2
1580 T5=T2*T3
1590 X2=X*X
1600 ERFCX=.25482959#*T-.28449673#*T2+1.4214137#*T3-1.45315202#*T4+1.06140542#*T5
1610 ERFCX=ERFCX*EXP(-X2)
1620 PER=.5*ERFCX
1630 GOTO 1660
1640 PER=A(N)
1650 EOVRNDB=CNR(N)
```

FIGURE 36 continued

```
1660 IF(PER>1!) GOTO 1930
1670 IF(ATMOS=2) GOTO 1750
1680 IF(PER>.1) GOTO  1920
1690 IF(PER<1E-09) GOTO 1760
1700 FOR KK=1 TO 37
1710 IF(PER<PE(KK))AND(PER>=PE(KK+1)) GOTO 1730
1720 NEXT KK
1730 RATIO=(FNLG10(PER)-FNLG10(PE(KK+1)))/(FNLG10(PE(KK))-FNLG10(PE(KK+1)))
1740 DBADD=DB(KK)+RATIO*(DB(KK)-DB(KK+1))
1750 IF(PER>1E-09) GOTO 1840
1760 IF(FLAG=1) GOTO 1920
1770 XPLT=.5
1780 RATIO=(LOG(PER1)/2.30259+9)/((LOG(PER1)/2.30259)-(LOG(PER)/2.30259))
1790 DBADDX=.54*(FNLG10(PER1)-FNLG10(PER))+DBADD
1800 YPLT2=6.8-(EOVRNDB+DBADD)*.2
1810 YPLT=YPLT1-RATIO*(YPLT1-YPLT2)
1820 FLAG=1
1830 GOTO 1880
1840 XPLT=9.5+LOG(PER)/2.30259
1850 YPLT=6.8-(EOVRNDB+DBADD)*.2
1860 IF(YPLT>6.8)OR(YPLT<.8) GOTO 1920
1870 IF(FLAG2=1) THEN LPRINT "PU",XPLT,YPLT
1880 LPRINT "PD",XPLT,YPLT
1890 FLAG2=0
1900 PER1=PER
1910 YPLT1=YPLT
1920 NEXT N
1930 LPRINT "PU",0!,0!
1940 REM
1950 REM TURN OFF PLOTTER
1960 REM
1970 LPRINT USING "&";CHR$(27);".Z"
1980 END
```

FIGURE 36 continued

APPENDIX B - SCHEMATIC DIAGRAM AND MEASURED CHARACTERISTICS OF TEST CIRCUITS

The pages in this appendix show schematic diagrams and measured characteristics for the custom circuit blocks used in conducting the experimental tests in this research.

In addition to the custom circuitry, commercially available equipment was also used. The function, type, and serial number of these instruments is listed here.

Functional Unit	Instrument
FSK Generator	Tektronix FG 504 Function Generator, Serial Number B044969
Noise Generator	General Radio 1390-B Noise Generator, Serial Number 9252
Interference Generator	Hewlett-Packard 3310A Function Generator, Serial Number 947-01817
Wideband RMS Voltmeter	Hewlett-Packard 3400A RMS Voltmeter, Serial Number 806-08059
Error Counter	Tektronix DC 504A Universal Counter/Timer, Serial Number B033519

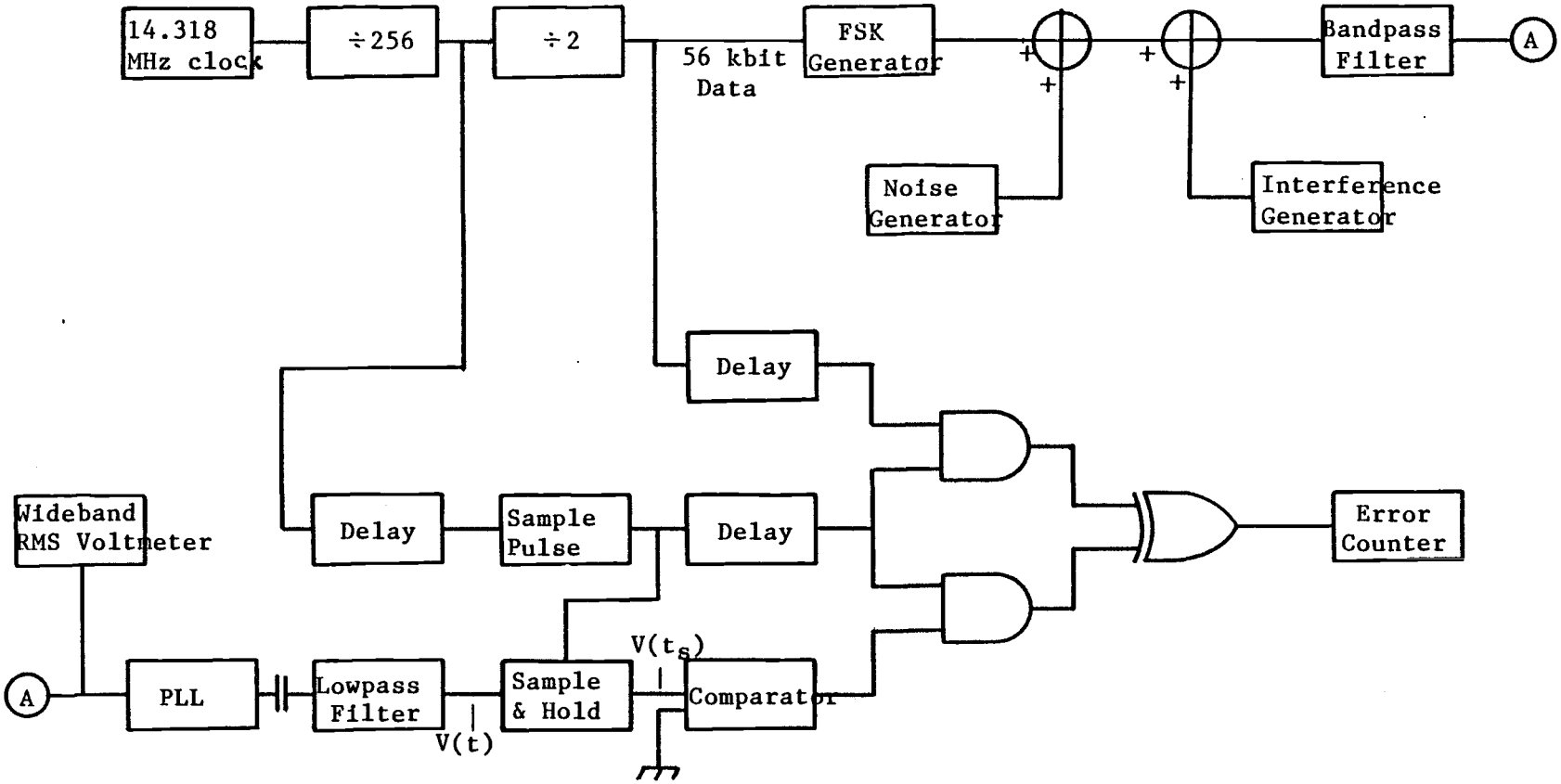

FIGURE 37 - Block Diagram of Equipment Connections for FSK Transmission Experiments

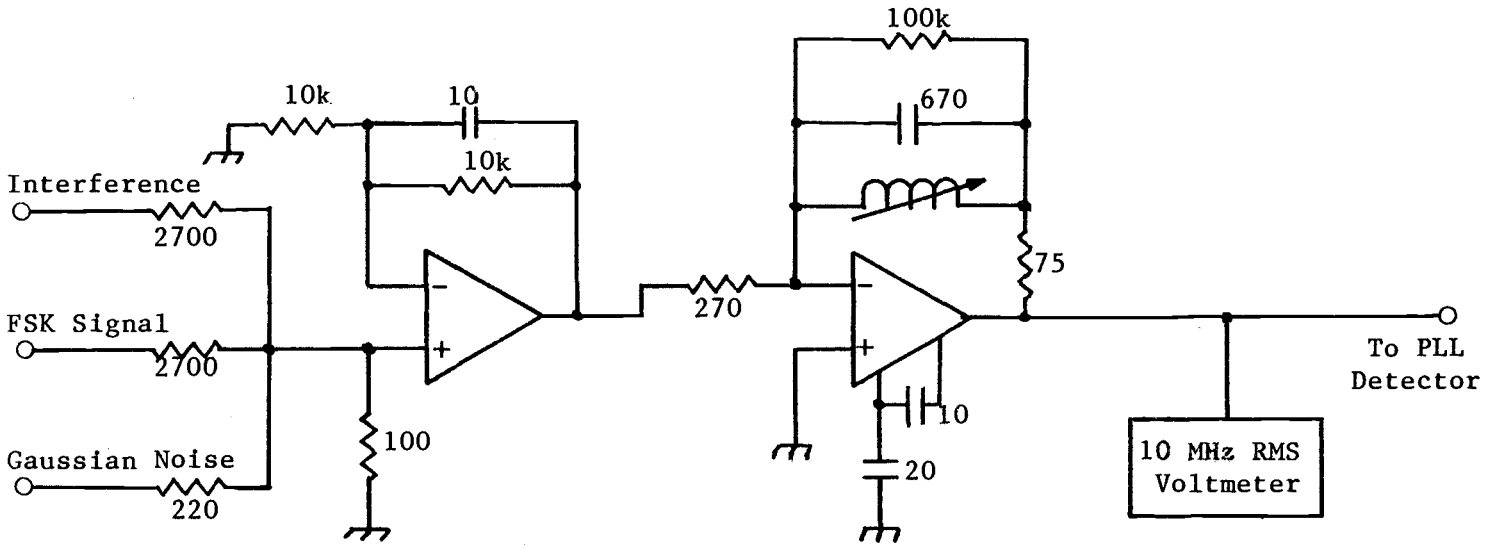

Opamps are LM318.
All resistances are in ohms.
All Capacitances are in picofrarads.

FIGURE 38 - Schematic Diagram of Bandpass Filter

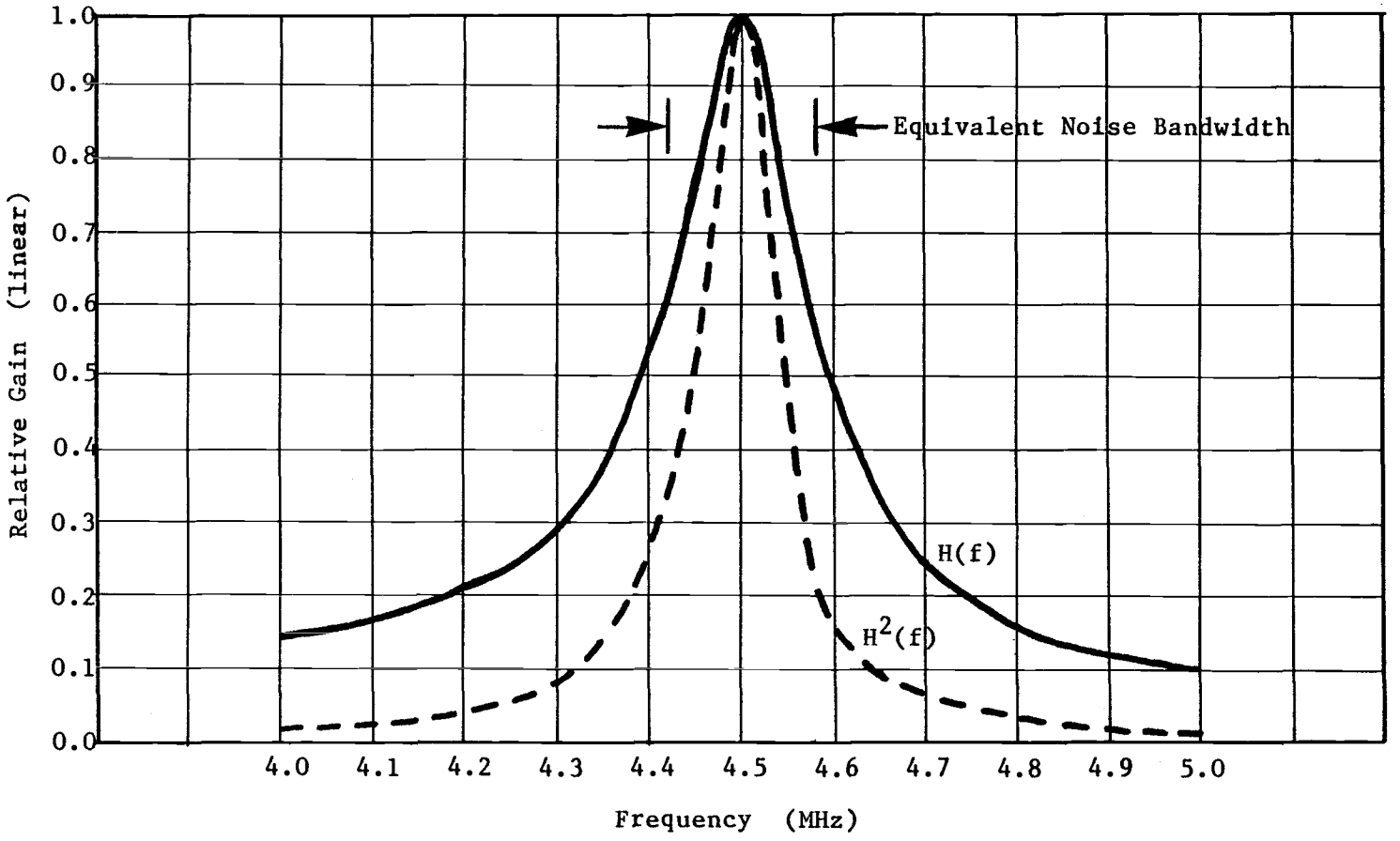

FIGURE 39 - Measured Response of Bandpass Filter

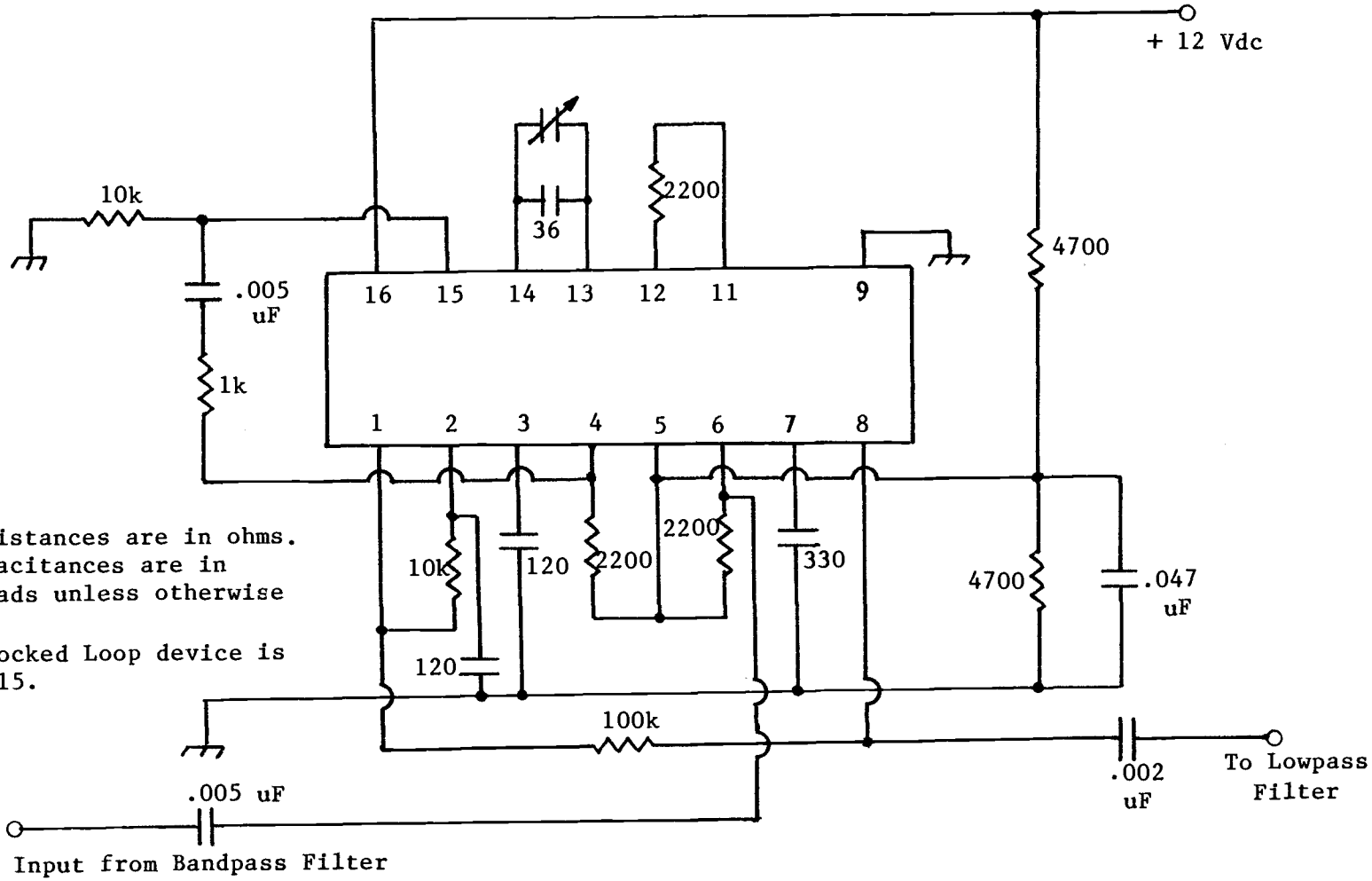

FIGURE 40 - Schematic Diagram of Phase Locked Loop Detector

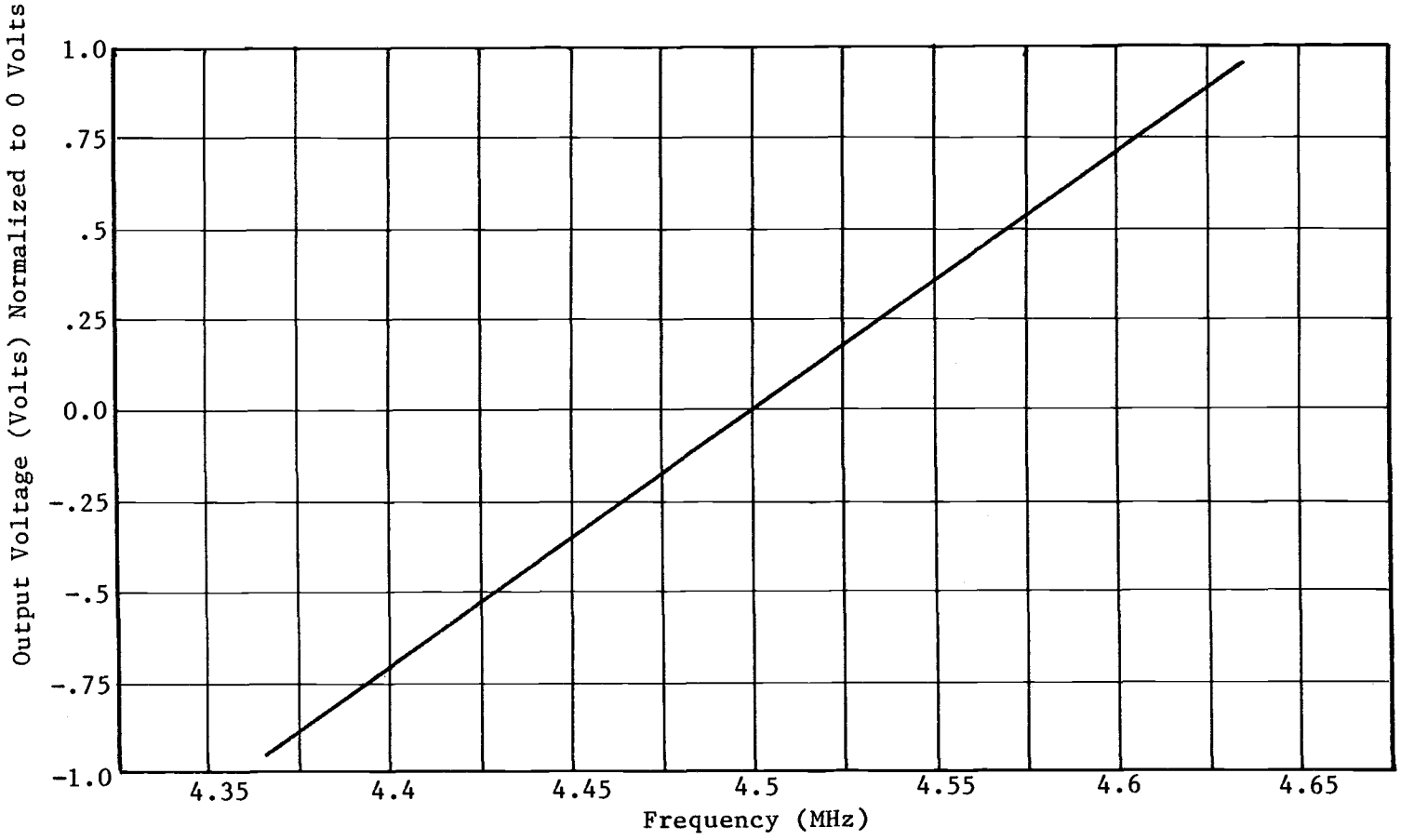

FIGURE 41 - Output Voltage of Phase Locked Loop Circuit Versus Input Frequency

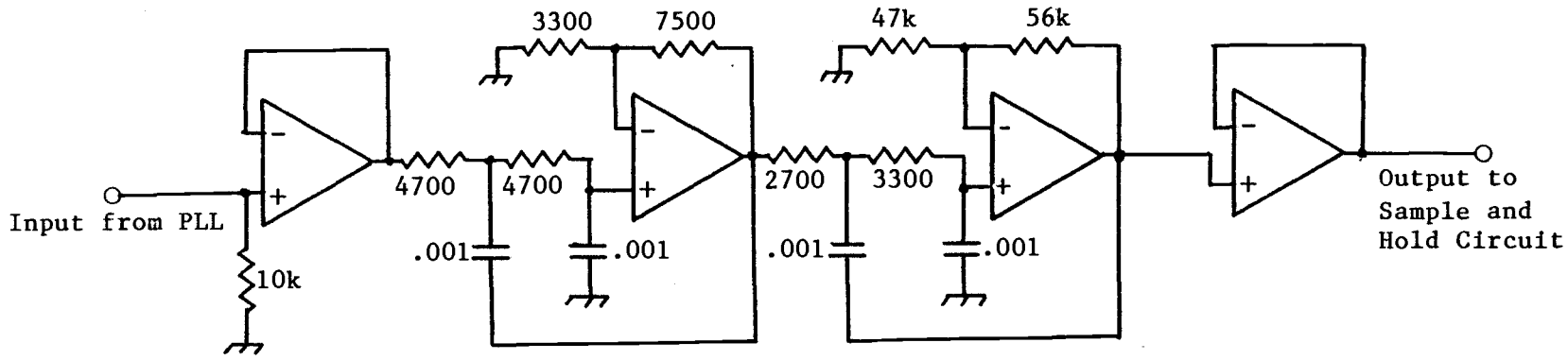

All resistances are in ohms.
All capacitances are in microfarads.
Opamps are 1/2 NE5532.

FIGURE 42 - Schematic Diagram of Lowpass Filter

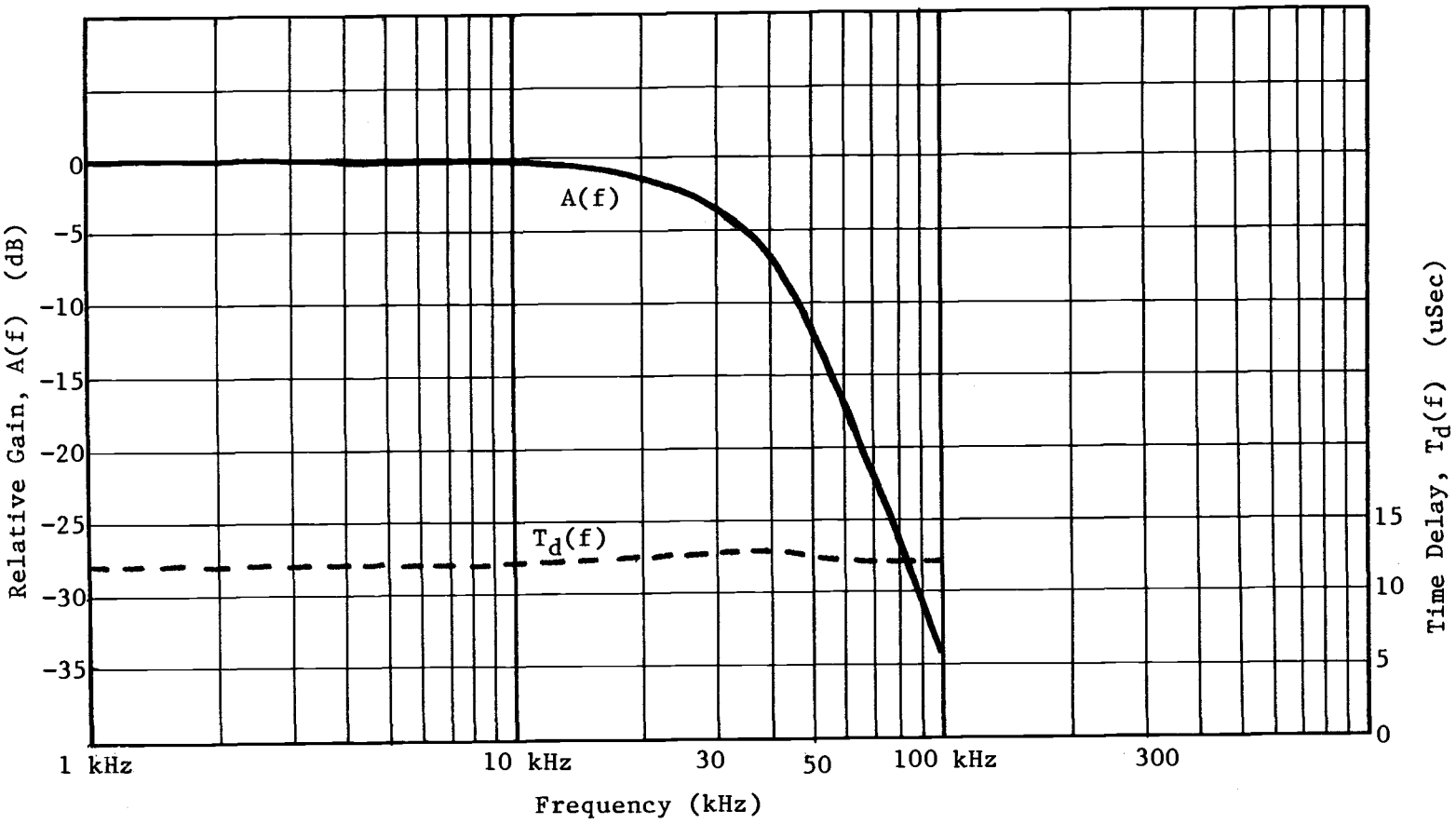

FIGURE 43 - Measured Frequency Response of Lowpass Filter

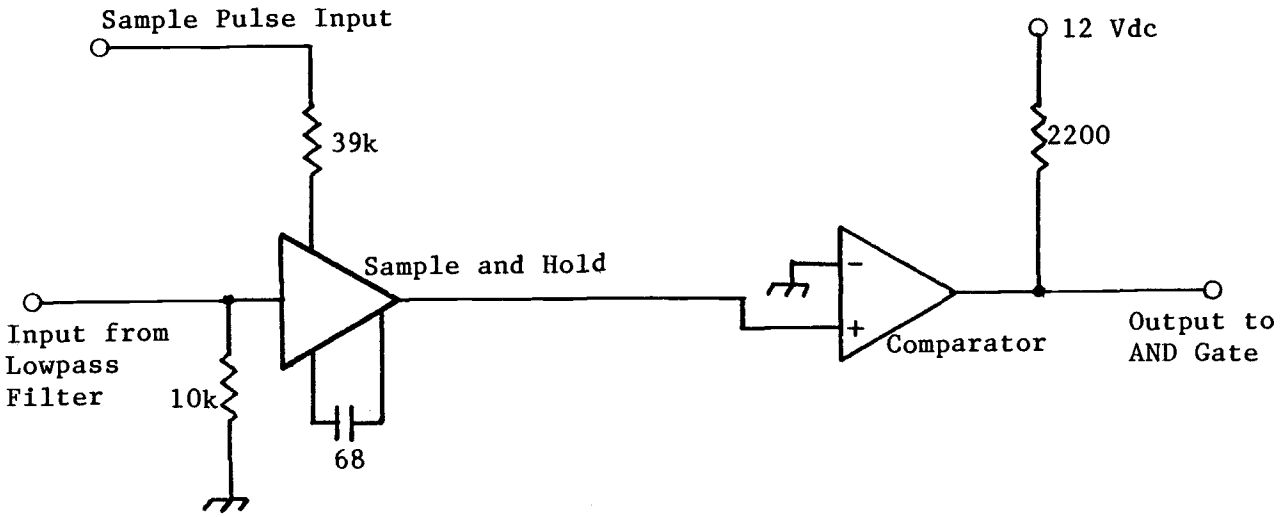

All resistances in ohms.
All capacitances in picofarads.
Sample and Hold device is a LM398.
Comparator device is a LM319.

FIGURE 44 - Schematic Diagram of Sample and Hold and Comparator Circuits